



POLITECNICO DI TORINO

Corso di Laurea Magistrale in Ingegneria Biomedica

Tesi di Laurea Magistrale

**Modeling Cardiac Effects of Vagus
Nerve Stimulation in Heart Transplant
Recipient**

Relatore

prof. Diego Gallo

Candidata

Silvia Frullini

Supervisor Esterni

Medical University of Vienna

prof. Francesco Moscato

Max Habermusch, MSc

Anno Accademico 2019-2020

Abstract

Heart transplantation (HTx) is the last resort for patients with severe heart failure, but an inevitable consequence of the surgery is cardiac denervation. This leads to a markedly increased resting heart rate and the inability of the heart to adapt to physical activity, thus reducing patient quality of life. Today, neuromodulation techniques such as vagus nerve stimulation (VNS) are successfully applied to treat various conditions including Parkinson disease, treatment-resistant depression, or epilepsy. As the vagus nerve (VN) has several projections to the heart, it plays a crucial role in chronotropic-, dromotropic- and inotropic control. Therefore, VNS may be a promising technique to artificially restore vagal cardiac control in those suffering from cardiac denervation. Although VNS is typically applied in an asynchronous fashion (A-VNS), for cardiac control it can be synchronized with respect to the cardiac cycle (S-VNS). This is often done by triggering a burst of impulses with the R-peak of the ECG. However, to this date, the cardiac effects of VNS are not fully understood, thus complicating the development of effective stimulation paradigms to restore cardiac control.

To further investigate the effects of VNS, in this thesis, a numerical model of the human cardiovascular system was extended to integrate a lumped parameter model of the VN that is target to extracellular stimulation. The model consists of (1) the hemodynamic system, comprising the heart and vessels; (2) the autonomic sympathetic cardiac control; (3) the sinoatrial node; (4) the VN realized as Hodgkin-Huxley-type multi-axon model; and (5) the VN terminals represented by a three-compartment acetylcholine release model. Moreover, a stimulator was integrated into the model as a pulse generator that allows eliciting action potentials within the VN axons by extracellular stimulation through a monopolar point electrode. The pulse generator is configurable allowing the manipulation of stimulation parameters including intensity (I), pulse width (PW), frequency (F), number of pulses (NP), and trigger delay (D). The model was then tuned based on published data on the cardiac effects of VNS obtained from in-vivo experiments in sheep.

To investigate the influence of the stimulation parameters on cardiac effects they underwent a global sensitivity analysis (GSA). The GSA was performed for A- and S-VNS, in both, the model of healthy individuals and HTx recipients. The results show that for S-VNS I has the greatest influence, followed by PW and NP, while F and D play a minor role. The results for A-VNS are similar as in S-VNS, however, F has a markedly increased influence on the cardiac effect. For both A-VNS and S-VNS, cardiac denervation following HTx shows no significant differences for chronotropism and dromotropism while an overall reduction for inotropism was found.

Finally, the model was validated, comparing the results to literature data, different from that used for tuning. The model was found capable to reproduce the chronotropic and dromotropic effects of VNS with good accuracy. However, for the inotropic response, the model predictions are in conflict with the findings in literature.

Overall, the study could help to identify potential targets stimulation parameters for the design of a closed-loop control strategy. Moreover, the model forms a viable foundation to further investigate the cardiac effects of VNS on the denervated heart.

Keywords: heart transplantation, vagus nerve stimulation, computer model, sensitivity analysis

Acknowledgements

Throughout the writing of this thesis, I have received a great deal of support and assistance.

I would like to express my sincere gratitude to my supervisors: Professor Diego Gallo, Professor Francesco Moscato, and Max Habermusch. Your support, guidance, and patience are invaluable to me. Thanks for including me on the NeuHeart team; this experience led me to face the world of research in a very positive way.

I would like to acknowledge the Center for Medical Physics and Biomedical Engineering, Medical University of Vienna (Austria), and the Ludwig Boltzmann Institute for Cardiovascular Research, Vienna (Austria), where this project was carried out. This project has been funded by the H2020-EU project: NeuHeart “A neuroprosthesis to restore the vagal-cardiac closed-loop connection after heart transplantation”. Grant agreement ID: 824071.

I would also like to thank the Vienna Scientific Cluster (VSC), who provides access to their supercomputer to obtain part of the results presented in this thesis.

Finally, I would like to acknowledge with gratitude the support and love of my family - my parents Maria Teresa and Stefano, my sister Ilaria, my brother Lorenzo - and my boyfriend Vittorio. You are my strength in times of despair, and those I always share with my times of joy.

Contents

List of Figures	vii
List of Tables	xii
1 Introduction	1
1.1 Cardiovascular Anatomy and Physiology	1
1.1.1 The cardiac cycle	3
1.1.2 Pressure-Volume Loops	4
1.2 Electrophysiology of the heart	7
1.3 The Neuron	10
1.3.1 The Action Potential	11
1.4 Autonomic Nervous System	15
1.4.1 Primary afferent neurons	16
1.4.2 Sympathetic Nervous System	17
1.4.3 Parasympathetic Nervous System	17
1.4.4 Neurotransmitters of the Autonomic Nervous System	20
1.4.5 Autonomic control of the cardiovascular system	21
1.4.6 Heart Rate Variability	25
1.5 Heart Failure	27
1.6 Transplanted pathophysiology	28
1.7 Vagus Nerve Stimulation	30
1.8 Numerical models of the cardiovascular system	31
1.9 Nerve Models	35
1.9.1 Hodgkin-Huxley neuron membrane model	35
1.9.2 Propagation of Action Potentials	36
1.10 Sensitivity Analysis	37
1.10.1 Sobol's method	38
1.11 Purpose of the study	39
2 Methods	41
2.1 Overview of the Model	41
2.2 Hemodynamic Model structure	43

2.3	Respiration	46
2.4	Sympathetic Cardiac Control	47
2.5	Physiological Model of Primary Afferent Neurons	49
2.5.1	Model of Baroreceptors	49
2.5.2	Model of Lung Stretch Receptors	50
2.6	Physiological Model of Autonomic Parasympathetic Premotor Neurons	50
2.7	Model of Vagus Nerve Axons	51
2.8	Acetylcholine Release Model	54
2.9	The Vagus Nerve	55
2.10	Sino Atrial Node	59
2.11	PR interval model	60
2.12	Tuning of the model: Global Sensitivity Analysis	61
2.12.1	Cardiac Effects' Markers	61
2.12.2	Two-phases Model Tuning	63
2.13	Validation Tests	64
2.13.1	Chronotropic Effect	64
2.13.2	Inotropic Effect	65
2.13.3	Dromotropic Effect	66
2.14	Hemodynamic Parameters	66
3	Results	69
3.1	S-VNS Effects on Chronotropy, Inotropy and Dromotropy	71
3.2	Global Sensitivity Analysis	75
3.2.1	S-VNS applied to Healthy condition	75
3.2.2	S-VNS applied to HTx condition	77
3.2.3	A-VNS applied to Healthy and HTx conditions	79
3.3	Model Validation	81
3.3.1	Chronotropism	82
3.3.2	Inotropism	82
3.3.3	Dromotropism	84
3.4	Effect of S/A-VNS on hemodynamic parameters	85
4	Discussion	87
4.1	S-VNS Effects on Chronotropy, Inotropy and Dromotropy	87
4.2	Global Sensitivity Analysis	88
4.2.1	S-VNS applied to the Healthy Condition	88
4.2.2	S-VNS applied to HTx condition	89
4.2.3	A-VNS applied to Healthy and HTx condition	90
4.3	Model Validity	91
4.4	Hemodynamic Parameters	92
5	Conclusion and Future Work	93

A	Model Parameters	95
A.1	Hemodynamic Model structure	95
A.2	Sympathetic Cardiac Control	97
A.3	Primary Afferent Neurons	99
A.4	Parasympathetic Premotor Neurons	99
A.5	CRRSS Model	100
A.6	Acetylcholine Release Model	101
A.7	Vagus Nerve	101
A.8	PR Interval Model	102
	Bibliography	103

List of Figures

1.1	The path of blood flow through the cardiovascular system. The pulmonary and systemic circuits and major blood vessels connecting with the heart are shown. Arrows indicate the direction of blood flow [1].	2
1.2	Changes in pressure and volume that characterize the cardiac cycle. Modified from [2]	4
1.3	PV loops: (a) main phases of the cardiac cycle with illustration of the ESPVR and EDPVR; (b) important features that can be easily extracted such as end-diastolic volume (EDV), end-systolic volume (ESV), end-systolic pressure (Pes) and left atrial pressure (LAP). Modified from [2].	5
1.4	(a) effect of preload, (b) effect of afterload and (c) effect of inotropy [3].	6
1.5	The conduction system of the heart [1].	8
1.6	Electrical activity in a SA node cell: a recording of the membrane potential showing pacemaker potentials (phase 4, slow depolarization) and action potentials (phase 0, depolarization; phase 3, repolarization). Modified from [1]	9
1.7	Representation of the neuron's main components: the nucleus, which resides in the soma, the axon in which the impulse travels, dendrites and synapses which connect the neuron with other cells. Modified from [5] .	11
1.8	Action potential is presented as a graph of voltage over time. Three main phases are distinguished: depolarization, repolarization and hyperpolarization [6].	12
1.9	Representation of a chemical synapse: the arrival of an AP triggers the fusion of some vesicles with the nerve membrane to locally release neurotransmitters. Neurotransmitters diffuse in the synaptic cleft and bind of the post-synaptic cell membrane receptors. Neurotransmitters are cleared from the synapse either by enzymatic degradation, neuronal re-uptake, or glial re-uptake. ([7] p.570)	14
1.10	Neuro-effector junction: the connection between autonomic fibers and target effectors. The neurotransmitter is released from varicosities, which interface the effector organ in many points [6].	16

1.11	Illustration of the sympathetic nervous system: preganglionic nerve fibers (solid lines) project to the ganglia; postganglionic nerve fibers (dashed lines) project to the effector organs [7].	18
1.12	Illustration of the parasympathetic nervous system: preganglionic nerve fibers (solid lines) project to the ganglia; postganglionic nerve fibers (dashed lines) project to the effector organs [7].	19
1.13	Schematic representation of the ANS's efferent nerves with their neurotransmitters: preganglionic fibers of both parasympathetic and sympathetic systems release ACh; ACh acts on nicotinic receptors (Nn) on the postganglionic nerves. ACh is also the neurotransmitter at cells of the adrenal medulla, releasing the CATs (Epi and NE) into the circulation. ACh is the predominant neurotransmitter of postganglionic parasympathetic nerves and acts on muscarinic (M) receptors. NE is the principal neurotransmitter of postganglionic sympathetic nerves, acting on adrenergic (α and β) receptors. [10]	20
1.14	Overview of cardiac innervation: Sensory nerves (blue), give feedback to the CNS which modulates the activity of parasympathetic (green) or sympathetic (red) nerves to either relax or stimulate the heart. The vagus nerve innervates the SA node, AV node and ventricular myocytes. [13].	23
1.15	Histology sample of the cervical vagus nerve. Fascicles are separated by perineurium and the epineurium surrounds the entire nerve. Arrows indicate sub-perineural vascular supply and in the magnification on the left side, sub-perineural supply is visible [16].	24
1.16	Power Spectral Density (PSD) of the interbeat interval showing the three main frequency bands: very low frequency (VLF), low frequency (LF) and high frequency (HF) [21].	27
1.17	Number of heart transplants per year and geographic region [24].	28
1.18	Models classification [35]	32
1.19	The Windkessel model proposed by Weber [36].	33
1.20	Hodgkin-Huxley neural membrane equivalent circuit [38]	36

2.1	Overview of the model structure: the first compartment (outer part of the scheme) is composed of the components of the cardiovascular system such as left and right heart, pulmonary and systemic arteries and veins; the second compartment represents the autonomic control of the heart by means of the sympathetic and the parasympathetic divisions. The sympathetic control releases isoprenaline (Iso) to the sino-atrial (SA) node on the basis of the afferent receptor input. The parasympathetic control also includes a more detailed representation of the afferent pathway through the lungs stretch receptors and baroreceptors models that deliver signals to the CNS that implement the efferent response. Pre-motor neurons activity leads to a release of acetylcholine (ACh) from the vagal varicosities to the SA node. The adrenal medulla releases circulating catecholamines (CAT). The amount of neurotransmitters that binds on the membrane of the SA node cells play a major role in determining the heart rate (HR). To deliver VNS, a simple pulse generator (third compartment) applies impulses to the vagus nerve. Each block of the scheme represents a sub-model which interface with one another.	42
2.2	Schematic diagram of the hemodynamic model structure: MV, mitral valve; AoV, aortic valve; TV, tricuspid valve; PV, pulmonary valve. Adapted from [42]	43
2.3	Electric analog of the arterial load model (left) and of the venous return (right) [44].	46
2.4	Sympathetic regulation mechanisms acting on the generic effector θ which can be systemic peripheral resistance, venous unstressed volume, end-systolic elastance of the right or left ventricle and changes in isoprenaline concentration. Modified from [45]	47
2.5	Equivalent circuit of the CRRSS model [38]	51
2.6	Three compartment ACh release model consisting of a main ACh neuronal store, the neuroeffector junction and extra junctional space. Concentrations of ACh within these stores are denoted by $[ACh_{ms}]$, $[ACh]$ and $[ACh_{ex}]$ respectively. k_1 and k_2 indicate the fractions of $[ACh_{ms}]$ released per vagal stimulus into the neuroeffector junction and extra junctional spaces and k_D is the effective diffusion rate between these latter two compartments. k_H is the rate of hydrolysis in the neuroeffector junction and k_E is the rate of escape from the extra junctional space to the vasculature. Modified from [50]	54
2.7	Illustration of the building of the vagus nerve (VN). Each fiber is a CRRSS model. In the VN there are hundreds of fibers, each with a proper diameter and distance for the electrode d_{el} (black rectangle).	56

2.8	Dimensionality reduction: inputs of the look-up table are the pulse width (P_w), a vector with n electrode distances d_{el} and a vector with n fiber diameters; output of the look-up table is a vector with the n activation thresholds (I_{thr}). I_{thr} is compared with the current intensity delivered from the stimulator (I_{stim}) and the number of activated fibers (N_{active}) is detected.	57
2.9	Diagram block of the entire vagus nerve, which contains the reduced axon models and the synaptic end (the ACh release model). The first provides the percentage of activated fibers ($N_{active\%}$) and the second the amount of ACh released by one fiber ($[ACh]_{RM}$). These two values are multiplied and a gain factor ($G_{ACh,stim}$) is applied to have the total amount of ACh released VNS ($[ACh]_{stim}$), which is also the amount of ACh released in vagotomy	58
2.10	Diagram block which describes the total amount of ACh released ($[ACh]_{tot}$) with the intact VN. The ACh released because of stimulation ($[ACh]_{stim}$) is summed to the one release by premotor neurons activity ($[ACh]_{pm}$). The 'Spikes' block transform the firing rate of premotor neurons ($f_{e,pm}$) in action potential (APs) with the right frequency.	59
2.11	Data processing for the calculation of the inotropism marker: from acquired pressure in the left ventricle (P_{lv}), the first derivative is calculated ($\frac{dP_{lv}}{dt}$) and its maximum detected. VNS is applied at 20s and maintained till the end of the simulation.	62
3.1	Generic simulation results for asynchronous vagus nerve stimulation (current intensity 0.6 mA, pulse width 150 μ s and frequency 25 Hz).	70
3.2	Generic simulation results for synchronized vagus nerve stimulation (current intensity 0.6 mA, pulse width 150 μ s, frequency 25 Hz, delay 156.2 ms and 4 pulses per burst).	70
3.3	The chronotropism marker (C_M) represents the percentage change in heart rate due to stimulation. It is calculated from the model (red dot) and compared to the Ojeda et al. study results [58] (in blue the mean value and in black the maximum and minimum). For each of the 75 parameter configuration, pulse width (P_w), current intensity (I_{stim}), frequency (F), number of pulses (N_p) and trigger delay (D) are given.	72
3.4	The inotropism marker (I_M) represents the percentage change of the rate of change of the left ventricle pressure due to stimulation. It is calculated from the model (red dot) and compared to the Ojeda et al. study results [58] (in blue the mean value and in black the maximum and minimum). For each of the 75 parameter configuration, pulse width (P_w), current intensity (I_{stim}), frequency (F), number of pulses (N_p) and trigger delay (D) are given.	73

3.5	The dromotropism marker (D_M) represents the percentage change of the PR interval due to stimulation. It is calculated from the model (red dot) and compared to the Ojeda et al. study results [58] (in blue the mean value and in black the maximum and minimum). For each of the 75 parameter configuration, pulse width (P_w), current intensity (I_{stim}), frequency (F), number of pulses (N_p) and trigger delay (D) are given.	74
3.6	Comparison of the estimation of the main and total sensitivity indices for chronotropism, inotropism and dromotropism performed by Ojeda et al. [58] with the ones obtained from the model with a parameter set of 1000 different quasi-random combinations.	76
3.7	Comparison of the estimation of the main and total sensitivity indices for chronotropism, inotropism and dromotropism performed in the healthy and the HTx conditions.	78
3.8	Estimation of Sobol's main and total indices for each A-VNS parameter on each cardiac effect.	80
3.9	Reduction in heart rate (chronotropic effect) in an isolated heart subjected to asynchronous vagus nerve stimulation obtained by the model compared to literature data [61], [62],[63].	82
3.10	PV loops of the vagotomy (a), healthy (b) and HTx (c) conditions with (right) and without (left) the application of asynchronous VNS (current intensity = 0.78 mA, pulse width = 0.15ms and frequency = 10 Hz). The black straight line represents the ESPVR.	83
3.11	Measurement of the PR interval applying A-VNS fixing the current intensity to 0.9 mA and the pulse width to 0.2 ms and increasing the stimulation frequency from 0 to 5 Hz.	85

List of Tables

1.1	Relative magnitude of effect on the heart of sympathetic and parasympathetic activity indicated by a positive (+) or negative (-) correlation [3].	22
2.1	Hydraulic-Electrical analogue components and unit of measures.	43
2.2	Synchronize VNS parameter ranges and notation from [58].	61
2.3	Resting hemodynamic parameters obtained from a polling of data from literature. Adapted from [65].	66
3.1	Comparison between the main and total sensitivity indices (mean±std [%]) for chronotropism, inotropism and dromotropism performed by Ojeda et al. [58] with the ones obtained from the model with a parameter set of 1000 different quasi-random combinations.	75
3.2	Estimation of main and total sensitivity indices (mean±std [%]) for chronotropism, inotropism and dromotropism obtained with the model in the HTx set up.	79
3.3	Global sensitivity indices (mean±std [%]) estimated with the Sobol's method of the asynchronized VNS parameters performed with 1000 different parameters combinations for the healthy and the HTx conditions.	81
3.4	Elastance (Ees) calculated as the slope of the ESPVR for when simulating dissected vagus, healthy condition and HTxR with and without VNS (continuous stimulation: current intensity = 0.78mA, pulse width = 0.15ms and frequency = 10 Hz)	84
3.5	Comparison between of the slope of increase of the PR interval obtained in the study performed by Pirola et al. [56] and the one obtained from the model when providing a supramaximal stimulation.	84
3.6	Comparison between hemodynamic parameters (heart rate (HR), cardiac output (CO), systolic blood pressure (SBP), diastolic blood pressure (DBP) and stroke volume (SV)) of the healthy control and HTxR with and without VNS (S-VNS: current intensity = 1mA, pulse width = 0.2ms, number of pulses = 4, frequency = 25.6 Hz and delay = 156.2 us and A-VNS: current intensity = 0.7 mA, pulse width = 0.1ms and frequency = 15 Hz)	86
A.1	Values used for the left ventricle model parameters	95

A.2	Values used for the right ventricle model parameters	96
A.3	Values used for the left (LA) and right (RA) atria model parameters	96
A.4	Values used for the valve models (M=mitral, A=aortic, T=tricuspid, P=pulmonary). R_{dir} and R_{inv} are the resistance in forward and backward direction respectively and L_{li} is the inertance.	97
A.5	Values used for the arterial load and venous return parameters.	97
A.6	Values used for the sympathetic control model.	98
A.7	Values used for the primary afferent neuron models.	99
A.8	Values used for the efferent premotor neuron models.	99
A.9	Values used for the CRRSS model.	100
A.10	Values used for the ACh release model.	101
A.11	Values of the vagus nerve reduced model.	101
A.12	Values used for the PR interval model.	102

Chapter 1

Introduction

1.1 Cardiovascular Anatomy and Physiology

The heart is the central organ of the cardiovascular or circulatory system. It has the primary function of circulating the blood through the body, and it does this by acting as a mechanical pump. It is formed by four chambers: two atria, which receive blood coming back to the heart by veins and two ventricles, which receive blood from atria and generate pressure to propel the blood in the arteries. As illustrated in Figure 1.1, the cardiovascular system is constituted by two divisions: the pulmonary circulation, composed of all vessels inside the lungs and those which connects the lungs to the heart, and the systemic circulation that comprises all other vessels that connect remaining parts of the body to the heart. Those circuits receive blood from different parts of the heart; that's why this latter is commonly divided in left and right heart, which deliver blood to the pulmonary and systemic circulation, respectively.

Both the pulmonary and the systemic circuit have a dense network of capillaries where both gasses and nutrients are exchanged. The blood picks up oxygen and delivers carbon dioxide passing through the pulmonary capillary bed, so it is called oxygenated blood since the end of this pathway. On the other hand, passing through the systemic capillary beds, which are contained in all organs except the lungs and tissues, it delivers oxygen and removes carbon dioxide and cellular wastes produced by cells with metabolism. Blood leaving those capillaries is called deoxygenated blood.

Also, the cardiovascular system provides cell-to-cell communication and immune function. Through the flowing in the cardiovascular system, the blood moves alternatively between the pulmonary and the systemic circuit coming back to the heart at the end of every cycle. This complex system can be seen in a simplified manner as a series of tubes (blood vessels) filled with fluid (blood) and connected to a mechanical pump (the heart). The heart's pumping activity consists of a rhythmic alternating contraction and relaxation of the cardiac muscle; this is called *cardiac cycle*. The pressure inside each chamber varies continuously during the cycle. The *gradient of pressure* is the propelling force for

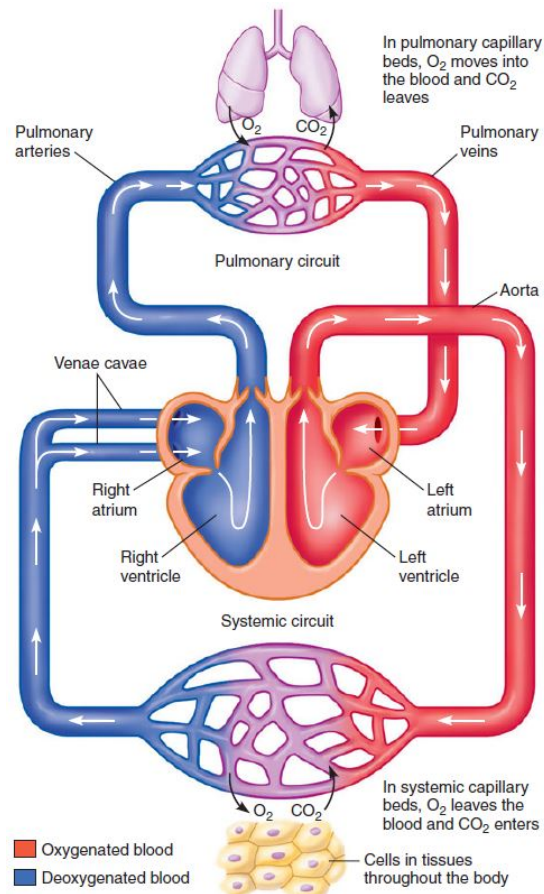


Figure 1.1: The path of blood flow through the cardiovascular system. The pulmonary and systemic circuits and major blood vessels connecting with the heart are shown. Arrows indicate the direction of blood flow [1].

moving the blood from atria to ventricle and from the latter to the arteries. It is fundamental that the flow is unidirectional; this is ensured by the pressure gradient and four cardiac valves. Atria are separated from ventricles by the atrioventricular (AV) valves: when the atrial pressure is greater than the ventricular one, the valve is open and vice versa, when the ventricular pressure is greater than the atrial one, the valve is closed. The semilunar valves separate ventricles from arteries: the aortic valve separated the left ventricle from the aorta, the pulmonary valve separates the right ventricle from the pulmonary trunk. Those two valves open when the ventricle's pressure overcomes the one in the relative artery, which happens when the ventricle is contracted. This allows the blood to leave the ventricles and move to the arteries to the point in which the ventricle's pressure becomes lower than the one in the arteries and the valve closes [1].

1.1.1 The cardiac cycle

The cardiac cycle comprises all the events associated with the blood flow through the heart during a heartbeat [2], and it is commonly divided into two major phases:

- *Systole*: from Greek meaning contracting is the period during which the muscle transforms from its totally relaxed state to the instant of maximal mechanical activation
- *Diastole*: from Greek meaning relaxation is the period in which the muscle relaxes from the end-systolic state back towards its resting state

In the following analysis, a particular focus is addressed to the hemodynamic of the left ventricle (LV), considering that all hemodynamic events occurring in the right ventricle have different timing and different levels of pressure but are similar. The mechanical events occurring during the cardiac cycle can be characterized by tracking changes in pressure and volume in the ventricle. In Figure 1.2 the most significant features are reported: ventricular volume (LVV), ventricular pressure (LVP), left atrial pressure (LAP) and aortic pressure (AoP) [2]. The analysis of each phase of the cardiac cycle is here analyzed by starting from the second half of the diastole in which both ventricles and atria are completely relaxed:

Late filling: before time A, the heart is in the second half of the diastole (relaxed state) and the blood, driven by the pressure gradient, moves from the systemic and pulmonary veins towards the atria. Then, it crosses the opened AV valve and fills the ventricle. LVP and LVV are relatively constant, and AoP is gradually declining. AoP falls as the blood ejected into the arterial system and gradually moves from the large arteries to the capillary bed.

Isovolumetric contraction: At time A, there is electrical activation of the heart, contraction begins, and pressure rises rapidly inside the chamber. Early after contraction begins, LVP rises to be greater than left atrial pressure and the mitral valve closes. LVP is less than AoP, so the aortic valve is closed as well. Since both valves are closed, no blood can enter or leave the ventricle during this time, and therefore the ventricle is contracting isovolumically.

Ejection: At time B, LVP slightly exceeds AoP and the aortic valve opens. During this phase, there is very little difference between LVP and AoP, provided that AoP is measured just on the distal side of the aortic valve. The blood is rapidly ejected from the ventricle into the aorta and LVV decreases. As the maximum contraction is reached, ejection slows down.

Isovolumetric relaxation: The muscles relax till the point, in time C, in which LVP falls below AoP and the aortic valve closes. At this point, ejection has ended and LVV reaches

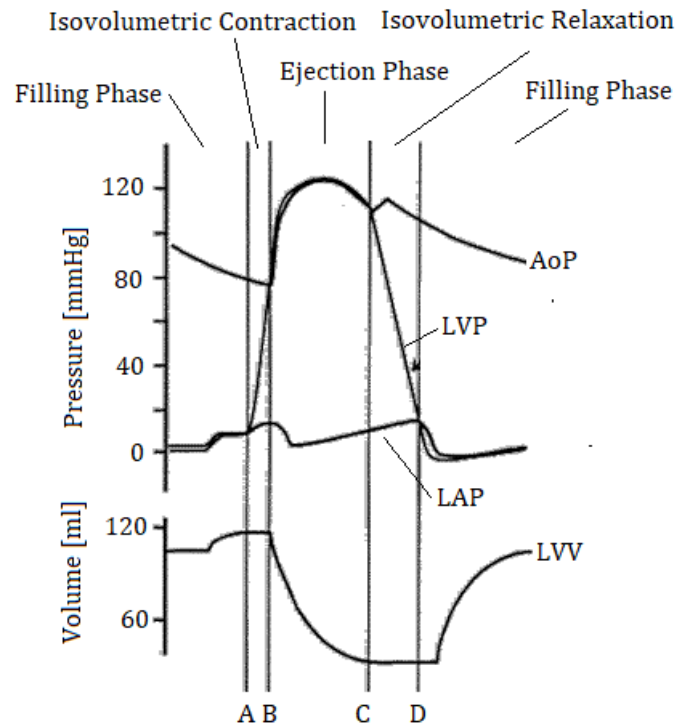


Figure 1.2: Changes in pressure and volume that characterize the cardiac cycle. Modified from [2]

and maintains its minimum because both mitral and aortic valves are closed. The continued decline of LVP indicates that the relaxation process continues.

Early ventricular filling: At time D, LVP falls below LAP and the mitral valve opens. At this point, blood flows from the left atrium into the LV as indicated by the rise of LVV; also note the slight increase in LVP as filling proceeds.

In general terms, systole includes isovolumic contraction and ejection; diastole includes isovolumic relaxation and (early and late) filling.

1.1.2 Pressure-Volume Loops

The cardiac cycle is usually illustrated by using the pressure-volume relation and this is done by plotting the LVP as function of LVV. As shown in Figure 1.3 (a), this originates a close loop which is called *pressure-volume loop* (PV loop). As time proceed, the PV points go around the loop in a counter clockwise direction. Some important features can be easily extrapolated (Figure 1.3 (b)) by this kind of representation:

- *end-diastolic volume (EDV)* is the maximum volume of the cardiac cycle
- *end-systolic volume (ESV)* is the minimum volume reached
- *stroke volume (SV)* is the value of blood ejected in each cycle:

$$SV = EDV - ESV \quad (1.1)$$

- *end-systolic pressure (Pes)* is identified by the pressure at the left upper corner of the loop
- *left atrial pressure (LAP)* is approximated with the pressure at the point in which the mitral valve opens which is in the left lower corner of the loop

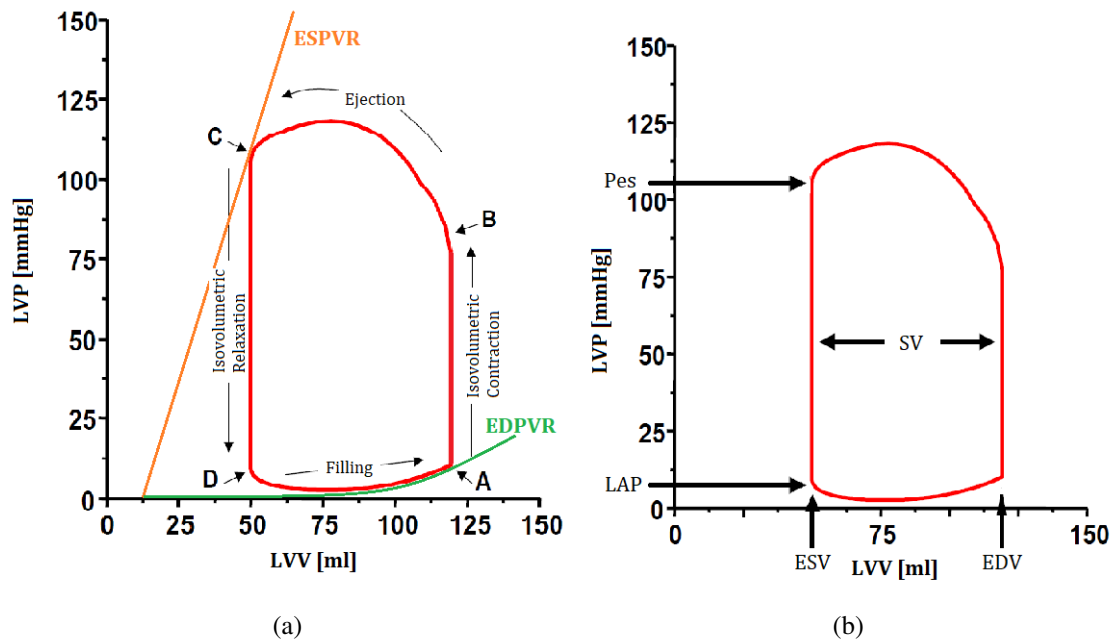


Figure 1.3: PV loops: (a) main phases of the cardiac cycle with illustration of the ESPVR and EDPVR; (b) important features that can be easily extracted such as end-diastolic volume (EDV), end-systolic volume (ESV), end-systolic pressure (Pes) and left atrial pressure (LAP). Modified from [2].

While the heart is contracting and relaxing, its chambers change stiffness, reaching the highest stiffness at the end of the systole and the lowest at the end-diastole. These two conditions describe the upper and lower border of the PV loop:

- *End-diastolic pressure-volume relationship (EDPVR)* describes the non-linear relationship between pressure and volume when the ventricle is assumed to be in his

total relaxed state. The green line illustrates this relation in Figure 1.3 (a). This curve creates the lower boundary of the PV loop, which falls on the EDP at the end of the diastole (the bottom right-hand corner).

- *End-systolic pressure-volume relationship (ESPVR)* describes the linear relationship between pressure and volume when the ventricle is assumed to be in his total contracted state. In Figure 1.3 (a), the ESPVR is represented by the orange line and the PV loop touches this curve at the end of the systole (the upper left-hand corner).

For both EDPVR and ESPVR, the curve intersects the volume axis at a slightly positive value (V_0), indicating that a finite amount of volume must fill the ventricle before it can generate any pressure, which is assumed to be the same for both.

Changes in preload, afterload and inotropy can be easily visualized by displaying the PV loop. These three effects are interdependent with the consequence that an increase or decrease in one of them in physiological conditions leads to change in the others. But for this explanation, it is assumed that they are independent, so while varying one of them, the others remain constants (Figure 1.4):

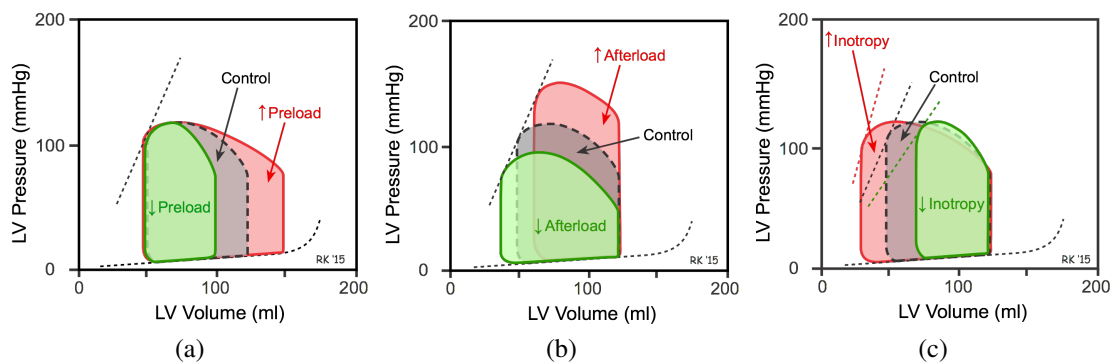


Figure 1.4: (a) effect of preload, (b) effect of afterload and (c) effect of inotropy [3].

- *Effect of preload:* Preload is defined as the stretch on the myocardial wall at the end of the diastole and on the PV loop can be well represented by the point with coordinates (EDP; EDV) which lay on the EDPVR. Moving this point on the EDPVR as shown by Figure 1.4 (a), the PV loop change accordingly. An increase in preload leads to an increased SV, vice versa, a decrease in preload leads to a decrease in SV.
- *Effect of afterload:* Afterload, in normal condition, is the load is imposed on the heart by the arterial system. This can be physiologically described by the aortic pressure (AoP) because ejection begins when the ventricular pressure slightly exceeds AoP. Thus, it is possible to consider P_{es} to be almost equal to AoP and be an indicator of afterload. In Figure 1.4 (b) is shown how SV decrease with increasing afterloads and increase for decreasing afterloads.

- *Effect of inotropy*: Inotropy, also defined contractility, indicate the intrinsic strength of the cardiac muscle. As an intrinsic property, it is independent of factors such as preload and afterload, and it typically refers to the velocity of muscle fibers shortening. The indicator of this effect is the slope of the ESPVR (also called *elastance*): a positive inotropic agent (which can be a pharmacological agent or an augmented sympathetic activity) increases the ventricle contractility and makes both the slope of the ESPVR and the SV increase (Figure 1.4 (c)); the opposite happens with a negative inotropic agent.

1.2 Electrophysiology of the heart

In contrast to skeletal muscle cells, cardiac cells are very different in their nature. There are different types, namely, *pacemaker, conducting and contractile cells*. In contrast with the skeletal muscles, the cardiac muscle does not receive contracting inputs from the central nervous system, but its contractions are generated from signals that originate inside the muscle itself. This is because a small number of cells that are embedded in the cardiac muscle can generate *action potentials* (APs) setting the cardiac rhythm; they are called *pacemaker cells*. Other few cells are *conductive fibers*, which allow the propagation of action potential in the heart in a very coordinated manner. The remaining cells of the cardiac muscle generate contractile force. This system allows to provide an adequate pumping function making the cardiac muscle to contract in a synchronized manner.

Pacemaker cells are mainly concentrated in the sinoatrial (SA) node and in the atrioventricular (AV) node, which are connected by conductive fibers. Although both are capable of generating APs, almost always, the heartbeat is controlled by the SA node. This is due to multiple reasons: first, the AP originated in the SA node travels to the AV node and all its pacemaker cells enter in the refractory period preventing the generation of a new AP; secondly, the rate of discharge of APs of the SA node is bigger than the one of the AV node. In fact, the AV node's intrinsic rate of isolated pacemaker cells is 40-60 impulses/minute and the one of the SA node is 90-100 impulses/minute. This implies that the AV node works as a kind of emergency system that permits ventricles contracting even if the SA node, for some reason, stops or decreases its function. If also the AV node is impaired, the heart has the last resource: Purkinje fibers can take control of ventricles, but the rate of discharge of APs is very low (30-40 impulses/minutes). The aforementioned rate values are intrinsic rates, but they are majorly influenced through the autonomic nervous system (sympathetic and parasympathetic) by segregation of neurotransmitters[1].

Origin and conduction of the impulse during a cardiac cycle

In Figure 1.5, the anatomical position and the sequence of electrical events that normally trigger the heartbeat is described. As the primary pacemaker, the SA node initiates APs, determining the cardiac rhythm. These action potentials travel to the AV node through the conduction fibers (internodal pathways). At the same time, it spreads through the bulk of

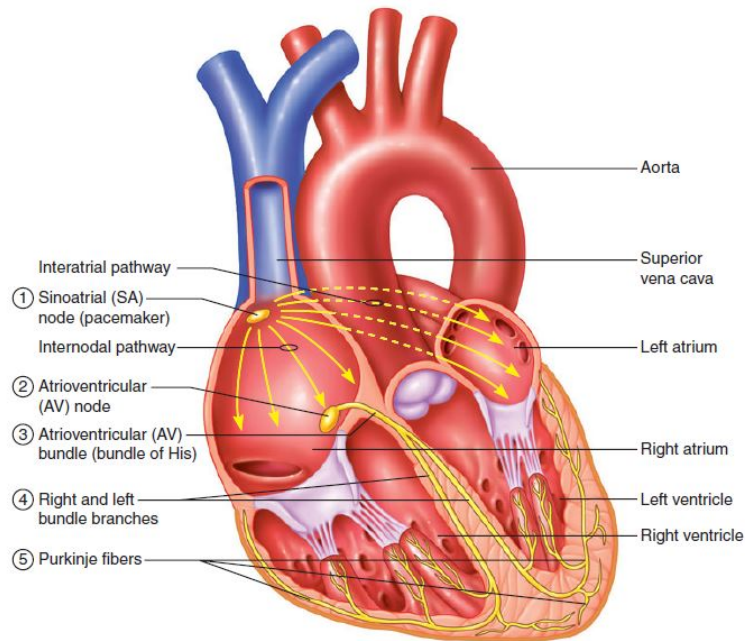


Figure 1.5: The conduction system of the heart [1].

the atrial muscle by way of interatrial pathways. Since the AV node cells conduct APs less rapidly, the impulse is delayed by about 0.1 seconds (called the AV nodal delay) before moving onward. From the AV node, the impulse travels through the bundle of His located in the interventricular septum. The signal travels only a short distance through it before splitting into left and right bundle branches, which conduct impulses to the left and right ventricles. From the bundle branches, impulses travel through an extensive network of branches referred to as Purkinje fibers, which spread through the ventricular myocardium from the apex upward toward the valves. From these fibers, impulses travel through the rest of the myocardial cells [1].

Ionic bases of the electrical activity of the heart

A pacemaker cell is capable of generating APs spontaneously because its resting membrane potential is unstable. Right after an AP, the pacemaker cell starts immediately to slowly depolarize until reaching the threshold potential that gives rise to a new AP. Those slow depolarizations are called *pacemaker potentials* [1]. The changes in membrane potentials are all provoked by modification in the permeability of the membrane to ions due to the timing of opening and closing of specific ion channels (principally Ca^{2+} and K^+ , and to a lesser extent Na^+). When a channel opens, a current that crosses the membrane is generated by an increased electrical conductance for that specific ion causing a change in the membrane potential [3].

The SA node cell AP can be divided into three major phases (Figure 1.6). Phase 4 is pacemaker potential, spontaneous depolarization due to the unstable resting potential. Once

that the potential threshold (between -50 and -40 mV) is reached, the AP starts. Then, phase 0 is the depolarization phase and phase 3 is the repolarization. Once the cell is completely repolarized at about -60 mV, the SA node cell spontaneously re-enters in phase 4.

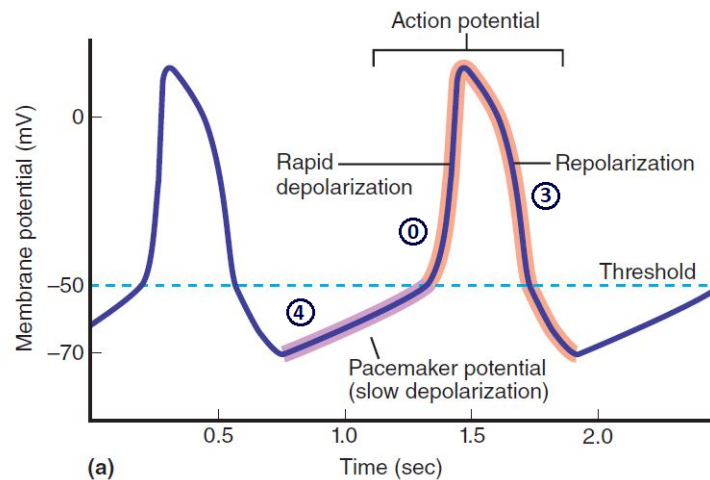


Figure 1.6: Electrical activity in a SA node cell: a recording of the membrane potential showing pacemaker potentials (phase 4, slow depolarization) and action potentials (phase 0, depolarization; phase 3, repolarization). Modified from [1]

- *Phase 4*: Right after the repolarization, the membrane potential is around -60 mV and the initial spontaneous slow depolarization is caused by the opening of the so-called *funny channels* that produces an inward (depolarizing) Na^+ current (I_f) [3]. The name 'funny' is given by their strange and not totally understood behavior: they allow the moving of both Na^+ and K^+ through the membrane. However, in this early stage of the pacemaker potential, the diffusion of K^+ to the outside of the cell decreases and the diffusion of Na^+ to inside the cell increases, becoming prominent. Funny channels stay opened only for brief time because they close when the membrane potential reaches -50 mV [1]. This voltage produces the opening of the voltage-dependent calcium channels called *T-channels*, where T stays for transient that allows the passing of calcium ions giving rise to the inward-directed Ca^{2+} current that further depolarize the cell. When the membrane potential of -40 mV is reached, another type of voltage-dependent calcium channels, the *L-channels*, where L stays for long-lasting, open and remain in this state for a longer time before slowly close.
- *Phase 0*: the depolarization is primarily the L-type Ca^{2+} channels that had already been opened during phase 4. Since the movement of Ca^{2+} through these channels

into the cell is not rapid, the rate of depolarization (slope of Phase 0) is not so steep.

- *Phase 3:* Two main mechanisms prevents the membrane potential to increase more than 20 mV: the L-type Ca^{2+} channels become inactivated and close, stopping the inward depolarizing Ca^{2+} currents and, at the same time, K^+ channels open producing an increased outward directed K^+ currents that give repolarization.

It is important to note that APs described for SA nodal cells are very similar to those found in the AV node since both nodes can generate spontaneous depolarization [3]. Therefore, in both cases, APs are mainly determined by changes in slow Ca^{++} and K^+ currents and do not involve fast Na^+ currents, as happens in the conductive nerve fibers (described in Section 1.3.1).

1.3 The Neuron

The neuron is a specialized cell that constitutes the nervous system's basic working unit whose aim is to transmit information to other nerve cells, muscles, or gland cells. Neurons in the human body have different shapes that reflect the different functions that each of them has to fulfill. Despite this shape variability, the main components of a neuron are the same (Figure 1.7) [4]:

- *Soma* is the body cell in which the nucleus and most of the organelles reside
- *Axon* is the longest extension of the neuron which serves for the conduction of electric impulse, called an action potential, outward, away from the cell body toward the axon terminus. The axon can be:
 - *Myelinated:* the axon is wrapped by several myelin sheets formed by Schwann cells that provide electrical insulation. The myelin interrupts periodically, leaving some gaps of 1-2.5 μm called Nodes of Ranvier. In vertebrates, myelinated fibers are the bigger fibers (diameter $> 1\text{-}2 \mu\text{m}$), the number of overlapped myelin sheaths can vary, in general, the myelin increases the fiber diameter by 20-40%, and the internodal length is about 100 times the outer diameter of the fiber. These properties confer to the myelinated fiber an increased speed of action potential conduction, which is linearly dependent on the diameter. It can be approximately calculated by multiplying for 4.5 the fiber diameter.
 - *Unmyelinated:* the axon has not a myelin cover. This happens in most of the smallest vertebrate fibers (diameter $< 1 \mu\text{m}$), which have the slowest conduction velocity proportional to the fiber diameter's square root.
- *Dendrites* extend outward from the cell body and are specialized to receive chemical signals from the axon termini of other neurons. Dendrites convert these signals into small electric impulses and transmit them inward, in the direction of the cell body.

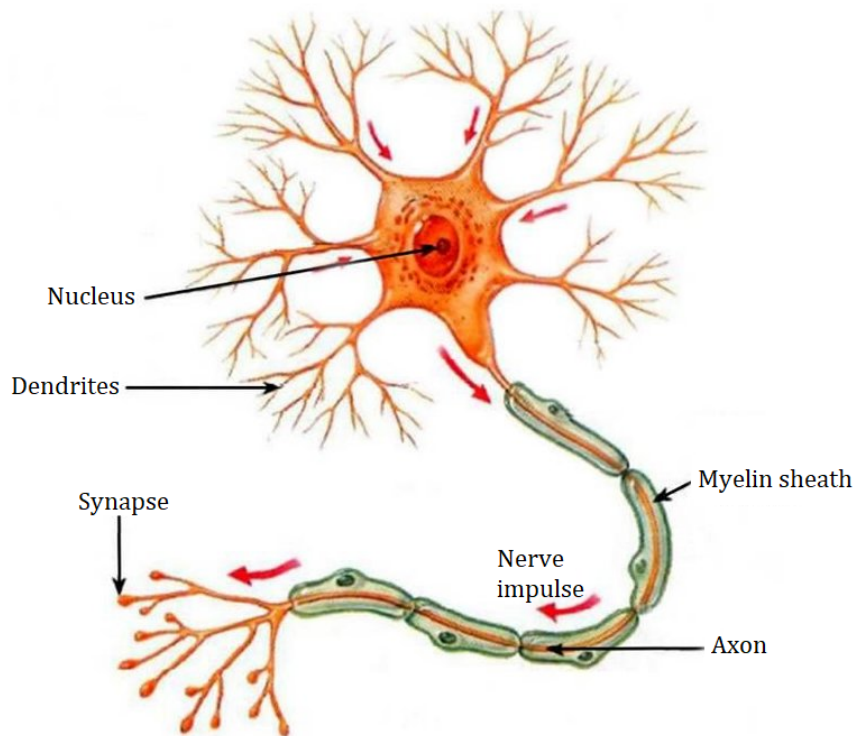


Figure 1.7: Representation of the neuron's main components: the nucleus, which resides in the soma, the axon in which the impulse travels, dendrites and synapses which connect the neuron with other cells. Modified from [5]

- *Synapse*: the axon ending normally branches in several fibers. The ending of those branches is called synapse, which is in close contact with other cells and allows the exchange of information from the pre-synaptic to the post-synaptic cell through the release of neurotransmitters (detailed explanation in Section 1.3.1). A single axon in the central nervous system can synapse with many neurons and induce responses in all of them simultaneously.

1.3.1 The Action Potential

The membrane of the neuron has a structure that prevents ions from passing through; however, a small conductivity is maintained even at rest. Different ion concentrations in the extracellular and intracellular space are maintained thanks to active ion pumps that move ions across the membrane in a very selective way. The potential between the inner and outer part of the membrane (*membrane potential*) is about -70 mV at rest. However, when a certain threshold is reached, an action potential (AP) occurs, provoking chain

reaction events responsible for generating the electric nerve impulse. As described in Figure 1.8, three main events are involved [6]:

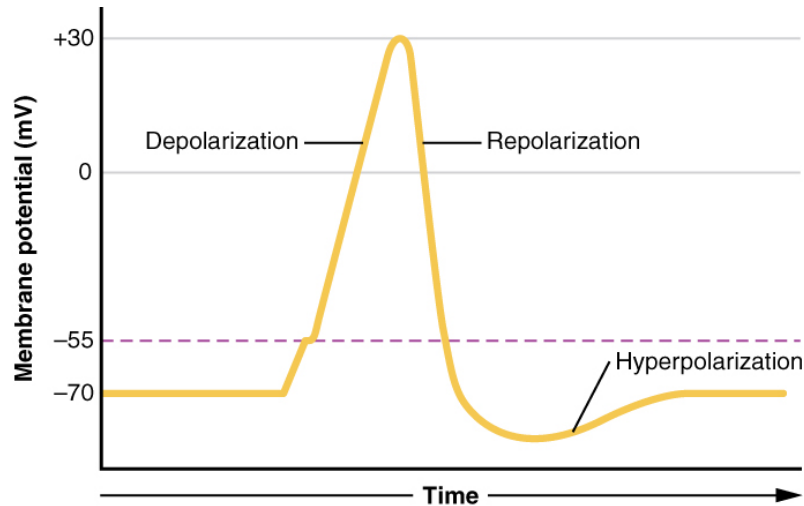


Figure 1.8: Action potential is presented as a graph of voltage over time. Three main phases are distinguished: depolarization, repolarization and hyperpolarization [6].

- *Depolarization*: sodium gates open and Na^+ ions flow into the cell because, in the resting state, the concentration of Na^+ is higher outside the cell than inside the cell and the concentration gradient drives those ions to enter the cell. Because of the sodium ion's positive charge, it makes the membrane potential increase up to 0 mV. The concentration gradient for Na^+ is so big that it will continue to enter the cell even after the membrane potential has become zero. This leads the voltage becomes positive (+30 mV).
- *Repolarization*: At 30 mV of membrane potential, potassium voltage-gated channels open and the concentration gradient makes K^+ leave the cell, making the membrane potential to move back toward its resting voltage of -70 mV.
- *Hyperpolarization*: Since K^+ ions reach equilibrium when the membrane voltage is below -70 mV, those channels are slightly delayed in closing, provoking a further decrease of the membrane potential for a brief period.

There are different kinds of Na^+ channels that, with their opening, provoke the initialization of the AP. Most of them are ligand-gated channels that open when the neurotransmitter binds to them; physical stimuli on a sensory receptor can also open other channels. Whatever Na^+ channel type it is, the AP starts when a certain *threshold* is reached, typically -55 mV. The AP cannot start below that threshold, but above that potential value, a large number of voltage-dependent channels spontaneously open and the AP proceed to complete its three phases. It is a '*all-or-nothing*' mechanism that makes the AP proceed

in the same deterministic way once the threshold is reached. Trains of APs act as digital signals: the timing of arrival of the APs codes the information delivered since there is no amplitude modulation.

As previously seen, the AP development is controlled by two voltage-gated channels, one for the sodium and the other for the potassium. The sodium one has an activation and an inactivation gate: when the threshold is reached, the activation gate opens, allowing Na⁺ to flow rapidly into the cell. When the depolarization peak is reached, the inactivation gate closes so that immediately no more sodium can enter the cell. Instead, the potassium channel only has one gate sensitive to a membrane voltage of -50 mV. However, it has some delay in opening and this time coincides with the peak of the AP, so voltage-gated K⁺ channels open just as the voltage-gated Na⁺ channels are being inactivated. At this point, the membrane potential repolarizes and the voltage passes -50 mV again. The channel closes, with a little delay leading to the hyperpolarization. The membrane can return to the resting potential because of the ongoing activity of the non-gated channels and the Na⁺/K⁺ pump.

While an AP is in progress, another one cannot be initiated because of the *refractory period*. This is divided into two phases: the *absolute refractory period* in which it is impossible to start a new AP because of the closing of the inactivation gate of the voltage-gated Na⁺ channel, and the *relative refractory period* which starts when the voltage becomes smaller than -55 mV, a new action potential could be started, but only by a stronger. This is because, in this situation, potassium ions still are flowing out of the cell, so more sodium ions are needed to depolarize the cell [6].

Action Potential Propagation

The AP travels through the axon membrane to carry the information to the next, post-synaptic cell. The propagation mechanism has its basis in the aforementioned concepts of depolarization, refractory period, and voltage-gated channels. Basically, the depolarization spreads because Na⁺ enters through the channels and moves along the inside of the cell membrane. As the Na⁺ flows, it depolarizes the axon's close proximity making that next segment reach the threshold and elicit a new AP. This happens segment by segment until the end of the axon. Moreover, this type of propagation ensures the AP's forward movement thanks to the absolute refractory period of the Na⁺ channels. Because of this, depolarization spreading back toward previously opened channels has no effect [6].

Neurotransmitter Release

The AP travels along the axonal membrane and when it reaches the axon terminal, it induces the release of neurotransmitters.

As already mentioned, the terminal ending is the synapse and the arrival of the AP triggers a localized rise in the level of Ca²⁺ in the cytosol. As shown in Figure 1.9, this causes some of the vesicles to merge with the plasma membrane of the pre-synaptic neuron releasing through exocytosis neurotransmitters into the small gap between the two cell membranes, the *synaptic cleft* [7]. The post-synaptic cell can be a dendrite or cell

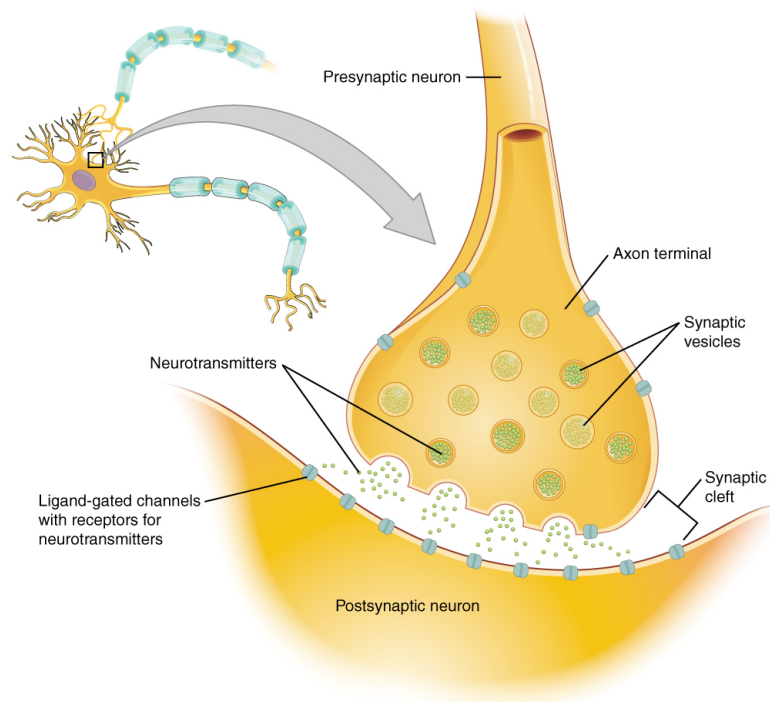


Figure 1.9: Representation of a chemical synapse: the arrival of an AP triggers the fusion of some vesicles with the nerve membrane to locally release neurotransmitters. Neurotransmitters diffuse in the synaptic cleft and bind of the post-synaptic cell membrane receptors. Neurotransmitters are cleared from the synapse either by enzymatic degradation, neuronal re-uptake, or glial re-uptake. ([7] p.570)

body of another neuron, a muscle or gland cell, or, rarely, even another axon. Neurotransmitters take about 0.5 ms to reach the post-synaptic cell membrane and bind its receptors, specific for only one type of neurotransmitter. The binding of the neurotransmitter triggers changes in the ion permeability of the post-synaptic plasma membrane, which, in turn, changes the membrane's electric potential at this point. If the post-synaptic cell is a neuron, this electric disturbance may be sufficient to induce an action potential. If the post-synaptic cell is a muscle, the change in membrane potential following binding of the neurotransmitter may induce contraction; if a gland cell, the neurotransmitter may induce hormone secretion. After some time, dependent on the type of cell, neurotransmitters are removed for the binding site by enzymatic degradation or re-uptake to the nerve terminal of the pre-synaptic cell [4].

1.4 Autonomic Nervous System

The autonomic nervous system (ANS) is the part of the nervous system, which controls cardiac and smooth muscle, as well as glandular tissue with the primary goal of maintaining the homeostasis. This balance is achieved by the controlled and complementary action of its two divisions: the sympathetic nervous system and the parasympathetic nervous system. The first is associated with the 'fight-or-flight' response and the latter with the 'rest and digest' [7]. Each target effector is innervated by both branches of the ANS which are tonically active: they provide some degree of nervous input to a given tissue continuously [8]. Therefore, the frequency of discharge of neurons in both systems can either increase or decrease and, as a result, tissue activity may be either enhanced or inhibited.

The signal that is delivered by the ANS is the result of the integration of signals coming from different receptors. The neural pathway that permits the *cardiovascular control* is composed of five classes of neurons [9]:

- *Primary afferent neurons* bring sensory information to the brain.
- *Interneurons* forward sensory information and inputs from higher brain centers to the premotor neurons.
- *Autonomic premotor neurons* control the activities of preganglionic neurons.
- *Preganglionic autonomic motor neurons* originate in the CNS with its cell body in the lateral horn of the gray matter of the spinal cord or in the brainstem and they project to the autonomic ganglion located outside the CNS, where they synapse with the postganglionic neuron.
- *Postganglionic autonomic motor neurons* that innervate the effector organ and implement the response.

Synapses between the autonomic postganglionic neuron and effector tissue, the so-called *neuroeffector junction*, differ greatly from neuron-to-neuron synapses (Figure 1.10). The postganglionic fibers in the ANS do not terminate in a single swelling like the synaptic knob and also they do not synapse directly with the cells of a tissue. Instead, the nerve fiber, in the proximity of the target tissue, contains multiple swellings called *varicosities*. When the neuron is stimulated, these varicosities release neurotransmitters along a significant length of the axon. Therefore, they diffuse over a large surface area of the effector tissue through the interstitial fluid binding on receptors located on the cell membranes. This leads to a simultaneous effect on different parts of the organ or more than just one organ per stimulus. Furthermore, cardiac muscle and most smooth muscle have gap junctions and through these intercellular communications, the electrical activity can spread from one cell to the neighborhood. As a result, the discharge of a single autonomic nerve fiber to an effector tissue may alter the entire tissue's activity.

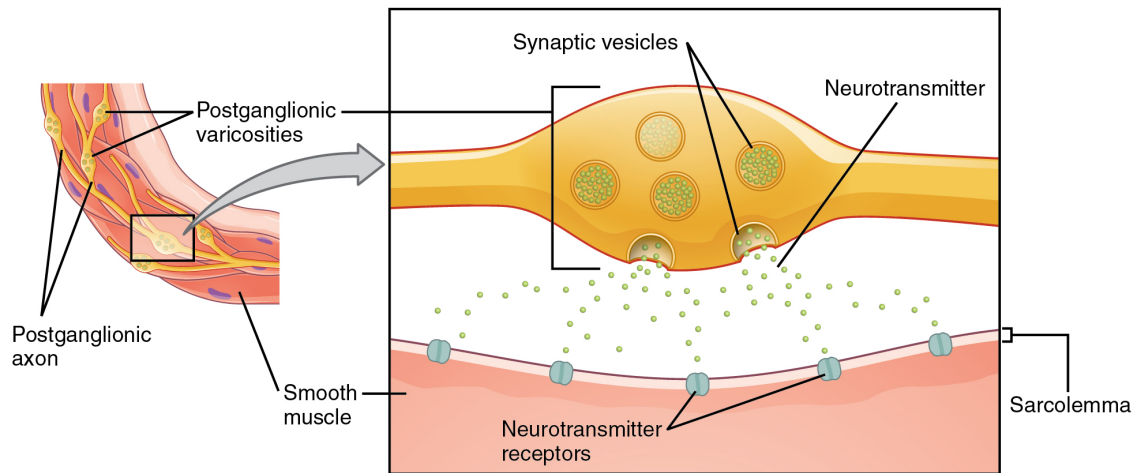


Figure 1.10: Neuro-effector junction: the connection between autonomic fibers and target effectors. The neurotransmitter is released from varicosities, which interface the effector organ in many points [6].

1.4.1 Primary afferent neurons

Afferent information arises from a network of afferent neurons distributed within key portions of the cardiovascular system. The peripheral endings of cardiovascular afferent neurons are unequally distributed. They are mainly concentrated in the central parts of the vascular tree (aorta, carotid artery, vena cava, and jugular vein) and within the heart.

Baroreceptors are stretch-sensitive mechanoreceptors located in the walls of the carotid arteries and aorta, where they monitor the pressure of blood flowing to the brain (carotid baroreceptors) and to the body (aortic baroreceptors). These receptors have their own baseline firing frequency, but when blood pressure increases in the arteries, the baroreceptor membrane becomes stretched and their firing rate increases. If the blood pressure falls, the firing rate decreases. They provide the afferent input to the *arterial baroreflex*, which is organized as a classic negative feedback system: an increase in arterial blood pressure activates mechanosensitive arterial baroreceptors that trigger reflex responses that ultimately reduce arterial blood pressure.

Pulmonary Stretch Receptors also belong to the family of mechanoreceptors. They are found in the bronchial smooth muscle, which senses and responds to airways' physical stretching. Stretch activates the pulmonary stretch receptors, which increase their afferent output. This behavior appears to decrease the respiratory rate largely by increasing the length of expiration [9].

1.4.2 Sympathetic Nervous System

To allow the fight-or-flight response, the sympathetic system causes divergent effects on many effectors that are activated together for a common purpose. More oxygen needs to be inhaled and delivered to skeletal muscle. To deliver more oxygen to the target organs, the respiratory, cardiovascular, and musculoskeletal systems are all activated together. In addition, sweating increases to maintain body temperature in the normal range because the increased muscle activity causes heating. On the contrary, the digestive system is shut down to focus on delivering enough oxygen to skeletal muscles. To fulfill those task in a coordinated way, the sympathetic innervation has a unique structure, represented in Figure 1.11, which allows the simultaneous effects on many organs [7].

The sympathetic system's preganglionic neurons arise from the thoracic and lumbar regions of the spinal cord (segments T1 through L2). Most of these preganglionic axons are short and synapse with postganglionic neurons within ganglia found in the sympathetic ganglion chains. Each of these ganglion chains, which run parallel immediately along either side of the spinal cord, consists of 22 ganglia. A single preganglionic neuron may synapse with several postganglionic neurons in many different ganglia. The long postganglionic neurons originating in the ganglion chain and then travel outward and terminate on the effector tissues. This divergence of the preganglionic neuron results in coordinated sympathetic stimulation to tissues throughout the body. An important feature of this system, which is quite distinct from the parasympathetic system, is that the sympathetic system's postganglionic neurons travel within each of the 31 pairs of spinal nerves. This allows for the distribution of sympathetic nerve fibers to the skin's effectors, including blood vessels and sweat glands. In fact, most innervated blood vessels in the entire body, primarily arterioles and veins, receive only sympathetic nerve fibers. Therefore, vascular smooth muscle tone and sweating are regulated by the sympathetic system only [8].

1.4.3 Parasympathetic Nervous System

The parasympathetic nervous system has a general structure similar to the sympathetic one, but few specific differences characterize it [7]. As illustrated in Figure 1.12, the preganglionic neurons of the parasympathetic system arise from several nuclei of the brainstem and from the sacral region of the spinal cord (segments S2-S4). The axons of the preganglionic neurons are quite long compared to those of the sympathetic system and synapse with very short postganglionic neurons within terminal ganglia, which are close to or embedded within the effector tissues. Because of this arrangement, there is typically little divergence in the parasympathetic system compared to the sympathetic one. In many organs, there is a 1:1 ratio of preganglionic fibers to postganglionic fibers. Therefore, the parasympathetic system's effects tend to be more discrete and localized, with only specific tissues being stimulated at any given moment, compared to the sympathetic system where a more diffuse discharge is possible [8].

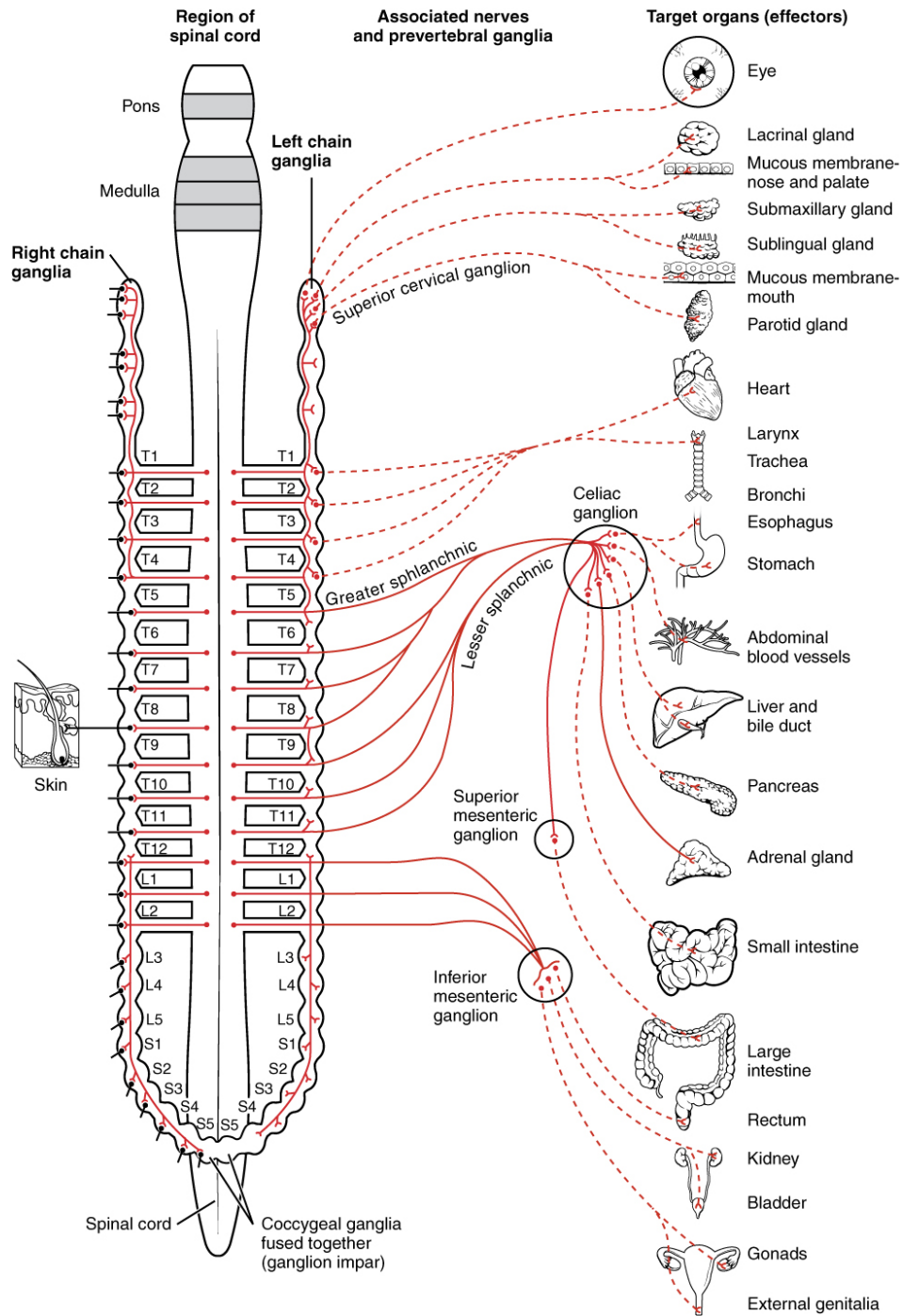


Figure 1.11: Illustration of the sympathetic nervous system: preganglionic nerve fibers (solid lines) project to the ganglia; postganglionic nerve fibers (dashed lines) project to the effector organs [7].

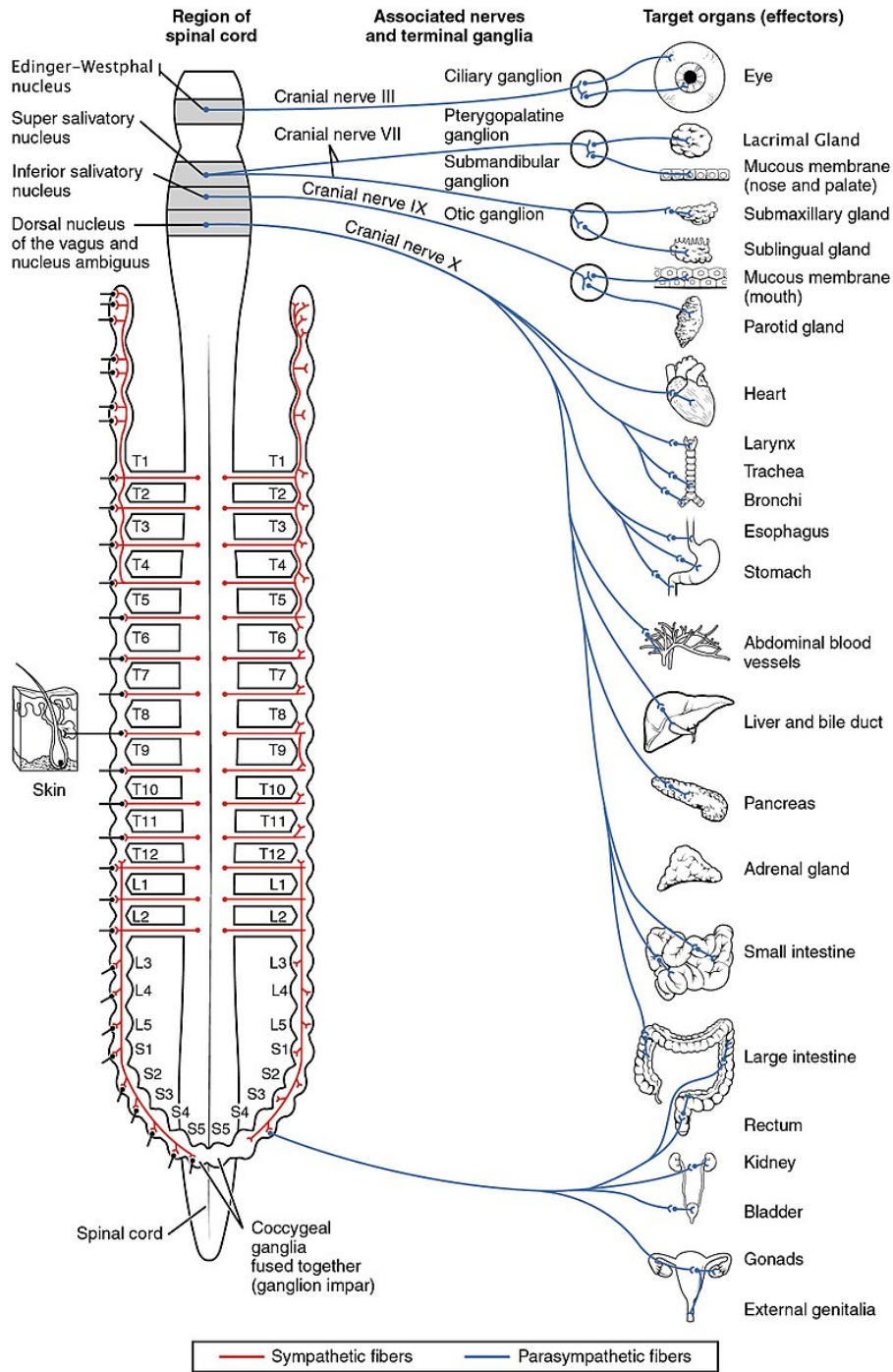


Figure 1.12: Illustration of the parasympathetic nervous system: preganglionic nerve fibers (solid lines) project to the ganglia; postganglionic nerve fibers (dashed lines) project to the effector organs [7].

1.4.4 Neurotransmitters of the Autonomic Nervous System

Neurotransmitters are synthesized in the axon varicosities and collected in vesicles for subsequent release. In Figure 1.13 a schematic representation of the efferent nerves of the ANS is given with their respective neurotransmitters. There are two main neurotransmitters released by neurons of the ANS:

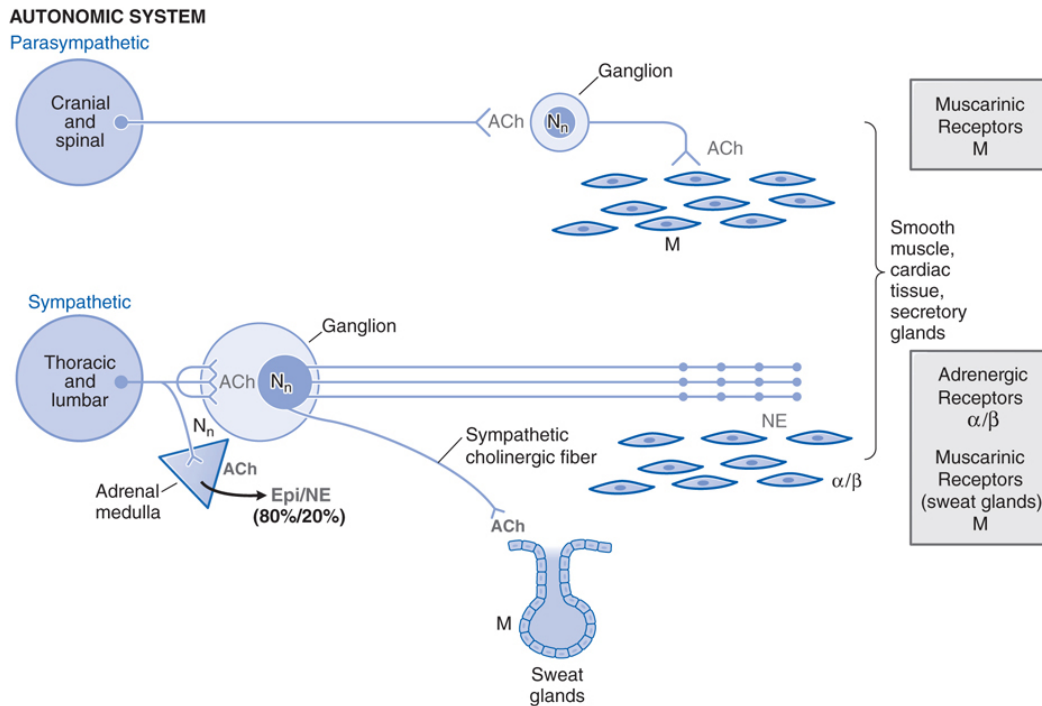


Figure 1.13: Schematic representation of the ANS's efferent nerves with their neurotransmitters: preganglionic fibers of both parasympathetic and sympathetic systems release ACh; ACh acts on nicotinic receptors (N_n) on the postganglionic nerves. ACh is also the neurotransmitter at cells of the adrenal medulla, releasing the CATs (Epi and NE) into the circulation. ACh is the predominant neurotransmitter of postganglionic parasympathetic nerves and acts on muscarinic (M) receptors. NE is the principal neurotransmitter of postganglionic sympathetic nerves, acting on adrenergic (α and β) receptors. [10]

- *Acetylcholine (ACh)* is released by all preganglionic neurons of the ANS, all postganglionic neurons of the parasympathetic nervous system, and some sympathetic postganglionic neurons to sweat glands. These types of fibers are called *cholinergic*. The receptor for ACh can be nicotinic, if it lays on the postganglionic neurons of both sympathetic and parasympathetic cell bodies or dendrites, or muscarinic if it is on the membrane of cells of the effector organ with parasympathetic innervation. The neurotransmitter terminates its function after enzymatic degradation by cholinesterase that hydrolyzes ACh forming choline and acetate.

- *Norepinephrine (NE)* is released by most sympathetic postganglionic. These types of fibers are called *adrenergic*. There are two types of receptors for NE: named the alpha (α)-adrenergic receptor and beta (β)-adrenergic receptor. NE is mostly removed from the neuroeffector junction by its reuptake into the adrenergic fiber that released it and it may then be metabolized intraneuronally by monoamine oxidase (MAO). The circulating CATs are inactivated by catechol-O-methyltransferase (COMT) in the liver.

For both ACh and NE, the inactivation or removal from the synapse must be rapid (in the order of few ms) to allow a new signal to get through and influence the effector tissue function [8].

Adrenal Medulla:

Cells of the adrenal medulla are considered modified sympathetic postganglionic neurons that release hormones into the blood. Approximately 20% of the hormonal output of the adrenal medulla is NE. The remaining 80% is *epinephrine (EPI)* due to the presence in the adrenal medulla of an enzyme that methylates NE to form EPI. These two hormones released by the adrenal medulla are indicated as *catecholamines (CAT)* and, since they travel in the blood, are able to reach many organs and tissues throughout the body. Therefore, they are capable of stimulating tissues that are not directly innervated by sympathetic nerve fibers. As a result, CATs have a much wider breadth of activity compared to NE released from sympathetic nerves. The duration of activity of the CATs is significantly longer than that of neuronally released NE due to the fact that the mechanism of inactivation of these substances takes place in the liver and the hepatic clearance of these hormones from the blood would require several passes through the circulation. Therefore, the effect of CATs is prolonged (up to 1-2 minutes) [8].

1.4.5 Autonomic control of the cardiovascular system

Although the contraction of the heart is not activated by stimuli from the central nervous system (CNS), the nervous system can regulate some aspects of the cardiac function such as heart rate (HR) control (*chronotropism*), myocardium contractility (*inotropism*), rate of myocardium relaxation (*lusotropism*) and velocity of the impulse in the conduction fibers (*dromotropism*). This function is mediated by the autonomic nervous system (ANS) whose fibers project to almost all the heart parts, including conduction fibers and myocardial tissue. The goal is to maintain and allocate blood flow that meets tissue demands over diverse circumstances such as exercise or postural changes. Thus, the ANS orchestrates optimal adjustments in the pump function of the heart by modulating the rate and the timing of events between atria and ventricles, altering the release of neurotransmitters and ensuring the maintenance of the homeostasis .

In Figure 1.14, the cardiac innervation is shown. The sympathetic innervation of the heart

is directed to the SA node, AV node and the myocardium. The innervation of the parasympathetic fibers is only directed to the SA node and the AV node because its innervation of the myocardium is relatively low so its influence on the cardiac muscle can be considered negligible.

Effects on the heart: The heart is innervated by vagal and sympathetic fibers eliciting opposite effects mediated by muscarinic and beta-adrenoceptors receptors, respectively. As shown in Table 1.1, activation of sympathetic efferent nerves to the heart increase heart rate (positive chronotropy) [11], contractility (positive inotropy), rate of relaxation (increased lusitropy), and conduction velocity (positive dromotropy) [12]. Parasympathetic effects are opposite. Parasympathetic effects on inotropy are weak in the ventricle, but relatively strong in the atria. When the body activates the sympathetic system, it generally down regulates parasympathetic activity, and visa versa, so that the activities of these two branches of the autonomic nervous system respond reciprocally. Sympathetic efferent nerves are present throughout the atria (especially in the SA node) and ventricles, including the conduction system of the heart.

	Sympathetic	Parasympathetic
Chronotropy	+++	---
Inotropy	+++	-
Lusitropy	+++	-
Dromotropy	++	---

Table 1.1: Relative magnitude of effect on the heart of sympathetic and parasympathetic activity indicated by a positive (+) or negative (-) correlation [3].

Effects on vessels: Sympathetic adrenergic nerves travel along arteries and their ending are found in the adventitia (outer wall of a blood vessel), while capillaries receive no innervation. Activation of sympathetic vascular nerves causes contraction of the vascular smooth muscle leading vasoconstriction of arteries and veins mediated by NE's binding on alpha-adrenoceptors. This leads to an increase of resistance given by vessels and a decrease in distal blood flow. When this occurs, the arterial pressure rises. Sympathetic-induced constriction of veins decreases venous compliance and blood volume and thereby increases venous pressure. Most blood vessels in the body do not have parasympathetic innervation; it is only present in salivary glands, gastrointestinal glands, and genital erectile tissue where it causes vasodilation. The overall effect of sympathetic activation is to increase cardiac output, systemic vascular resistance, and arterial blood pressure. Enhanced sympathetic activity is particularly important during exercise, emotional stress, and during hemorrhagic shock.

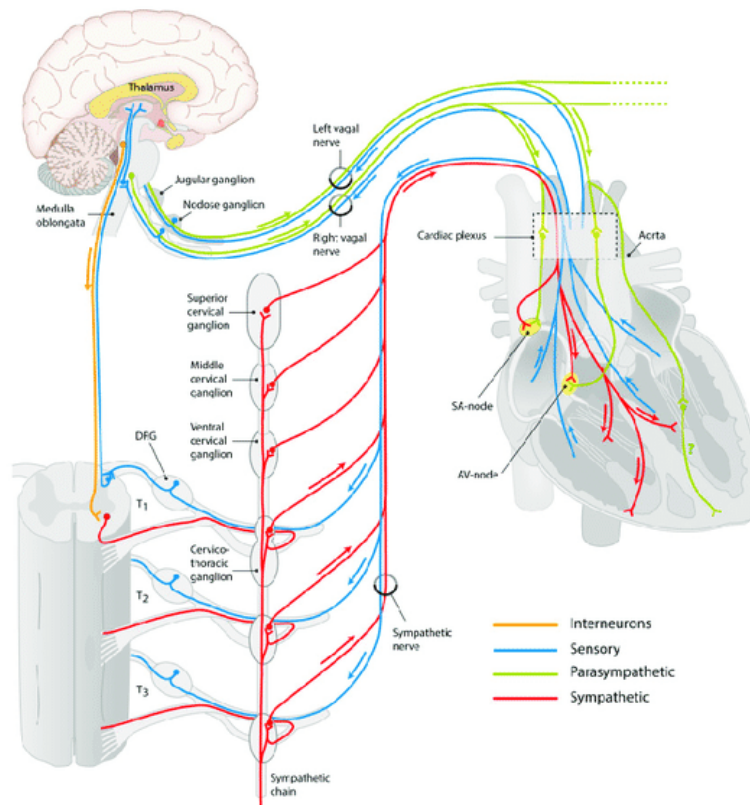


Figure 1.14: Overview of cardiac innervation: Sensory nerves (blue), give feedback to the CNS which modulates the activity of parasympathetic (green) or sympathetic (red) nerves to either relax or stimulate the heart. The vagus nerve innervates the SA node, AV node and ventricular myocytes. [13].

The Vagus Nerve:

The vagus nerve (VN) is the tenth cranial nerve, CN X, and the ANS's longest nerve in the human body. It has a mixed nerve composition made of 20% efferent fibers and 80% afferent (sensory) fibers. Only the efferent fibers are part of the ANS and in particular, they constitute the major component of the parasympathetic division. In contrast, all the remaining afferent fibers in the VN have the role of transmitting and/or mediating sensory information from throughout the body to the brain. The right and left VNs exit from the brainstem, and they course through the neck (in the carotid sheath between the carotid artery and jugular vein), upper chest (along the trachea), lower chest and diaphragm (along the esophagus), and into the abdominal cavity. During this course, branches enervate various structures such as the larynx, pharynx, heart, lungs, and gastrointestinal tract (Figure

1.12. In the brainstem, the sensory afferent fibers are directed in the nucleus tractus solitarius, sending fibers that connect to different brain regions directly or indirectly [14]. The right vagus nerve primarily innervates the SA node, whereas the left vagus innervates the AV node. The atrial muscle is also innervated by vagal efferents, whereas vagal efferents only sparsely innervate the ventricular myocardium. Parasympathetic innervation of the heart mediates the reduction of the heart rate. In a healthy subject, the parasympathetic tone from these sources is well-matched to sympathetic tone to provide an appropriate heart rate. Also, when hyperstimulated, the left vagal branch predisposes the heart to conduction block at the AV node.

Fibers in the Vagus Nerve

The VN is composed of hundreds of nerve fibers arranged in fascicles, each surrounded by the *perineurium*, which is a protective sheath. Moreover, many fascicles are arranged together in bundles enclosed by the *epineurium*, which is a layer of dense irregular connective tissue that provides blood supply: vessels branch from the epineurium and enter in the perineurium to reach the axons inside each fascicle (Figure 1.15) [15]. A histological study on 27 cadavers reports that the inner diameter of the VN at the cervical level is 4.1 ± 1.3 mm and the outer diameter is 5.1 ± 1.5 , meaning that the epineurium thickness is around 1 mm [16].

In the VN there are different types of fibers. A first classification can be done by divid-

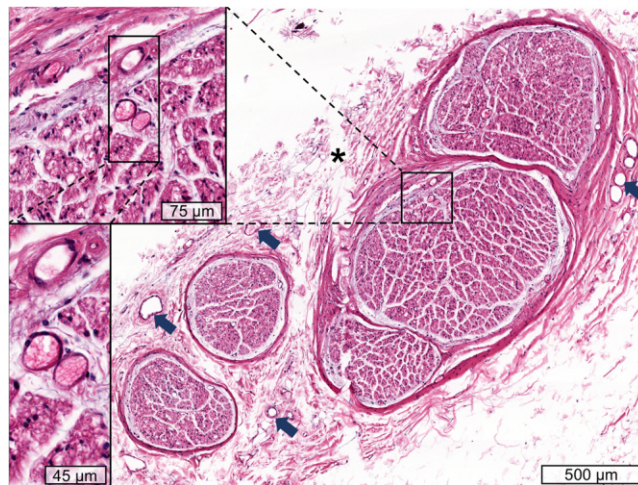


Figure 1.15: Histology sample of the cervical vagus nerve. Fascicles are separated by perineurium and the epineurium surrounds the entire nerve. Arrows indicate sub-perineural vascular supply and in the magnification on the left side, sub-perineural supply is visible [16].

ing them in afferent and efferent fibers. The first are responsible for carrying information from the periphery (receptors) to the CNS and they constitute the majority of the VN fibers (around 80%); the latter delivers information from the CNS to the target organ

(20% of the VN fibers).

A second classification divides fibers in *myelinated* and *un-myelinated*. Myelin is an insulator formed by Schwann cells wrapped around the fiber's axon with a diameter bigger than 1-2 μm . The degree of myelination indicates the number of overlapped concentric wrappings and its number can vary between 10 and 160. The myelin interrupts periodically, forming some gaps of 1-2.5 μm called *nodes of Ranvier*, which allow the saltatory conduction. The space between two consecutive nodes of Ranvier is called *internode* and have a length between 0.2 and 2 mm. The conduction velocity (CV) in the bigger fibers is higher than in the smaller ones, and this is determined by both the degree of myelination and the internode length, which are in value proportional to the fiber diameter. Generally, the myelin thickness is 20-40% of the fiber diameter and the internode length is 100 times the outer fiber diameter. This implies that the bigger the fiber, the higher is the degree of myelination and the internode length and the higher is the conduction velocity. For myelinated fiber, the CV is directly proportional to the fiber diameter; in particular, it can be calculated in *m/s* by multiplying the diameter in μm per 4.5. On the other hand, unmyelinated fibers do not have this property and their CV is only dependent on the axonal membrane and proportional to the square root of the diameter. Fibers below 1 μm in vertebrates are slow conducting unmyelinated fibers [17].

A third complementary classification is diameter based [18]:

- *A fibers* are myelinated with a diameter of 5–12 μm and the constitute around 8% of the total amount of fibers.
- *B fibers*: are myelinated with a diameter of 1-5 μm and the constitute around 12% of the total amount of fibers. They have more nodes of Ranvier per unit length than A fibers, so their CV is lower.
- *C fibers*: are the biggest amount of fibers in the VN (around 80%) and they are the only un-myelinated. The diameter is 0.5-2 μm and they are afferent fibers.

1.4.6 Heart Rate Variability

Oscillations on the HR in a healthy subject are physiological and in continuous changing and they reflect the complex response of the cardiovascular system to external stimuli to maintain the homeostasis. Heart rate variability (HRV) is defined as the beat-to-beat variation in HR and is used to measure the autonomic nervous system influence on the heart non-invasively.

As a result of certain diseases, the complexity of the interaction between different control systems, which operates at a different time and spatial scales, can change, resulting in a decrease or an increase of the HRV.

On the base of the length of the recording, a common classification divides the short-term HRV (5-10 minutes of ECG recording) and long-term HRV (24 hour Holter monitoring). They both have to be carried out under standardized conditions. For assessing autonomic

activity, the short-term analysis is usually preferred to the 24 hour Holter monitoring [19]. The analysis of the HRV can be performed either in the time domain and in the frequency domain [20]. In the first case, what is analyzed is the interbeat interval, which is the time interval between two consecutive heartbeats. A typical frequency-domain analysis is shown in Figure 1.16, it estimates the power distribution of into four frequency bands:

- Ultra-low-frequency (ULF), frequency ≤ 0.003 Hz: it can be analyzed by performing a long recording period (at least 24 hours). There is no evidence that is correlated with the autonomic function, so it is neglected in this discussion.
- Very-low-frequency (VLF), frequency between 0.0033 Hz and 0.04 Hz
- Low-frequency (LF), frequency between 0.04 Hz and 0.15 Hz: it is mainly attributed to the baroreceptors' activity. Moreover, in resting condition, a prevalent power is provided by the parasympathetic nervous system while the sympathetic nervous system only gives power to frequency components in the upper extremity (above 1 Hz) of the LF band.
- High-frequency (HF), frequency between 0.15 Hz and 0.40 Hz: it is also called the respiration band. It corresponds to the HR variations related to the respiratory cycle, which are mainly attributed to the vagal tone. Respiratory sinus arrhythmia (RSA) is a physiological phenomenon that is commonly associated with the cardiovascular and respiratory system coupling: the HR accelerates during inspiration and slows during expiration. This behavior is modulated by the vagal outflow, which is increased during expiration (augmented acetylcholine release) and inhibited during inhalation. As a consequence, the HF peak is placed at the breathing frequency. When the latter goes below 9 breaths/minute (0.15 Hz), the component of HRV relative to RSA is part of the LF spectrum, and the HF disappears. In this case, if any HF component is observed, it should be considered a different entity or an artifact.

Baroreceptors and chemoreceptors contribute to spectral components from the VLF to HF. The baroreflex links HR, BP, and vascular tone. Oscillation in one of them causes identical oscillations in the others since they are strictly correlated.

The power can be expressed as an absolute (ms^2/Hz) or relative values. This latter can be estimated as a percentage of total HRV power or in normal units [20] by dividing the absolute power for a specific frequency band by the summed absolute power of the LF and HF bands. This allows comparing frequency-domain measurements of different individuals even if they have differences in absolute values given by healthiness, age, etc.

The ratio of LF to HF power may estimate the ratio between sympathetic and parasympathetic activity under controlled conditions. Analyzing HRV over a short time period, the autonomic, cardiovascular, central nervous, endocrine, and respiratory systems influences' can be evaluated.

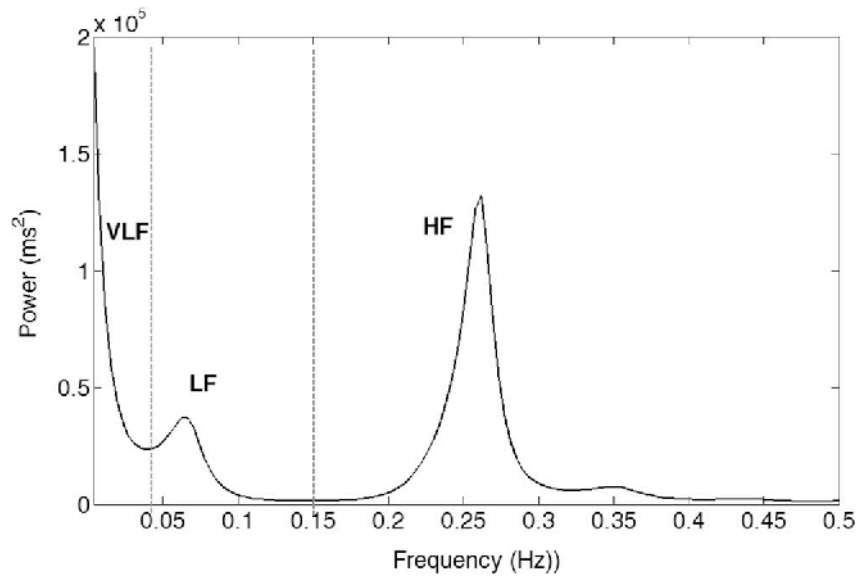


Figure 1.16: Power Spectral Density (PSD) of the interbeat interval showing the three main frequency bands: very low frequency (VLF), low frequency (LF) and high frequency (HF) [21].

1.5 Heart Failure

Heart failure (HF) is a cardiovascular disease and, according to the definition of the European Society of Cardiology [22], it is defined as:

”a clinical syndrome characterized by typical symptoms (e.g. breathlessness, ankle swelling and fatigue) that may be accompanied by signs (e.g. elevated jugular venous pressure, pulmonary crackles and peripheral edema) caused by a structural and/or functional cardiac abnormality, resulting in reduced cardiac output and/or elevated intracardiac pressures at rest or during stress.”

There are two main types of HF [23]:

- *Systolic HF*, which occurs when the heart is too weak to pump enough blood through the arteries. In this case, the ejection fraction (EF), defined as the percentage of blood ejected by the left ventricle at each beat, decreases.
- *Diastolic HF* in which the heart is lacking elasticity to be filled with enough blood. In this case, EF is maintained.

In both cases, the consequence is that vital organs such as the brain, kidneys and muscles, do not receive enough oxygen and nutrients to aim their functions. The main causes of HF are coronary heart disease, where the arteries that deliver blood to the heart reduce

in diameter, due to the build-up of plaque (atherosclerosis), and consequently make the blood supplied to the heart muscle small in volume, and high blood pressure (hypertension). Together, they account for around 70% of HF. Heart valve disease, abnormal heart rhythm, and heart defects at birth can also lead to HF and many other diseases can contribute to making HF more probable.

In most cases, chronic HF is treated via pharmacologic and devices, but despite the continuous improvement, long-term morbidity and mortality remain high, and many patients progress to end-stage heart failure. In this case, a heart pump can be implanted but usually it is only a target to delay the last resort that is heart transplantation.

1.6 Transplanted pathophysiology

A heart transplant (HTx) is a surgical operation in which a diseased, failing heart is replaced with a healthier donor heart. HTx is usually reserved to people as the last resort when the heart condition has not improved enough with medications, the implant of a device, or surgeries. Unfortunately, due to the lack of donors, only a few of those on the waiting list for the new heart can have one.

The International Society for Heart and Lung transplantation reports that every year between 4000 and 5000 heart transplantation surgeries are performed and that the majority is carried in North America and Europe (Figure 1.17) [24]. In 2018 in Italy, 233 heart transplant were performed: data reports that one year after transplant the 80,9% of the patients are survived and the 90,1% of them work or is able to work [25].

The surgery procedure leads to cardiac denervation which results is an elevated resting heart rate (around 90 bmp) and subnormal exercise response, which negatively affects patients' quality life and clinical outcomes. This happens because the donor heart's intrinsic heart rate control allows the heart to continue its main function of pump, but what is lacking is the fine autonomic control. Because of the surgical operation required for

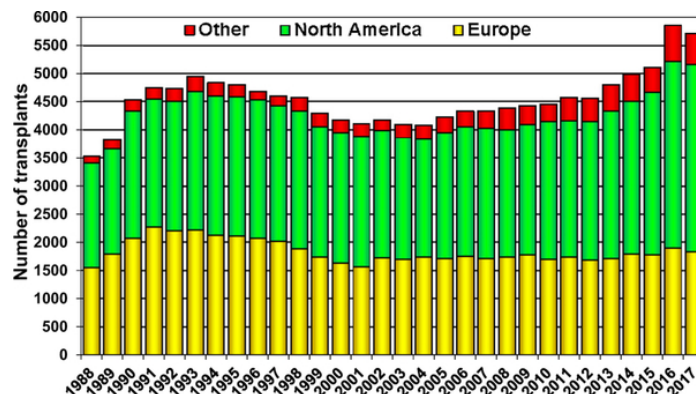


Figure 1.17: Number of heart transplants per year and geographic region [24].

the HTx, the parasympathetic vagal neurons are interrupted, which also implies the loss of the SA node innervation, and the efferent postganglionic sympathetic nerve fibers and afferent nerve fibers directed from the myocardium to the CNS are interrupted as well. A comprehensive overview of evidences of early and long-term HTx is given by Awad M. et al. [26].

In early HTx recipients, cardiac denervation alters cardiovascular control in HTx recipients whose effects are:

- *Increased HR* due to the lack of parasympathetic vagal efferent nerve connections than normal HR at rest. A resting HR ≥ 90 or 100 bpm in recipients at 1-year post-HTx was found to be an independent predictor of lower survival rates at 3, 5, and 10 years post-HTx when compared with recipients with HR < 90 bpm.
- *Diminished exercise capacity* because denervated hearts must rely on circulating, rather than cardiac, CAT release to adapt to the increased needs of exercise and this adaptation is insufficient to reach normal HR and contractility. Furthermore, the lack of sympathetic direct input to the heart causes a lower increase in HR in response to exercise and the maximum HR reached is lower than the normal. Also, the decrease in HR during recovery from exercise is slower than the normal rate. In addition, cardiac denervation causes an abnormal cardiac output (CO) response to exercise.
- *Lower HRV* because the denervation leaves the heart under hormonal and internal control loops only.
- *Higher sensitivity to circulating CAT* due to the lack of presynaptic neuronal inputs, which may affect inotropic responses and increase the frequency of arrhythmias, and altered response to adrenergic drugs, which requires adjustments to pharmacotherapy in HTx recipients.

Cardiac reinnervation has been shown to occur in 40% to 70% of recipients late after HTx and sensory reinnervation may occur as well. Sympathetic reinnervation occurs at least 5 to 6 months after HTx. It requires the presence of functional nerve terminals occurring outside the heart that are connected to nerve terminals in the transplanted heart. In contrast, parasympathetic reinnervation seems to occur more than 1 to 3 years following HTx. It has to be noted that ventricular reinnervation seems to be time-dependent, whereas SA node reinnervation does not and the latter may be present in some but not all patients. Awad M. et al. [26] reports that some improvements in autonomic cardiac control can be observed as a consequence of cardiac reinnervation:

- In response to exercise, late HTx recipients reach the peak HR with a higher rate in respect to early HTx recipients suggesting cardiac reinnervation late after HTx.

- HRV is shown to increase after 3 years post-HTx, but this increase seemed to differ among HTx recipients confirming cardiac reinnervation's heterogeneity. Moreover, the increase in LF - and HF - power of the HRV spectrum differ:
 - The LF power component of HRV was directly associated with sympathetic reinnervation in the sinus node post-HTx and it was observed to be higher in the reinnervated and late HTx recipients than in the early ones. Additionally, the LF spectrum was similar between late HTx recipients and control subjects, suggesting potential good reinnervation.
 - Even 3 years post-HTx, none of the recipients showed any increase in HF-power, confirming the absence of parasympathetic reinnervation.

1.7 Vagus Nerve Stimulation

Nowadays, *functional electrical nerve stimulation* has a wide field of applications such as cardiac pacemakers, phrenic pacemakers to compensate respiratory insufficiency, motor nerve stimulation, electrical nerve stimulation for urinary or anal incontinence, etc. [17]. The term 'functional' underlines the aim of nerve stimulation: the restoring of a function. For an optimal nerve stimulation application, some basic knowledge about the mechanism of natural excitation is needed. In this field, Pioneers were Hodgkin and Huxley that in 1952 discovered the process of the excitability of nerve fibers by performing experiments on giant squid axons [27] that made them earn a Nobel prize.

The term *vagus nerve stimulation* (VNS) is generally used to indicate any technique that stimulates the VN. It is usually applied invasively: the implant procedure is performed under anesthesia. It requires surgical subcutaneous implantation of a commercially available programmable pulse generator and an electrode in contact with the VN through a second incision in the neck area. The pulse generator is usually placed in the upper chest area and attached to a lead wire which is passed through a subcutaneous tunnel. Parameters of stimulation are usually chosen individually to provide the expected response. They are set using an external device placed on the skin over the implanted device. The programmable parameters are:

- *Current intensity* which indicates the amplitude of the electrical stimulus measured in milliamperes (mA)
- *Pulse width* which is the duration of the pulse measured in microseconds (ms)
- *Interpulse period* or *frequency* measured in seconds (s) or Hertz (Hz) respectively
- *ON/OFF duty cycle* which describes the stimulus on-time and off-time measured in seconds (s); this is needed only when the stimulation is not applied continuously

In 1997, the US Food and Drug Administration (FDA) approved the implantation of a medical device for VNS as adjunctive therapy for reducing the frequency of seizures in patients >12 years of age with partial-onset seizures refractory to antiepileptic medications and in 1999, the FDA approved the use VNS for the long-term treatment of chronic treatment-resistant depression (chronic TRD) in patients >18 years. Small open-label studies and case series reports have described the use of VNS for rapid cycling bipolar disorder, treatment-resistant anxiety disorders, Alzheimer’s disease, chronic refractory headaches, and obesity, although none of these uses has been given FDA approval [28, 14].

The electrode can be applied either to the left or the right cervical vagus nerve. In *left VNS*, the electrode implanted is a lead wire. It is the standard procedure to treat refractory epilepsy [29] and depression and both field VNS has moved beyond the experimental phase and into the clinic; clinicians are faced with deciding who is an appropriate patient for this surgical implant and how to integrate VNS into existing treatment in order to optimize both efficacy and safety [30].

Instead, when *right VNS* is applied, the main target of this treatment is inducing a cardiac response. The heart’s vagal innervation is asymmetrical in nature, such that the right branch has a major effect on the heart the left. The type of electrode implanted is a cuff electrode that can be more selective in activating vagal efferent fibers. The deterioration of heart functions can be irreversible and difficult to control and, despite recent advances in therapy, mortality and morbidity remain high. In search of alternative treatments for managing HF, clinicians have been investigating the use of VNS. Preclinical studies [31] and one phase II human study [32] suggest that chronic right cervical VNS is safe and effective for treating HF.

The adverse effects of VNS are mostly stimulation-related. They can be due to the stimulation of any body structure enervated by the vagus nerve, but mainly, since 80% of the VN fibers are afferent, they are caused by the propagation of the electrical pulses from the point of attachment of the electrode toward the brain leading to an indirect response.

1.8 Numerical models of the cardiovascular system

Numerical models are a simplification of reality that can contribute to understanding complex systems, evaluate their perturbation and make predictions [33]. The research in this field is spreading in recent years due to the potential benefits they can carry in a wide range of applications. Their strength resides in the capability of representing complex environments in a simplified way helping in various stages a study to define the right operative choices. Even if the development of the model is often time-consuming, it can improve the accuracy of an experimental set-up, allowing, in many cases, to save money and time by preventing experimental failures and high-risk attempts on animals or humans and increasing productivity.

The process of modelling is usually divided into four stages, namely *building*, *studying*,

testing and *use* [33]. Unfortunately, it is hardly ever the case that stages proceed linearly from building to use. Most commonly, defects found at the studying and testing stages result in the necessity to return to the building stage to perform the corresponding corrections. Of course, any changes that are made to the model require the repetition of the studying and testing stages, leading to an elongation of the process. The testing stage can be divided in two sub-stages: in the first one, a cluster of experimental data is used (test set); once that the model can reproduce them, another cluster of data (validation set) is used for the *validation* of the model. The use of the model can be involved to show some important features difficult to be measured in experiments but also to predict the response of the modeled system to certain perturbations.

Diseases of the cardiovascular system are one of the main problems in contemporary health care, causing many deaths in mid-aged people [34]. Mathematical models of the human cardiovascular system can help to understand better hemodynamics and their changes induced by disease. Through a model, many aspects can be tested more than the mechanics itself, such as the effect of a therapy or of a medical device.

Models, as illustrated in Figure 1.18, are generally classified in two big families: *lumped parameter*, also called zero-dimensional (0D), and *distributed parameter* models that can be in one, two or three dimensions (1D, 2D, 3D) [35].

0D models simulate the hemodynamics of the circulatory system under the assump-

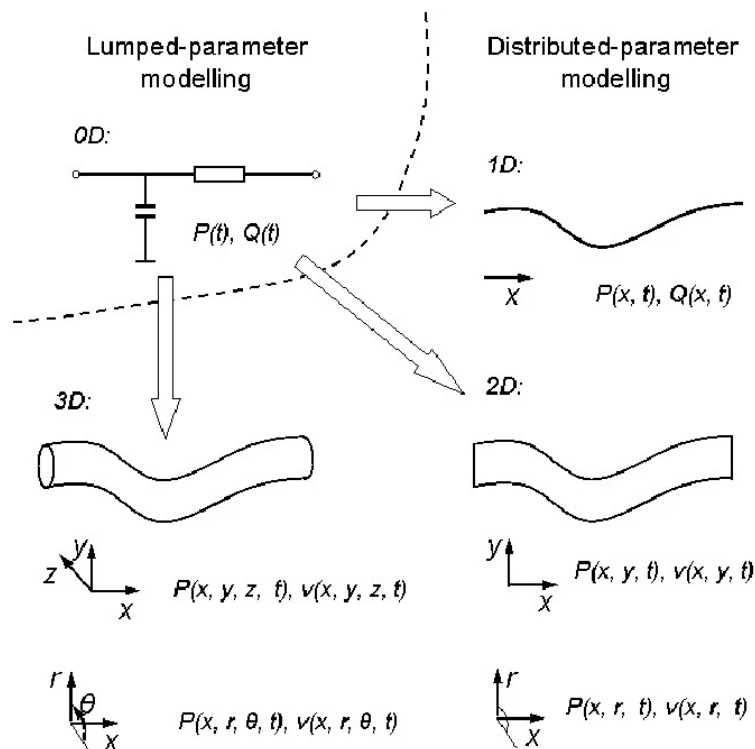


Figure 1.18: Models classification [35]

tion of a uniform distribution of the fundamental variables (pressure, flow and volume) within any compartment (organ, vessel or part of vessel) of the model at any instant in time, whilst the higher dimensional models recognize the variation of these parameters in space. The choice of the appropriate dimensionality, depends on the question that the model should help to answer and on the required accuracy.

The basic assumption of the lumped model is the *hydraulic-electrical analog* which reflects the similarity between the cardiovascular and the electric circuit:

- Blood flowing in the circulatory system corresponds to the current flowing in an electric circuit
- Blood pressure gradient corresponds to the voltage gradient
- Hydraulic impedance towards whom the blood is pushed corresponds to the electric impedance. In particular, the hydraulic impedance represents the combined effect of the frictional loss, vessel wall elasticity and blood inertia in the blood flow. Those features have their analog in the electric impedance in resistance (R), capacitance (C) and inductance (L).

Under this assumption, the investigation of cardiovascular dynamics can be described by using methods for the analysis of electric circuits such as the Kirchhoff's current law instead of the continuity equation for mass conservation and Ohm's law instead of the Poiseuille's Law to describe the flowing in a tubing. The electrical analog is unable to describe the non-linearities that sometimes feature in cardiovascular mechanics; in that case, integration with the governing equations of that phenomena can be added.

The Windkessel model [36] was the first lumped parameter model proposed to describe the arterial flow. This was subsequently expanded to cover the modeling of other organs such as the heart, heart valves, and veins. It is known that the pressure in the arterial

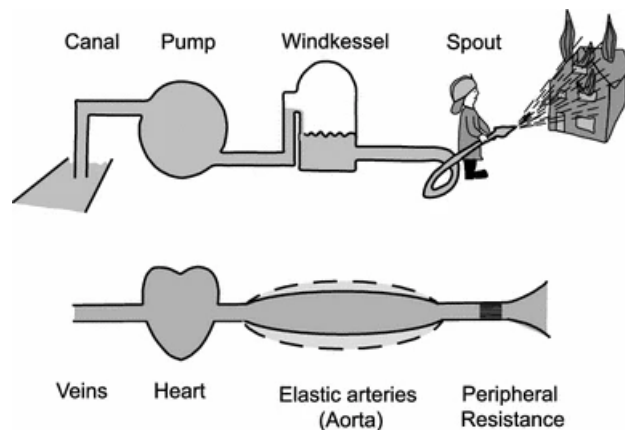


Figure 1.19: The Windkessel model proposed by Weber [36].

system is not constant but varies over the heartbeat and this is related to the elasticity of the large arteries. Weber was probably the first who proposed a comparison of the volume elasticity of the large arteries with the Windkessel present in fire engines (Figure 1.19). In 1899 Frank proposed the quantitative formulation of the so-called two-element Windkessel model. This latter is constituted by:

- A resistance element: the Poiseuille's law states that the drop in pressure ΔP (1.2) is proportional to the dynamic viscosity (μ), length of the tubing (L) and the volumetric flow rate (Q) and inverse proportional to the fourth power of the radius (R) as described by Equation (1.3):

$$\Delta P = \frac{8\mu L Q}{\pi R^4} \quad (1.2)$$

By applying the electric analog, the resistance of the vessel (R_v) is described by Equation (1.3):

$$R_v = \frac{8\mu L}{\pi R^4} \quad (1.3)$$

Considering the vascular system as a series of tubes of different diameters where the arteries have the biggest radius and capillaries and arterioles the smallest, these latter provide the highest resistance. When all individual resistances are added, the total peripheral resistance (R_{as}) is obtained, which can be approximated with capillaries' resistance. In the analog, the Q corresponds to the CO and the ΔP is the difference between the aortic pressure (P_{ao}) and the venous pressure (P_v) that can be assumed almost zero because of its order of magnitude, which is one or two times smaller than the P_{ao} . With these assumptions, the R_{as} can be simply calculated as described in Equation (1.4):

$$R_{as} = \frac{\Delta P}{Q} = \frac{P_{ao} - P_v}{CO} \simeq \frac{P_{ao}}{CO} \quad (1.4)$$

- A compliant element: compliance (C) is defined as the change in volume (ΔV) for a given change in pressure (ΔP) as in Equation (1.5).

$$C = \frac{\Delta V}{\Delta P} \quad (1.5)$$

In the vascular system, it is mainly determined by the elasticity of the large arteries. It can be obtained by the addition of the compliances of all vessels and is therefore called total arterial compliance (C_{as}). Its value is not easy to be directly measured in an experiment by injecting a volume in the arterial system avoiding losses at the periphery; Frank estimated its value from pulse wave velocity in the aorta.

In the 1930s and 1940s, numerous researchers tried to improve the two-element Windkessel by adding resistance and/or inertance terms and by adding effects of reflected waves developing the three/four elements Windkessel [36]. Since then, many models were developed to describe the cardiovascular system. In [34] a wide overview of those models is given; in 2006, Hassani et al. [37] has even proposed a 42-compartment model in which every compartment includes a resistor, a capacitor and an inductor.

1.9 Nerve Models

Modeling the axon membrane behavior can help to understand the mechanism of generation and propagation of the APs. In particular, precise models are currently studied and applied to acquire knowledge about the possible interactions with the nerve from the external. This is the case of the simulation of functional electrical nerve stimulation: it is possible to simulate both intra- and extracellular stimulation of the nerve membrane. This procedure accompanies research of more efficient functional electrical stimulation methods needed for the biomedical engineering and neuromodulation. [38]. Many models were developed through in the past years: the first was the Hodgkin-Huxley membrane model, which built the basis for all the following ones, the Frankenhaeuser-Huxley model, which was introduced for myelinated axons, the Fitzhugh model, the CRRSS model and many others [17].

1.9.1 Hodgkin-Huxley neuron membrane model

Hodgkin and Huxley were the first to provide a description of the behavior of the membrane potential of neurons, also simulating ion channels [27]. They based their work on the giant squid axon that, thanks to its big diameter, is easier to be investigated. With the patch-clamp technique, they measured the current flowing in an ion channel by applying a constant voltage and then developing equations for different types of channels. The equivalent circuit that models the membrane is constituted by (Figure 1.20) [17, 27, 38]: a channel for the potassium and another for the sodium, which allow the flowing of ion currents through the membrane; a leakage conductance current; and a capacitance in parallel which represents the dielectric properties of the phospholipid bilayer constituting the membrane. Referring to the equivalent circuit in Figure 1.20, by applying the basic laws of circuitry and the Kirchhoff's current law, it is possible to obtain:

$$I^{active} + g^{lk} \cdot (V^m - E^{lk}) + \frac{dV^m}{dt} \cdot c = 0 \quad (1.6)$$

where I^{active} includes of the current flowing in both the sodium and potassium (active) channels, g^{lk} is the conductance, V^m is the membrane potential, E^{lk} is the reversal or Nernst potential and c is the capacitance of the membrane.

Reordering the equation, the rate of change of the membrane voltage is:

$$\frac{dV^m}{dt} = -(I^{active} + g^{lk} \cdot (V^m - E^{lk}))/c \quad (1.7)$$

Active channels are voltage dependent and this behavior is modelled with the use of a time and voltage dependent conductance $g(t, V^m)$:

$$g(t, V^m) = \bar{g} \cdot \prod m_i(t, V^m)^{p_i} \quad (1.8)$$

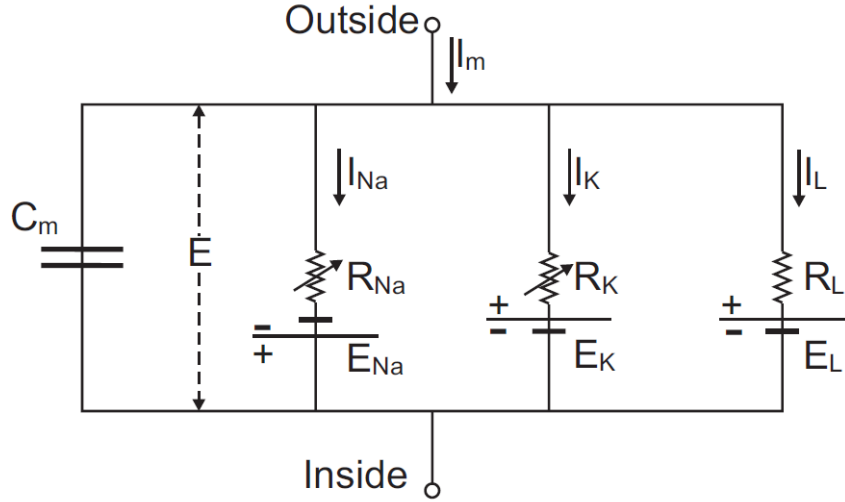


Figure 1.20: Hodgkin-Huxley neural membrane equivalent circuit [38]

where \bar{g} is the maximal conductivity of the sodium/potassium channels, p_i is an integer and m_i is the probability to have open gates which leads ions pass through [17]. It is defined as:

$$\frac{dm(t, V^m)}{t} = \alpha_m(V^m) \cdot (1 - m) - \beta_m(V^m) \cdot m \quad (1.9)$$

where α define the opening rate, β the closing rate, they are determined experimentally with patch and voltage clamp methods and differ between cell types and ion channels. Having $m = 1$ means that all gates are opened, $m = 0$ means that they are all closed. The Hodgkin-Huxley model is called *local* [17] because it describes the behavior of the membrane in a fixed point.

1.9.2 Propagation of Action Potentials

To describe the propagation of an action potential through the axon or dendrites, the cable theory can be applied to calculate the current flux. The neuron is divided in many parts called compartments and each of them have different geometric properties and assumed to be an isopotential element. Every compartment can be connected to n other compartments, this means that more than currents flowing in and out of the membrane described by equation (1.7), also currents coming from other compartments have to be taken into account. Under this assumption, the membrane potential can be described by [38]:

$$\frac{dV^m}{dt} = -(I^{active} + g^{lk} \cdot (V^m - E^{lk}) + \sum_n I_n^{int})/c \quad (1.10)$$

where I_n^{int} represent the current influx from the n -th compartment:

$$I_n^{int} = \frac{E_k^i - E_n^i}{(R_k + R_n)/2} \quad (1.11)$$

where k is the connected compartment and E^i is the intracellular voltage.

1.10 Sensitivity Analysis

Sensitivity Analysis (SA) is the study of the uncertainty of the model output attributed to different sources of uncertainty of the model input [39]. SA applied to mathematical models is an important tool to define between a high number of free parameters, which ones have a major influence on the output. There are different aim of the SA:

- *Ranking*: provides an ordering of the inputs based on their effect on the variability of the model output.
- *Screening*: defines which inputs are uninfluential on the variability of the model output. Typically, to those input a constant value is attributed.
- *Mapping*: observe the effect of the inputs on the output. This is useful to find a combination of parameters which makes the model stable or maximize the output.

There are different methods to conduct the SA, but none of them is suitable for all these three aims. To choose the appropriate SA method, other characteristic has to be taken into account.

A first distinguish is done between *local* and *global* methods. The first evaluates the model inputs at a specific point of the input space, while the second evaluates the sensitivity at a different point in the input space and then performs the mean of these sensitivities, which represents the influence that the input has of the output uncertainty. Moreover, most of the global methods also measure the interactions of the given input in combination with some other(s).

Another classification of the methods is based on the number of varied inputs for each successive model simulation. In the *one-at-a-time* (OAT) only one input can change whereas in the *many-at-a-time* (MAT) two or more inputs are changed per model evaluation. Local methods can only be OAT-based, while the global ones can be either OAT or MAT but are computationally more expensive.

The process that generates the input samples with which the model is iteratively evaluated is called *sampling* and different strategies are used:

- *Random sampling*: random values in the interval [0,1] are generated and associated with the input value. The previously assigned values do not influence the newly generated value with the risk that the parameter space is not uniformly covered.

- *Latin hypercube sampling*: near-random samples are generated from a multidimensional distribution, ensuring a more evenly distributed values.
- *Sobol sequence* generates quasi-random values ensuring that the input space is uniformly covered. Successive quasi-random points know about the position of previously sampled points and fill the gaps between them. Consequently, with this kind of sampling, the model needs a lower number of iterations to converge.

1.10.1 Sobol's method

Based on the classification above, Sobol's method is *global and MAT* and allows the evaluation of the inputs through *ranking and screening*. As global, it has a high computational cost and allows the evaluation of non-linearities and interactions.

The model output (Y) is considered a function of the n model inputs (X_i) as described in equation 1.12.

$$Y = f(X_1, X_2, \dots, X_i, \dots, X_n) \quad (1.12)$$

The Sobol's method is a variance-based technique which decomposes the model variance into contributions from each factor as well as interactions. The calculation of two indices can be performed by means of conditional variances:

- *First-order index or main effect* (S_i) measures the direct influence of each input to the output variance and it is calculated by equation 1.13.

$$S_i = \frac{V_{X_{\sim i}}(E_{X_{\sim i}}(Y | X_i))}{V(Y)} \quad (1.13)$$

where E is the expected value, V the variance, $X_{\sim i}$ denotes all models factor except the i th. This value can also be interpreted as the expected reduction in the output variance if X_i was to be fixed. Main indices are mainly used for ranking.

- *Total-order index or total effect* (S_{T_i}) measures the first and higher order effects (interactions) of factor X_i [40] and it is defined by equation 1.14.

$$S_{T_i} = \frac{E_{X_{\sim i}}(V_{X_{\sim i}}(Y | X_{\sim i}))}{V(Y)} \quad (1.14)$$

This value also represents the variance that would be left if all factors but X_i were to be fixed. Meaning that if the total index of X_i is zero, X_i is non-influential. Total indices are suitable for screening [39].

1.11 Purpose of the study

This study was carried out as part of the European project called *NeuHeart* [41] whose aim is to build a smart neuroprosthesis to restore the vagal-cardiac closed-loop connection after heart transplantation. The idea is to find a solution to the main clinical impairment given by the denervation of the heart due to the transplant: chronotropic incompetence. The neuroprosthesis shall restore the vagal-cardiac heart rate control by applying vagus nerve stimulation that is adjusted based on certain physiological parameters acquired by sensors, creating a closed-loop control of the heart.

The purpose of the study was to gain a better understanding of the acute cardiovascular effects of VNS. A pre-existing model, developed at the Medical University of Vienna, was extended, integrating a vagus nerve model and nerve stimulation. Finally, the influence of each parameter of stimulation on chronotropism, inotropism and dromotropism was studied performing an extensive sensitivity analysis to build the basis for implementing their automatic control in the future stages of the project.

Chapter 2

Methods

2.1 Overview of the Model

The model was implemented in Simulink and MATLAB®(The MathWorks®Inc, Natick, Mass), and it can be classified as a lumped, zero-dimensional model.

A schematic overview of the model is given in Figure 2.1 and it is described by diving it in three main compartments:

- **Hemodynamic model** which includes the entire cardiovascular system: left and right ventricles and atria, heart valves, systemic and pulmonary circulations.
- **Autonomic control model** which includes the sympathetic and the parasympathetic nervous system that, based on the signals from baroreceptors and lung stretch receptors, release neurotransmitters (norepinephrine, which is substituted in the model by the sympathomimetic drug isoprenaline (Iso), acetylcholine (ACh) and circulating catecholamines (CAT)) to the SA node determining its rate of depolarization and therefore the heart rate (HR). A detailed modeling of the parasympathetic nervous system is provided and includes pre-motor neurons and the vagus nerve, which consists of a multi-axon model whose nerve terminals innervating the SA node are represented with the ACh release model. The autonomic control provides a closed-loop feedback system that regulates peripheral resistance, venous unstressed volume, ventricular elastance and heart period.
- **Stimulator** which is a simple pulse generator that drives impulses to the vagus nerve. Vagus nerve stimulation (VNS) can be asynchronized (A-VNS) if it is provided continuously, or synchronized (S-VNS) if a burst of impulses is triggered when a certain heart-related event is detected (e.g. the P wave in the ECG).

The model can be operated in various conditions: healthy, heart transplant (HTx), healthy with VNS and HTx with VNS.

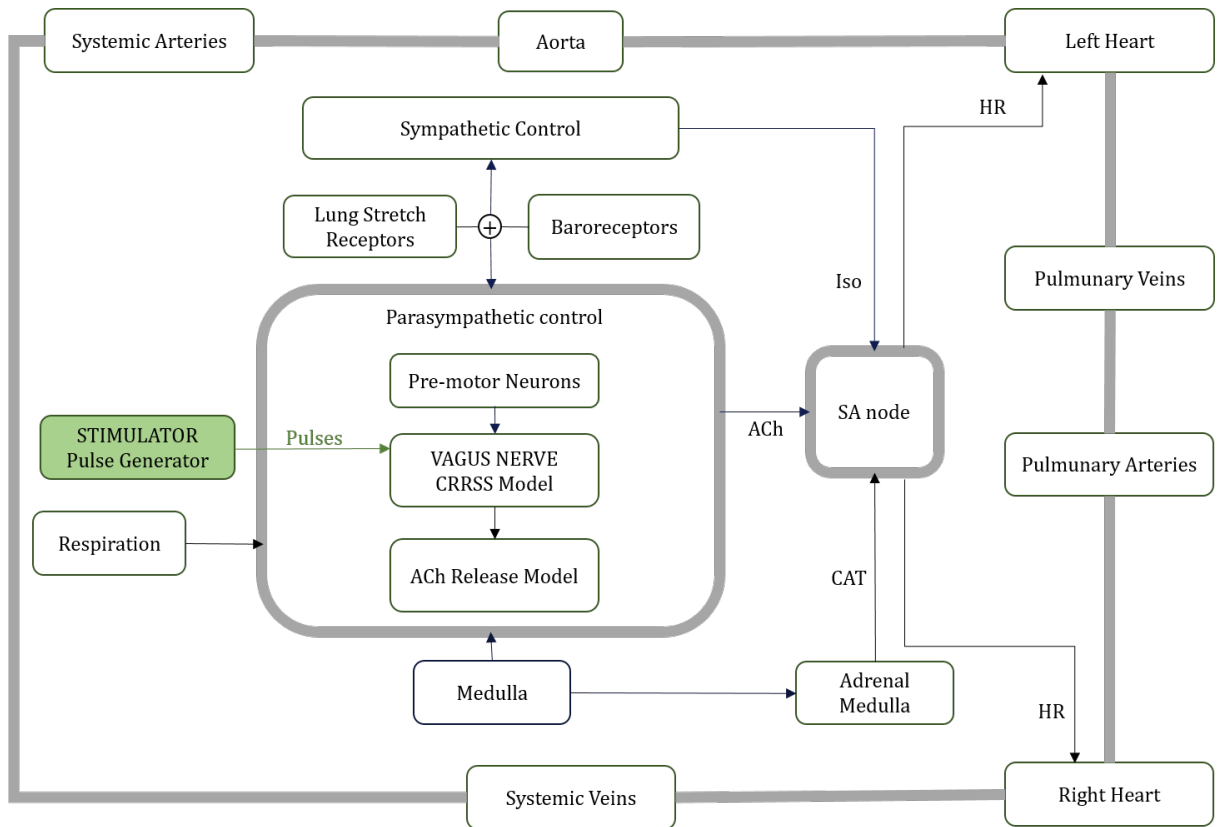


Figure 2.1: Overview of the model structure: the first compartment (outer part of the scheme) is composed of the components of the cardiovascular system such as left and right heart, pulmonary and systemic arteries and veins; the second compartment represents the autonomic control of the heart by means of the sympathetic and the parasympathetic divisions. The sympathetic control releases isoprenaline (Iso) to the sino-atrial (SA) node on the basis of the afferent receptor input. The parasympathetic control also includes a more detailed representation of the afferent pathway through the lungs stretch receptors and baroreceptors models that deliver signals to the CNS that implement the efferent response. Pre-motor neurons activity leads to a release of acetylcholine (ACh) from the vagal varicosities to the SA node. The adrenal medulla releases circulating catecholamines (CAT). The amount of neurotransmitters that binds on the membrane of the SA node cells play a major role in determining the heart rate (HR). To deliver VNS, a simple pulse generator (third compartment) applies impulses to the vagus nerve. Each block of the scheme represents a sub-model which interface with one another.

2.2 Hemodynamic Model structure

The hemodynamic model is based on the work of Moscato et al. [42] and it is structured in multiple compartments of the cardiovascular system. In Figure 2.2, the main compartments are illustrated and each of them is modeled through equations based on the hydraulic-electrical analog (described in Section 1.8). A summary of the analog is given in Table 2.1.

Hydraulic component	Electric component
Pressure [mmHg]	Voltage [V]
Fluid flow [l/s]	Current [A]
Resistance to flow [mmHg · s/m ³]	Resistance [Ω]
Compliance [l/mmHg]	Capacitance [F]
Inertia [kg · m ²]	Inductance [H]

Table 2.1: Hydraulic-Electrical analogue components and unit of measures.

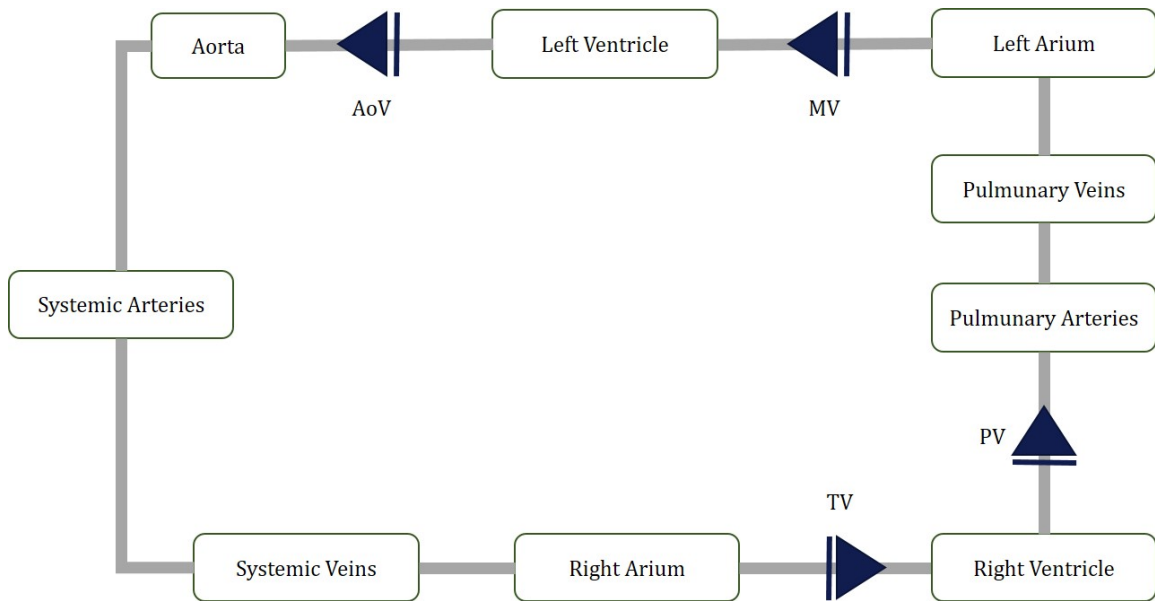


Figure 2.2: Schematic diagram of the hemodynamic model structure: MV, mitral valve; AoV, aortic valve; TV, tricuspid valve; PV, pulmonary valve. Adapted from [42]

Heart chambers

The heart is composed of 4 chambers (two atria and two ventricles) and four valves. The mathematical representation of the relation between blood pressure (P) and volume (V), described in equation 2.1, is valid for all the four chambers.

$$P(t) = \varphi[V(t), t] - R_i \cdot \frac{dV(t)}{dt} \quad (2.1)$$

where t is the time, $V(t)$ and $P(t)$ are the instantaneous blood volume and pressure inside the chamber and R_i is the internal resistance that takes into account the dissipation of energy due to ejection and therefore is negligible in the atria. The function $\varphi[V(t), t]$, formulate in equation 2.2, represents the non-linear time-varying elastance and its slope is the elastance ($E(t)$).

$$\varphi[V(t), t] = \varphi_p + \varphi_a[V(t)] \cdot F_{iso}(t) \quad (2.2)$$

where $F_{iso}(t)$ represents the ventricular contraction function normalized with respect to cardiac cycle duration (T) and peak amplitude (E_{max}). φ_p and φ_a are the active and passive pressure-volume pump relationships, respectively which are proper of each chamber. φ_p also represents the end-diastolic pressure-volume relation (EDPVR) and $\varphi_p + \varphi_a$ the end-systolic pressure-volume relation (ESPVR). The function φ_a is modeled for all chambers by using a parabolic relation described in equation 2.3.

$$\varphi_a[V(t)] = \left[1 - \left(\frac{V^* - V(t)}{V^* - V_d} \right) \right] \cdot P^* \quad (2.3)$$

V^* and P^* are the peak isovolumetric pressure and volume, respectively and their position is used to locate the ESPVR curve in the pressure-volume (PV). The point with coordinates (V^* , P^*) is also the vertex of the downward concavity of the parable passing from the point with coordinates ($V_d, 0$), where V_d is the ventricular dead volume, which is the volume of the chamber when the pressure is zero.

Since the relation between $F_{iso}(t)$ and $\varphi[V(t), t]$ is direct, $F_{iso}(t)$ is determinant in defining the level of contraction of the chamber at a given time instant. The easiest way to model it is to adopt as a function the positive half of a sin function, whose peak corresponds to the ventricular systole. However, according to experimental data, the more accurate model in this work set it as piecewise cubic functions.

Left Ventricle

As already mentioned, φ_p represents the passive characteristic of the ventricular muscle (the EDPVR), which defines the stiffness of the ventricle when it is in the relaxed state. Therefore, this characteristic is an index of the preload sensitivity, which describes how much blood the ventricle will deliver depending on its filling pressure (the atrial pressure or preload pressure). In equation 2.4, the formulation of φ_p for the left ventricle is given.

$$\varphi_p = \begin{cases} (c_3 \cdot V^3 + c_2 \cdot V^2 + c_1 \cdot V + c_0) + P_{offset} & \text{if } V_d < V < V_0 \\ \alpha \cdot V^\beta + P_{offset} & \text{if } V > V_0 \end{cases} \quad (2.4)$$

V_0 is the ventricular unstressed volume modeled as an exponential function for a volume greater than this value and as a cubic function for lower volumes. This because when the volume is lower than V_0 , the EDPVR has inflection and the pressure has a faster decrease.

Right Ventricle

The right ventricle differs from the left one only for the function that describes φ_p , but except for the parameters values, the others equation stays the same. In this case φ_p is modelled by means of a hyperbole reported in equation 2.5.

$$\varphi_p(V) = \frac{HR \cdot (Pec + b) \cdot V - [100 \cdot Kr \cdot (Pec - V) + 1000 \cdot a + V \cdot HR \cdot (Pec + b)]}{HR \cdot V - (1000 \cdot Kr + V \cdot HR)} \quad (2.5)$$

Right and Left Atria

Atria differ from ventricles mainly for the contraction strength, which is lower and for the timing of the beginning of the contraction. This latter is achieved by shifting the F_{iso} function by the 20% of the heart period before. Left and right atria are modeled in the same way and the function that describes the passive characteristic φ_p is linear, as shown in equation 2.6.

$$\varphi_p(V) = (V - V_0) \cdot E_{min} + P_0 \quad (2.6)$$

Heart Valves

The main aim of valves is to direct the flow in the forward direction. For this reason, valves are modeled as resistors and the value of the resistance in the forward direction (R_{dir}) is low, allowing the flow to follow the pressure gradient, while the value in the backward direction (R_{inv}) is very high, simulating the valve closure. Equation 2.7 describes the valve behavior in mathematical terms by means of the blood flowing through the valve (Q_{in}). Moreover, an inertance term was added (L_{li}) in series to the resistance to simulate filling and ejection dynamics. The resistance values attributed to each valve (mitral, aortic, tricuspid and pulmonary) are reported in Table A.4.

$$R_{valve} = \begin{cases} R_{dir} & \text{if } Q_{in} > 0 \\ R_{inv} & \text{if } Q_{in} \leq 0 \end{cases} \quad (2.7)$$

Arterial and Venous circulation

The systemic and pulmonary arterial systems are modelled by using an evolution to a five-compartment model of the Windkessel model developed by Otto Frank and described in Section 1.8 [36]. While the systemic and pulmonary venous system is modelled according to [43]. The electric analogue schemes are given in Figure 2.3 and the attributed values in Table A.5.

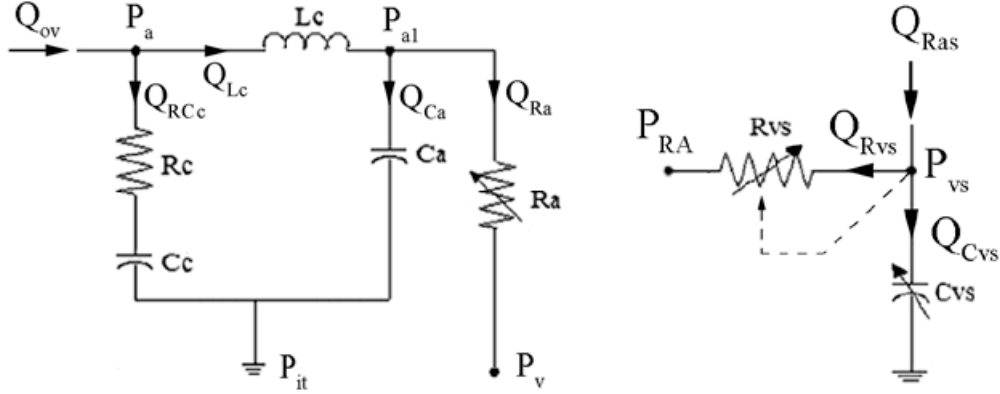


Figure 2.3: Electric analog of the arterial load model (left) and of the venous return (right) [44].

2.3 Respiration

The mechanical modelling of respiration was implemented according to the model proposed by Ursino et al. [45] to build the basis for the implementation of the effects of lung stretch receptors. In particular, the model provides a time-varying formulation for the intrathoracic pressure (P_{thor}) based on a given breathing frequency. It is described in the system of equation 2.8.

$$P_{thor} = \begin{cases} -5 \cdot \alpha \cdot \frac{T_{resp}}{T_i} - 4 & \text{if } 0 < \alpha < \frac{T_i}{T_{resp}} \\ -5 \cdot \frac{T_i + T_e - \alpha \cdot T_{resp}}{T_e} - 4 & \text{if } \frac{T_i}{T_{resp}} < \alpha < \frac{T_i + T_e}{T_{resp}} \\ -4 & \text{if } \frac{T_i + T_e}{T_{resp}} < \alpha < 1 \end{cases} \quad (2.8)$$

where T_{resp} is the respiratory period, and T_i and T_e denote the duration of inspiration and expiration, respectively; α is a normalized variable which represents the fraction of the respiratory cycle. Conventionally, $\alpha = 0$ corresponds to the beginning of inspiration.

$$\frac{d\epsilon}{dt} = \frac{1}{T_{resp}} \quad (2.9)$$

$$\alpha(t) = frac(\epsilon) \quad (2.10)$$

where the function “fractional part” $frac(\epsilon)$ resets $\alpha(t)$ to zero when it reaches the value 1.

The lung volume (V_L), determinant variable to assess the activity and influence of the

lung stretch receptors (see Sections 2.4 and 2.5.2), is linearly obtained from P_{thor} , as illustrated in equation 2.11.

$$V_L = 1.9 - 0.1 \cdot P_{thor} \quad (2.11)$$

2.4 Sympathetic Cardiac Control

The sympathetic regulation mechanisms use afferent information provided by arterial baroreceptors and lung stretch receptors. However, differently for what is performed to model the parasympathetic regulation in which a more physiological modeling approach is used by modeling all the neural pathways (afferent and efferent), more straightforward description of the sympathetic effect is performed according to the model proposed by Ursino and Magosso [45]. In their work was adapted by excluding the parasympathetic influence and creating proportional variables to gain an effect on the desired model output.

The information from receptors modulates various cardiovascular parameters such as systemic peripheral resistance, venous unstressed volume, heart contractility and heart period. The first three control actions are purely sympathetic in nature and, therefore, no adaptation on the model proposed in [45] was needed. As shown by the block diagram in Figure 2.4, the control mechanism of these quantities is described by a first order dynamic. Instantaneous mean aortic pressure P_{ao} and lung volume V_L are continuously compared to the respective set point value ($P_{ao,ref}$ and $V_{L,ref}$) calculating the differences which is considered an error. These values are then multiplied by a gain proper of each effector ($G_{a\theta}$ for the pressure and $G_{p\theta}$ for the lung volume). Subsequently, the weighted errors are summed together and passed to a sigmoidal static function that imposes upper and lower saturation limits for the response. A pure delay (D_θ) and a first-order low-pass dynamic with time constant $\tau_{\theta s}$ are then applied accounting to reproduce the timing of the response.

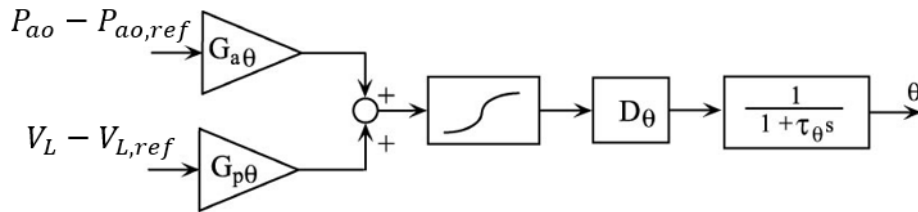


Figure 2.4: Sympathetic regulation mechanisms acting on the generic effector θ which can be systemic peripheral resistance, venous unstressed volume, end-systolic elastance of the right or left ventricle and changes in isoprenaline concentration. Modified from [45]

The block diagram described in Figure 2.4 is mathematically formulated as illustrated in equations 2.12-2.14.

$$x_\theta = G_{a\theta} \cdot (P_{ao} - P_{ao,ref}) + G_{p\theta} \cdot (V_L - V_{L,ref}) \quad (2.12)$$

$$\sigma_\theta = \frac{\theta_{min} + \theta_{max} \cdot e^{\pm x_\theta/k_\theta}}{1 + e^{\pm x_\theta/k_\theta}} \quad (2.13)$$

$$\frac{d\theta(t)}{dt} = \frac{1}{\tau_\theta} \cdot [\sigma_\theta(t - D_\theta) - \theta(t)] \quad (2.14)$$

where θ represents the generic effector for: the systemic peripheral resistance (R_{as}), unstressed systemic venous compliance volume (V_{usv}), end-systolic elastance (E_{max}) of the right or left ventricle. All the parameter values are presented in table A.6

For what concerns the heart rate, the model provided by Ursino and Magosso [45] was modified. In our model, the heart period is governed by the SA node model, whose depolarization rate depends on the concentration of neurotransmitters such as Iso and ACh. Since the concentration of ACh depends on the ACh release by the acetylcholine release model, which is part of the parasympathetic control (see Section 2.8), the only branch related to the sympathetic influence of the model in [45] was maintained leading to a model with the same block diagram presented in Figure 2.4 that describe the changes in the Iso concentration. Moreover, the adrenal medulla releases catecholamines directly into the circulation. Therefore a first-order dynamic system (equation 2.15 and 2.16) describes the release and spillover from vascular beds.

$$\frac{dk_{circ}}{dt} = \frac{nora - k_{circ}}{\tau_{k_{circ}}} \quad (2.15)$$

$$\frac{dnora}{dt} = c_{nora} \frac{(P_{ao} - P_{ao,ref}) \cdot G_{a,am} + (V_L - V_{L,ref}) \cdot G_{p,am}}{\tau_{k_{circ}}} \quad (2.16)$$

The total amount of Iso released by the sympathetic nervous system to the SA node cells is the sum of three components: the Iso released directly by the sympathetic fibers that project to the SA node, the Iso release indirectly through the circulation by the adrenal medulla $k_{circ,T}$ and a baseline Iso value Iso_{base} , as described in equation 2.17 and 2.18.

$$x_s(t) = (P_{ao} - P_{ao,ref}) \cdot G_{a,T_s} + (V_L - V_{L,ref}) \cdot G_{p,T_s} \quad (2.17)$$

$$Iso(t) = x_s(t - D_s) \cdot c_s + k_{circ} \cdot c_{circ,T} + Iso_{base} \quad (2.18)$$

To simulate changes in HTxR, selected parameters were modified in all the sympathetic regulation mechanism models to induce a change in hemodynamics due to altered sympathetic cardiac control. Parameter values used to simulate healthy individuals and HTxR are given in Table A.6 of the Appendix.

2.5 Physiological Model of Primary Afferent Neurons

A wide range of sensory neurons monitor the cardiovascular state and inform the CNS. The present model only accounts for the two most relevant receptor types: arterial baroreceptors and pulmonary stretch receptors.

2.5.1 Model of Baroreceptors

Baroreceptors belong to the class of mechanoreceptors and they are stretch-sensitive. They are located in the walls of the carotid arteries (carotid baroreceptors), to monitor the pressure of blood flowing to the brain, and in the aorta to control the pressure of blood flowing to the body (aortic baroreceptors).

When blood pressure increases, the arteries stretch the baroreceptor membrane and leading to an increase of firing rate. Otherwise, if the blood pressure falls, the firing rate decreases. Their mechanism provides the set of the normal mean arterial pressure (about 95 mmHg in adults) that is taken as a reference for a continuous comparison with the instantaneous pressure. Small deviations from the setpoint induce a large change in the firing rate of baroreceptors, as previously described. However, the setpoint and response shape is not fixed because it can adapt to prolonged deviations.

The afferent baroreflex was modelled by Ursino et al. in [46] on experimental data as a linear derivative first-order dynamic block (equation 2.19) and a sigmoidal static characteristic (equation 2.20).

$$\tau_p \cdot \frac{d\tilde{P}}{dt} = P_{ao} + \tau_z \cdot \frac{dP_{ao}}{dt} - \tilde{P} \quad (2.19)$$

$$f_{cs} = \frac{f_{min} + f_{max} \cdot \exp\left(\frac{\tilde{P} - P_{ao,ref}}{k_a}\right)}{1 + \exp\left(\frac{\tilde{P} - P_{ao,ref}}{k_a}\right)} \quad (2.20)$$

$$k_a = \frac{f_{max} - f_{min}}{4 \cdot G_b} \quad (2.21)$$

where f_{cs} is the firing rate of the carotid baroreceptors in response to the pressure sensed \tilde{P} which is the output variable of the dynamic block and depends on the arterial (aortic) pressure P_{ao} ; f_{max} and f_{min} are the maximum and minimum firing rate reachable of the receptors; τ_p and τ_z are the time constants for the real pole and the real zero in the linear dynamic block; $P_{ao,ref}$ is the value of baroreceptor pressure at the central point of the sigmoidal function; k_a is a parameter, with the dimension of pressure, related to the slope of the static function at the central point calculated by equation 2.21; G_b is the maximum baroreceptor gain.

2.5.2 Model of Lung Stretch Receptors

Inflation of lungs at low pressure activates slowly adapting stretch receptors which project to the medulla. Their activity depends on the tidal volume (V_T). Equations 2.22 and 2.23 describe how the firing rate (f_{ap}) increases with increased V_T .

$$\frac{df_{ap}}{dt} = \frac{1}{\tau_c} \cdot (-f_{ap} + \varphi_{ap}) \quad (2.22)$$

$$\varphi_{ap} = G_{ap} \cdot (4 \cdot V_L - 9.2) \quad (2.23)$$

where f_{ap} is the firing rate of the pulmonary stretch receptors in response to changes in tidal volume T_V ; τ_c is a time constant of the lung inflation; G_{ap} is a constant gain.

2.6 Physiological Model of Autonomic Parasympathetic Premotor Neurons

Parasympathetic premotor neurons control parasympathetic preganglionic neurons which protrude to the SA node, AV node, atria and ventricles. They are excited by increased activity (firing rate) of baroreceptors (and chemoreceptors) and inhibited by increased activity of lung stretch receptors. On this basis, equation 2.24 describes the firing rate $f_{ev,pm}$ of vagal premotor neurons.

$$f_{ev,pm} = \frac{f_{ev,0} + f_{ev,\infty} \cdot e^{\frac{f_{cs} - f_{cs,0}}{k_{ev}}}}{1 + e^{\frac{f_{cs} - f_{cs,0}}{k_{ev}}}} - W_{p,v} \cdot f_{ap} - \theta_v \quad (2.24)$$

where k_{ev} and $f_{ev,\infty}$ are constants, θ_v is an offset term, $W_{p,v}$ is the synaptic weight of the lung stretch receptor activity and $f_{ev,0}$ is the resting vagal tone which describes a continuous parasympathetic tonic activity. In fact, the intrinsic depolarization rate of pacemaker SA node cells is around 1.67 Hz (100 bpm), but thanks to the parasympathetic tone, the resting rate of a normal adult is lowered at around 1.17 Hz (70 bpm).

2.7 Model of Vagus Nerve Axons

The vagus nerve (VN) at the cervical level is formed by thousands of fibers [16] and each of them is a neuron axon. A widely used mammalian nerve fiber model was developed by five authors who gave its name: the Chiu-Ritchie-Rogart-Stagg-Sweeney (CRRSS) model [47, 48]. It models a myelinated fiber and it is similar to the one proposed by Hodgkin and Huxley with the main difference that the potassium current is neglected. Therefore, only the sodium and the leakage currents across the membrane are taken into account. The electrical equivalent model of the CRRSS is shown in figure 2.5. It consists of two compartments alternatingly chained together. The first of them represents the *node of Ranvier*, which contains a sodium channel in parallel to the leak conductance and a capacitance, while the second compartment is the *internode* which takes into account the insulation provided by the myeline, therefore it is simply modeled with a capacitance in parallel with a conductance.

As described in Section 1.9.2, each compartment can be modelled as in equations 1.10

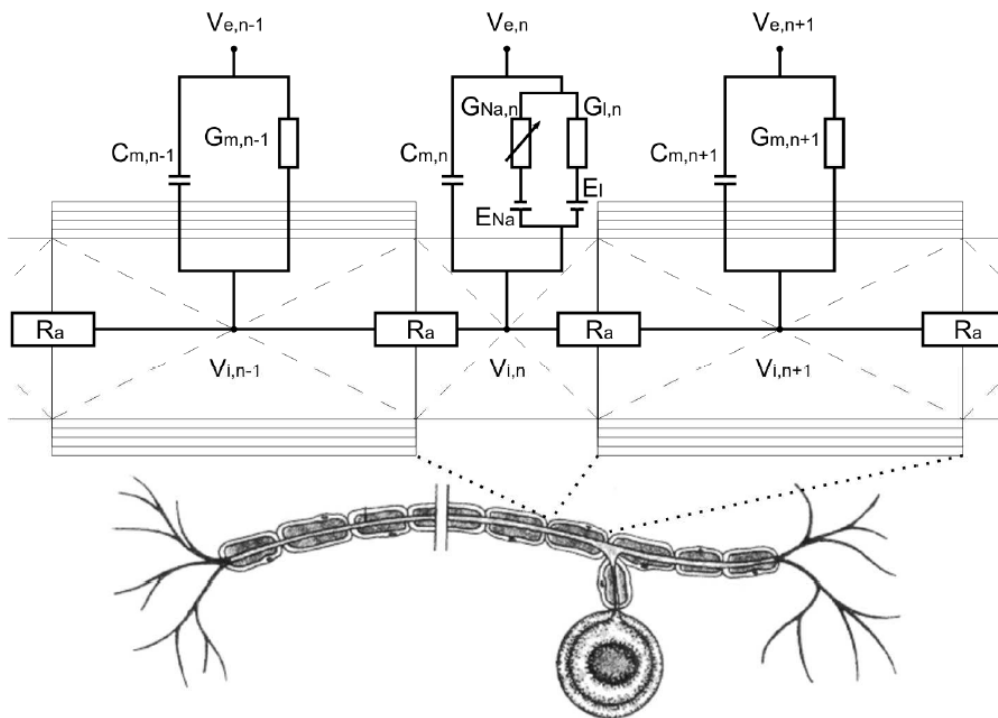


Figure 2.5: Equivalent circuit of the CRRSS model [38]

and 1.11. Taking into account of the external stimulation, the current flowing through the membrane because of it (I^{ext}) is described by means of the extracellular potential (V^e)

as in equation 2.25. Thus equation 1.11 can be re-written as in 2.26

$$I^{ext} = \sum_n \frac{V_n^e - V_k^e}{R_a} \quad (2.25)$$

$$\frac{dV^m}{dt} \cdot c = -(I^{active} + g^{lk} \cdot (V^m - E^{lk})) + \sum_n \frac{E_n - E_k}{R_a} + \sum_n \frac{V_n^e - V_k^e}{R_a} \quad (2.26)$$

where n indicates the number of connected compartments, c is the membrane capacity calculated from equation 2.27 for the node and by dividing its result for the number of myeline sheaths (N) for the internode compartment. R_a is the axonal resistance of the k -th compartment calculated with equation 2.28. The leakage conductance g_{lk} is calculated for the internode by equation 2.29.

$$c = c_m d \pi l \quad (2.27)$$

$$R_a = \rho \frac{4l}{d^2 \pi} \quad (2.28)$$

$$g_{lk} = \frac{g_m}{N} d \pi l \quad (2.29)$$

where d is the compartment diameter, l its length, c_m the specific membrane capacity and ρ the axoplasmic resistivity.

As illustrated in the electric scheme of the axonal membrane in Figure 2.5, the node of Ranvier is the only crossed by I^{active} which is given by the presence of the sodium channel. It is calculated by equation 2.30 by means of the sodium conductivity G^{Na} calculated in equation 2.31.

$$I^{active} = G^{Na} m^2 h (V^m - E^{Na}) \quad (2.30)$$

$$G^{Na} = g^{Na} d \pi l \quad (2.31)$$

E^{Na} is the sodium reversal potential and m and h are gating variables described by equations from 2.32 to 2.38.

$$\frac{dm}{dt} = [\alpha_m(1 - m) - \beta_m m]k \quad (2.32)$$

$$\frac{dh}{dt} = [\alpha_h(1 - h) - \beta_h h]k \quad (2.33)$$

$$k = 3^{0.1T-3.7} \quad (2.34)$$

$$\alpha_m = \frac{97 + 0.363V^m}{1 + e^{\frac{31-V^m}{5.3}}} \quad (2.35)$$

$$\beta_m = \frac{\alpha_m}{e^{\frac{V_m - 23.8}{4.17}}} \quad (2.36)$$

$$\alpha = \frac{\beta_h}{e^{\frac{V_m - 5.5}{5}}} \quad (2.37)$$

$$\beta = \frac{15.6}{1 + e^{\frac{24 - V_m}{10}}} \quad (2.38)$$

Extracellular stimulation modelling

Rattay et al. [49] developed a model to describe the complex, non-linear behavior of the membrane potential, under the influence of a time-varying electrical field. The stimulation is given by a single point electrode which constitutes the center of an orthogonal Cartesian coordinate system. The medium in which the electrode resides is considered homogeneous and the electric field can be calculated for a point with coordinates (x,y) by means of which the distance d_{el} between the electrode and the point can also be calculated, as shown in equation 2.39.

$$V^e = \frac{\rho_e I_{el}}{4\pi} \cdot \sqrt{x^2 + y^2} = \frac{\rho_e I_{el}}{4\pi} \cdot d_{el} \quad (2.39)$$

where $I_e I$ is the current delivered by the electrode.

The so-called *Activating function* drives the extracellular potential and represents the rate of change of the membrane voltage when the neuron is in its resting state right before the stimulation. As shown in equation 2.40, it is proportional to the second-order spatial differential along with the fiber.

$$f = \frac{d}{4\rho_e c} \cdot \frac{\partial^2 V_e}{\partial x^2} \quad (2.40)$$

It follows that in the discrete domain, taking into account that each compartment (n) is in contact with its two only neighbours ($(n - 1)$ and $(n + 1)$), it is presented in the form of equation 2.41.

$$f_n = \frac{d\Delta x}{4\rho_e Lc} \cdot \frac{V_{n-1}^e - 2V_n^e + V_{n+1}^e}{\Delta x^2} \quad (2.41)$$

where Δx is the node-to-node distance and L the node length. With the above consideration, equation 2.26 can be rewritten as shown in equation 2.42.

$$\frac{dV_n^m}{dt} = \left[-I^{active} - g^{lk} \cdot (V^m - E^{lk}) + \frac{d\Delta x}{4\rho_e L} \cdot \left(\frac{V_{n-1}^m - 2V_n^m + V_{n+1}^m}{\Delta x^2} + \frac{V_{n-1}^e - 2V_n^e + V_{n+1}^e}{\Delta x^2} \right) \right] / c \quad (2.42)$$

Values used in the CRRSS are given in Table A.9 in the Appendix.

2.8 Acetylcholine Release Model

Acetylcholine (ACh) is released in the neuroeffector junction by vagal stimulation and binds on the membrane of the SA node cells to muscarinic receptors with the effect of decreasing the rate of pacemaker depolarization and, therefore, the heart rate. After its release, the action of ACh is terminated by the combined processes of hydrolysis, performed by the acetylcholinesterase which form choline that is transported back into the nerve terminal to resynthesise ACh, and washout from the synaptic cleft. In his work, Dokos [50] developed a three-compartment model which is illustrated in Figure 2.6. It describes a bi-exponential decline of ACh concentration in the neuroeffector junction ($[ACh]$). The main store of ACh located in the nerve terminal, releases a certain fraction of its contents (k_1) at each vagal stimulus. Simultaneously a fixed fraction (k_1) is also released into an extra junctional space and therefore is not effective on the SA node cells and escapes unhydrolyzed. In the neuroeffector junction compartment $[ACh]$ decline is rapid due to hydrolysis (k_H) and uptake back into the main store. While in the extra junctional space, ACh decline and uptake into the main store occurs at a lower rate because it is only due to the vasculature.

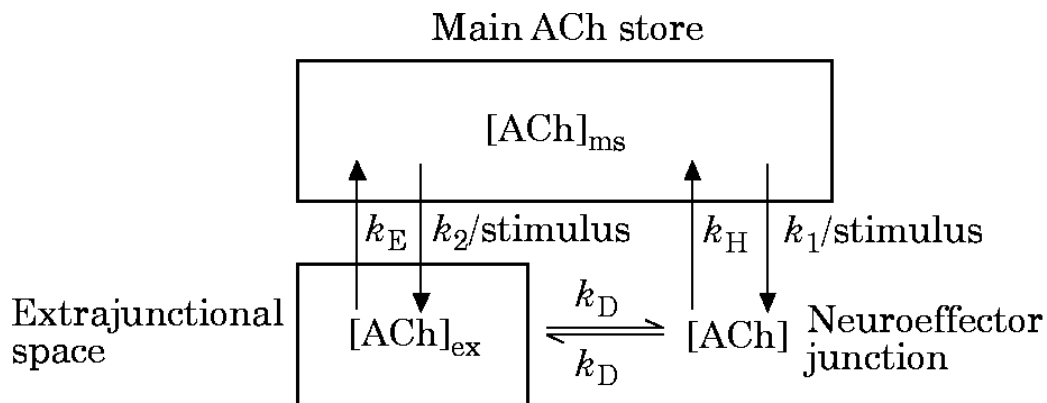


Figure 2.6: Three compartment ACh release model consisting of a main ACh neuronal store, the neuroeffector junction and extra junctional space. Concentrations of ACh within these stores are denoted by $[ACh_{ms}]$, $[ACh]$ and $[ACh_{ex}]$ respectively. k_1 and k_2 indicate the fractions of $[ACh_{ms}]$ released per vagal stimulus into the neuroeffector junction and extra junctional spaces and k_D is the effective diffusion rate between these latter two compartments. k_H is the rate of hydrolysis in the neuroeffector junction and k_E is the rate of escape from the extra junctional space to the vasculature. Modified from [50]

The kinetics of the model described in Figure 2.6 are mathematically described by the three equations 2.43-2.45.

$$\frac{d[ACH]_{ms}}{dt} = \left(\frac{k_H}{F_{ms}} \right) [ACH] + \left(\frac{k_E}{F_{ms}} \right) [ACH]_{ex} \quad (2.43)$$

$$\frac{d[ACH]}{dt} = -k_H[ACH] - k_D([ACH] - [ACH]_{ex}) \quad (2.44)$$

$$\frac{d[ACH]_{ex}}{dt} = \left(\frac{k_E}{F_{ex}} \right) [ACH]_{ex} + \left(\frac{k_D}{F_{ms}} \right) ([ACH]_{ex} - [ACH]) \quad (2.45)$$

where F_{ms} and F_{ex} denote the fractional volumes of the main store and extrajunctional space relative to the neuroeffector junction. Moreover, at the arrival of each vagal stimulus there is an instantaneous transfer between compartments according to equations 2.46-2.48.

$$[ACH]_{ms,0} = (1 - k_1 - k_2)[ACH]_{ms} + [ACH]_T \quad (2.46)$$

$$[ACH]_0 = [ACH] + k_1 F_{ms} [ACH]_{ms} \quad (2.47)$$

$$[ACH]_{ex,0} = [ACH]_{ex} + k_2 \left(\frac{F_{ms}}{F_{ex}} \right) [ACH]_{ms} \quad (2.48)$$

where $[ACH]_{ms,0}$, $[ACH]_0$, $[ACH]_{ex,0}$ denote the values of ACh concentration in the respective compartment right after the vagal stimulus.

Values associated with the ACh release model are reported in Table A.10 and they are the same provided in [50] except for the value of the hydrolysis constant k_H which is reported to be of tricky measure. In particular, a comparison study reports that the k_H value differs greatly between studies (between 0.2260 Hz and 50 Hz) [51]. For this reason, this value underwent a fine-tuning, which was performed on the entire built model, described in Section 2.12.

2.9 The Vagus Nerve

The VN at the cervical level is formed by thousands of nerve fibers (described by the CRRSS model in Section 2.7). It is clear from Figure 2.7, that two aspects, directly dependent from the CRRSS model, are the most crucial for this model: the diameter of fibers (d_i) and their distance from the electrode ($d_{el,i}$), which also influences the parameter r needed to calculate the activating function.

Due to the leak of literature histological studies performed on the human VN which reports a count or a proportion between of the number of A, B and C fibers, the choice of the number of fibers to include in the VN model was based on a histological study performed on the porcine left VN at the mid-cervical level [18]. This study states that 80%

of the fibers at this level are C fibers and provides a count of A and B fibers, which have a proportion of 40%/60%, respectively.

Unmyelinated C fibers were not included in our model. The main reason for that is that they are primarily afferent (sensory) fibers only and, for the purpose of this study, we are only interested in modeling the efferent ones that are the target of the VNS. Moreover, since C fibers are the smallest, their activation threshold is so high that it is assumed that with the VNS therapeutic intensity levels, they would never be elicited [52].

Secondly, for what concerns the fiber topology, no information was found to be reliable. Therefore a set of electrode distances equal in number to the amount of fibers was randomly generated with a normal distribution.

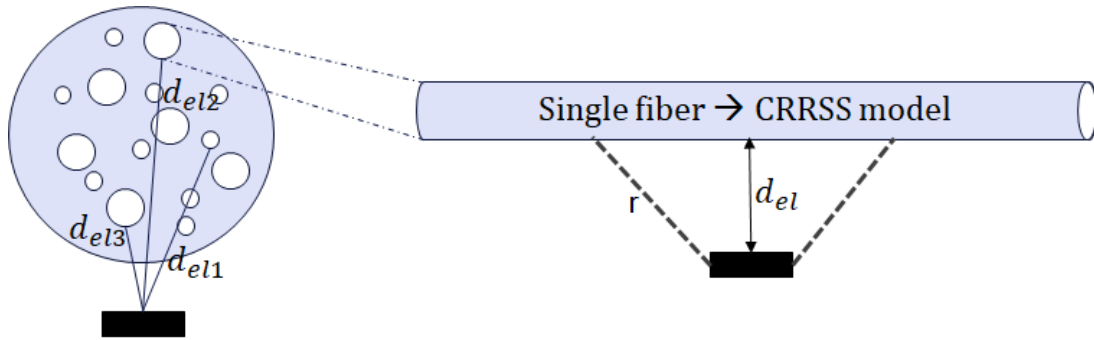


Figure 2.7: Illustration of the building of the vagus nerve (VN). Each fiber is a CRRSS model. In the VN there are hundreds of fibers, each with a proper diameter and distance for the electrode d_{el} (black rectangle).

Model dimensionality reduction

The considerations above imply that, in theory, the VN should be modeled by means of hundreds CRRSS models to model A and B fibers each with its own d and d_{el} , but this approach requires a rather high computational power and therefore, the need of a super-computer.

For this reason, a strategy for model dimensionality reduction was developed by using the approach described in [53]. In simple words, it consists in the construction of a look-up table whose ground is constituted by 3 axes that report the pulse width (Pw), the electrode distance (d_{el}) and the fiber diameter (d). The output value is the current intensity threshold (I_{thr}) needed to elicit the fiber with those features.

To calculate the I_{thr} for the implementation of the 3D look-up table, the CRRSS model was iteratively run by setting all possible combinations of the ground parameters in a defined range: [0.05 0.2] ms with steps of 0.05ms for the Pw , [0.1 3] cm with steps of 0.1 cm for the d_{el} and [1 12] μm with steps of 0.5 μm for the d .

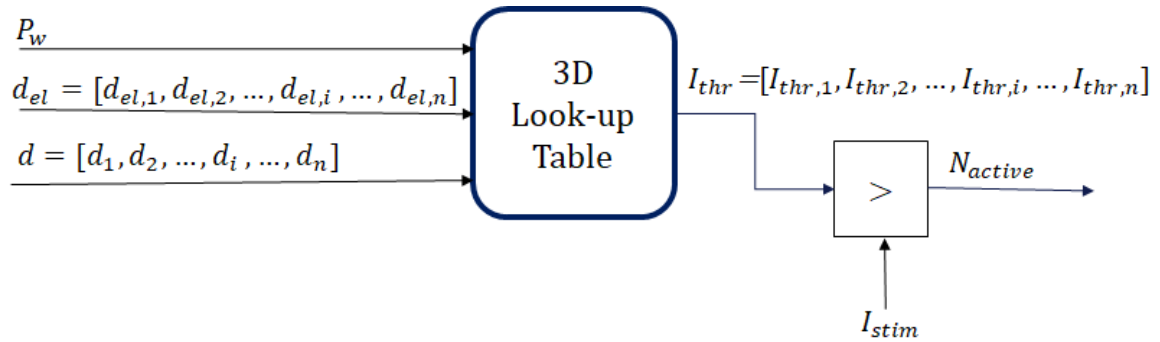


Figure 2.8: Dimensionality reduction: inputs of the look-up table are the pulse width (P_w), a vector with n electrode distances d_{el} and a vector with n fiber diameters; output of the look-up table is a vector with the n activation thresholds (I_{thr}). I_{thr} is compared with the current intensity delivered from the stimulator (I_{stim}) and the number of activated fibers (N_{active}) is detected.

Once that the look-up table was obtained, it was integrated in the Simulink model with the target of providing the number of activated fibers. As described in Figure 2.8, its inputs are the pulse width delivered by the stimulator, a vector with the n values of electrode distances (one for each of the modeled fiber) and a vector with n fiber diameters. The output is a vector I_{thr} , which provides the n threshold intensities needed to elicit the modeled fibers. Each value of the vector I_{thr} is then compared to the current intensity (I_{stim}) delivered by the stimulator and the number of activated fibers (N_{active}) is calculated.

Integration of Vagus Nerve Axons' with the ACh Release Model

To integrate the ACh release model with the reduced VN model, the percentage of activated fibers is calculated and multiplied by a term proportional to the $[ACh]$ released by a unique ACh release model.

Assuming that the timing of each burst of ACh release is synchronized with the pattern of stimulation, the stimulator is directly attached to the ACh release model. This is not a perfect representation of reality since, in this way, it is assumed that all fibers are releasing ACh at the same time. But, as seen in Section 2.7, the diameter of the fiber determines its conduction velocity. Therefore, bigger fibers release ACh with some advance in time with respect to the smaller ones. However, the timing difference is not so significant (in the order of μs) and, therefore, this assumption provides a well explanation of the dynamic as well.

The diagram block in Figure 2.9 describes the integration of the ACh release model and the reduced VN and provides the description of the amount of ACh released in the condition of vagotomy, which is necessary when performing a heart transplant.

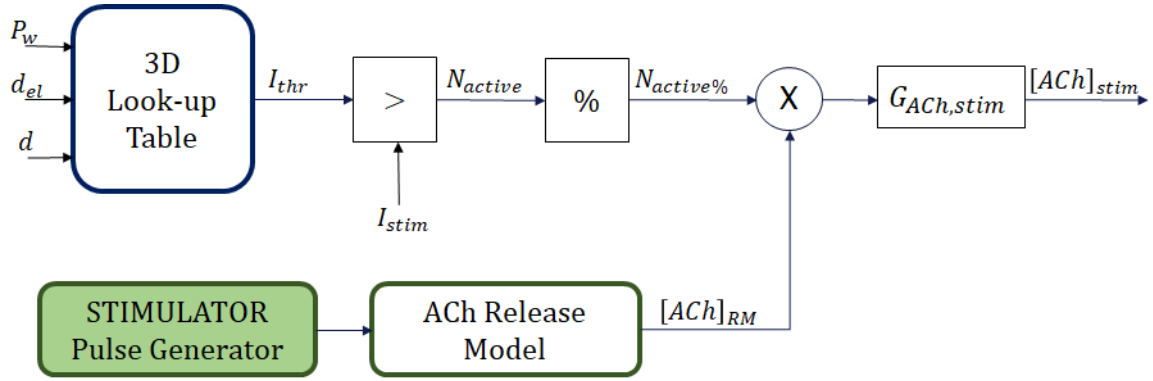


Figure 2.9: Diagram block of the entire vagus nerve, which contains the reduced axon models and the synaptic end (the ACh release model). The first provides the percentage of activated fibers ($N_{active\%}$) and the second the amount of ACh released by one fiber ($[ACh]_{RM}$). These two values are multiplied and a gain factor ($G_{ACh,stim}$) is applied to have the total amount of ACh released VNS ($[ACh]_{stim}$), which is also the amount of ACh released in vagotomy

Integration of the Vagus Nerve with Premotor Neurons

To simulate the intact vagus, the premotor neurons are integrated. The basic assumption that the VN firing rate is equal to the one of the premotor neurons is made. In this way, there is no need to include into the intact vagus model an anatomical description of the VN itself. The firing rate of the premotor neurons ($f_{ev,pm}$) directly determines the release of ACh.

Since the ACh release model is sensitive to the instant of arrival of the impulse (or action potential AP), the $f_{ev,pm}$ was converted into a spike signal with the given frequency which is the input to the ACh release model. As described in the diagram block in Figure 2.10, again $G_{ACh,pm}$ is applied to the released ACh and the amount of ACh released thanks to premotor neurons activation ($[ACh]_{pm}$) is summed with the previously calculated ACh released because of stimulation ($[ACh]_{stim}$) providing the total amount of ACh released by the VN ($[ACh]_{tot}$).

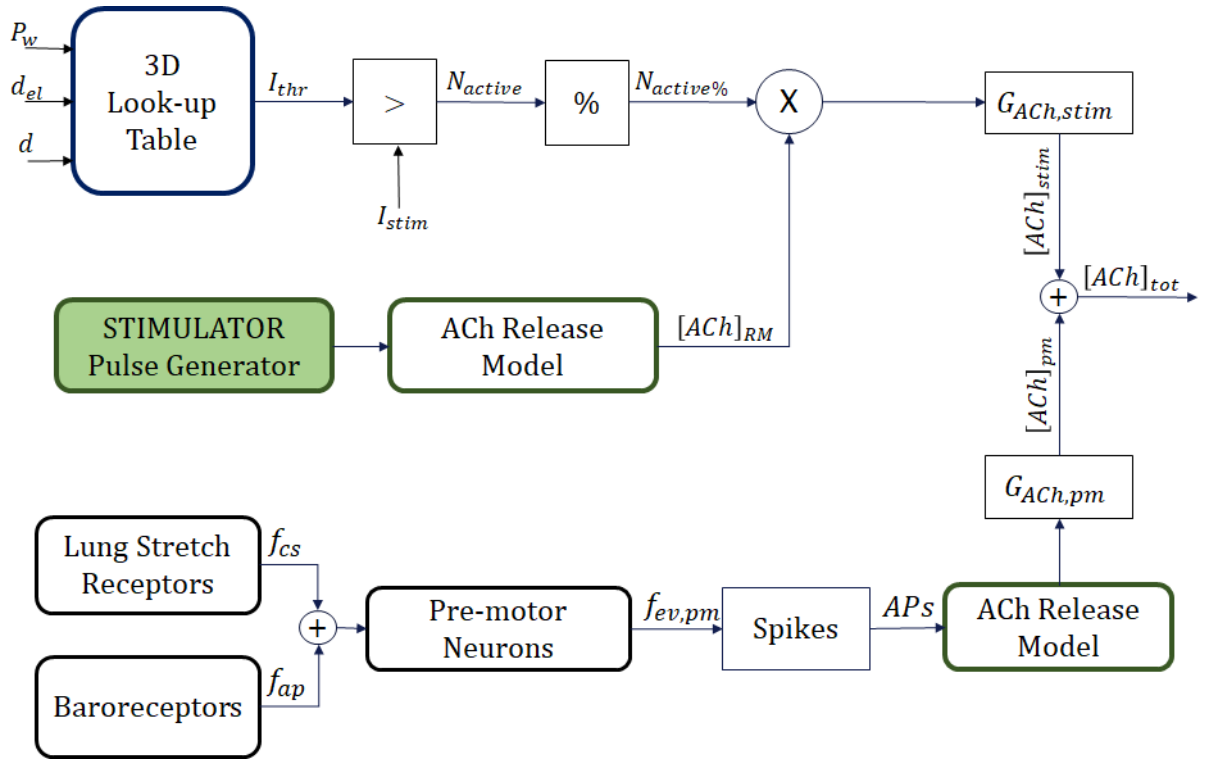


Figure 2.10: Diagram block which describes the total amount of ACh released ($[ACh]_{tot}$) with the intact VN. The ACh released because of stimulation ($[ACh]_{stim}$) is summed to the one release by premotor neurons activity ($[ACh]_{pm}$). The 'Spikes' block transform the firing rate of premotor neurons ($f_{e,pm}$) in action potential (APs) with the right frequency.

2.10 Sino Atrial Node

The implementation of the SA node was based on a Hodgkin-Huxley-type single-cell human SA node model proposed by Fabbri et al. [54] who developed the rabbit SAN cells model proposed by Severi et al. [55]. This model can reproduce the SA node cell's spontaneous depolarization, including variations in voltage and ionic conductance due to autonomic control. This is made by elaborating the concentration of Acetylcholine (ACh) and Isoprenaline (Iso, a sympathomimetic drug of norepinephrine), which are the input of the SA node model. The authors provide a detailed description of the model in [54].

2.11 PR interval model

The conduction speed of the atrioventricular (AV) pathway determines the delay of the contraction between the atria and the ventricle. The conduction velocity is modulated by the autonomic nervous system and, therefore, affected by VNS. The atrioventricular conduction is visible on the ECG by means of the PR interval. This latter depends on two opposite effects: the *indirect effect* which induce a prolongation of the PR interval caused by the slowing of the HR and the *direct effect* which provokes its increases in response to the direct action of the vagus on atrioventricular nodal cells [56].

Accordingly, with this explanation, a study [57] reports a negative linear correlation between the PR interval and the HR obtained in the absence of VNS. It is shown in equation 2.49 and represents the indirect effect.

$$PR_{ind} = -c_{PR,ind} \cdot HR + PR_{baseline} \quad (2.49)$$

To model the direct effect (PR_{dir}), a term proportional to the ACh released by the VN is added applying a first dynamic, as shown in equation 2.50 and 2.51.

$$\frac{dPR_{dir}}{dt} = \frac{[ACh] \cdot c_{PR,dir} - PR_{dir}}{\tau_{PR,ind}} \quad (2.50)$$

$$PR = PR_{dir} + PR_{dir} \quad (2.51)$$

2.12 Tuning of the model: Global Sensitivity Analysis

The study performed by Ojeda et al. [58] analyzes the acute cardiac response to different VNS configurations, considering the chronotropic, dromotropic and inotropic cardiac effects. In particular, they apply to the intact right VN at the cervical level synchronized VNS (S-VNS) with 75 different parameter configurations to six healthy sheep while acquiring the associated cardiovascular response. By using a gaussian process regression, they built a surrogate model that predicts the response of any parameter configurations fitting the observed data acquired from each sheep. Then, a global sensitivity analysis (GSA) with Sobol’s methods was performed to obtain the main and total sensitivity indices and determine the main influencing stimulation parameters to elicit the cardiac response.

Differently from the asynchronous VNS (A-VNS) in which the stimulation is constantly delivered at a certain frequency, intensity and pulse width, S-VNS delivers a burst with a certain amount of impulses when a certain even is detected. In [58], the S-VNS is triggered by the R peak of the recorded ECG and the 75 different parameter configuration are chosen with an optimized Latin Hypercube sampling with the aim to cover as best as possible the range in which the parameters are made vary. In Table 2.2, the parameters with their intervals are defined as reported by Ojeda et al. [58].

Parameter	Notation	Range
Current	I_{stim}	0,2 mA to 1 mA
Number of pulses	N_p	1 to 4
Pulse width	P_w	0,05 ms to 0.20 mA
Frequency	F	21,3 Hz to 41 Hz
Delay	D	16 ms to 156 ms

Table 2.2: Synchronize VNS parameter ranges and notation from [58].

2.12.1 Cardiac Effects’ Markers

Cardiac effects of VNS are assessed in [58] by calculating markers for each VNS parameter configuration (a detailed explanation of the markers is given in a previous study [59]). The model output was processed to reproduce their experiments and compare results. S-VNS is applied using the depolarization of the SA node cell model as a trigger. A simulation protocol of 50 s was tested: the first 20 s define the baseline (no VNS), at t=20s VNS is applied and maintained until the end of the simulation.

Chronotropism marker

The chronotropism marker was evaluated from the HR model signal calculating the baseline HR value ($HR_{baseline}$) defined as the mean value of the last 15 s before VNS stimulation is applied and the HR during VNS (HR_{VNS}) defined as the mean HR after the

transitory due to the beginning of VNS is passed (between 35 s and 50 s).

$$C_M = \left(1 - \frac{HR_{VNS}}{HR_{baseline}} \right) \cdot 100 \quad (2.52)$$

Inotropism marker

The inotropism marker was calculated by means of the left ventricle pressure signal (P_{lv}). The signal processing is shown in Figure 2.11: the first derivative $\frac{dP_{lv}}{dt}$ is calculated and the its maximums are detected, one for each heartbeat. To define the baseline value, the mean of the last three cycles before VNS is applied is taken ($dPdt_{baseline}$) and the 'during VNS' value is the minimum of those maximum when VNS is applied ($mindPdt_{VNS}$). The marker (I_M) is calculated as in equation 2.53.

$$I_M = \frac{mindPdt_{VNS} - dPdt_{baseline}}{dPdt_{baseline}} \cdot 100 \quad (2.53)$$

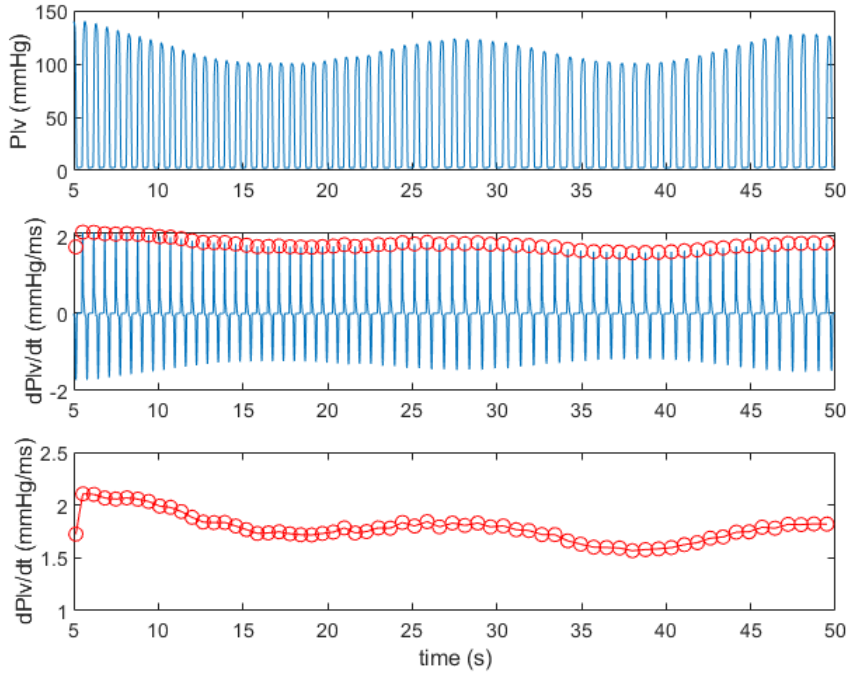


Figure 2.11: Data processing for the calculation of the inotropism marker: from acquired pressure in the left ventricle (P_{lv}), the first derivative is calculated ($\frac{dP_{lv}}{dt}$) and its maximum detected. VNS is applied at 20s and maintained till the end of the simulation.

Dromotropism marker

The dromotropism marker was evaluated on the PR interval signal. As the chronotropism marker, also here it is simply calculated as the percentage reduction between 'during stimulation' mean value (PR_{VNS}) and the mean baseline value ($PR_{baseline}$) as illustrated in equation 2.54.

$$D_M = \left(1 - \frac{PR_{VNS}}{PR_{baseline}}\right) \cdot 100 \quad (2.54)$$

2.12.2 Two-phases Model Tuning**First Phase: Marker's Comparison**

On the base of the reported markers from Ojeda et al. [58] measured on 12 sheep, a first tuning was performed. Their data were processed, calculating the mean, the maximum and the minimum value of each marker for each of the 75 parameter configurations. The model was run iteratively comparing the model's output, in terms of calculated markers (C_M, I_M and D_M), with the elaborated data from [58]. To produce the best fit of their data certain model variables were manually tuned such as: A and B mean fiber diameters (d_A, d_B), A and B amount and ratio of fibers (N_A, N_B), electrode distance (d_{el}), hydrolysis rate constant (k_H) and gain factors ($G_{ACh,stim}, G_{ACh,pm}$).

Second Phase: Global Sensitivity Analysis

The second stage of the tuning was finer and performed using the GSA results provided by Ojeda et al. [58]. For this aim, the *Global Sensitivity Analysis Toolbox* [60] was used, which is a set of routines provided by MathWorks and developed to calculate both the main and the total indices of the GSA with Sobol's method. The model was set in healthy condition and the GSA was performed by defining 1000 parameters combinations whose values are in the ranges defined in Table 2.2. The tuning was focused on the same model parameters which were target of the first phase of tuning ($d_A, d_B, N_A, N_B, d_{el}, G_{ACh,stim}, G_{ACh,pm}$). The GSA was run iteratively and small manual variations in the model parameters values were applied. This is possible because small deviations from the values obtained in the first stage of tuning do not produce a strong deviation from the marker calculation result.

Global Sensitivity Analysis on S-VNS parameters

To assess possible changes, the GSA for HTx condition was also run calculating main and total indices. The same setup used for the healthy condition was applied in terms of the number of iterations and S-VNS parameters ranges.

Global Sensitivity Analysis on A-VNS parameters

Nowadays, VNS has usually applied asynchronously (A-VNS) to the vagus nerve. For this reason, the choice to investigate the influence of the only three parameters is definable when A-VNS is applied: current, frequency and pulse width. Due to the lack of experiments, no comparison with experimental data is possible. Therefore, the model is considered reliable to compare the stimulation parameter influence on each cardiac effect between the healthy and the HTx conditions.

The intervals given to the GSA tool for each parameter are: [0.1 - 1] mA for the current, [0.05 - 0.2] ms for the pulse width and [0 - 15] Hz for the frequency. Main and total indices were calculated for both the healthy and the HTx condition and their values compared between one and others.

It has to be noted the performing the GSA with 1000 parameters combination is highly time-consuming with a 'common' computer (ASUSTeK Computer Inc. Intel(R) Core(TM) i7 -6500 CPU @2.50 GHz 2.59 GHz), around 4 days to obtain both main and total indices. Therefore, it was run using the Vienna Scientific Cluster (VSC-4) which is a supercomputer (Intel Skylake Platinum 8174 CPU @3.1 GHz 3.9 GHz) using 100 cores. This produces a drastic reduction of the computation time up to a few minutes to obtain the GSA results.

2.13 Validation Tests

To demonstrate the model's validity, some tests were performed using literature studies different from the one used for tuning. In this way, the model is evaluated on animal species different from sheep, whose data were used for the tuning. Furthermore, the great majority of the literature studies are performed applying VNS in an asynchronized manner, giving the opportunity to verify if the model can reproduce A-VNS cardiac effects even if the tuning was performed using data obtained applying S-VNS.

2.13.1 Chronotropic Effect

Three studies were identified to evaluate the chronotropic effect: [61] and [62] are performed with Langendorff perfused rabbit hearts (isolated hearts) to investigate the effects of direct sympathetic and vagus nerve stimulation while [63] is performed in vivo on dogs with a setup which mimics the isolated heart.

In all of them, A-VNS is applied and the stimulation parameters were chosen to achieve a submaximal heart response. As described in [62], to identify the proper combination of parameters to achieve this target, pulse width and frequency were fixed to 200 μ s and 5 Hz, respectively and the model current intensity was increased iteratively up to reach the minimum HR before inducing heart blockade. The same procedure was applied to the model considering that the heart blockade is here interpreted as SA node blockade. The stimulation current was then chosen as the value right before the one that produces the

block and resulted in being 0.9 mA.

A frequency sweep stimulation protocol was applied using the following parameterization: VNS was 100 s OFF/100 s ON to ensure the reach and maintain a stable HR for an adequate period. The pulse width and the current were kept fixed at 200 μ s and 0.9 mA while the frequency was increased according to the values reported in the three studies (1, 2, 3, 5, 7, 10 Hz). The reduction in HR was then calculated in respect to the baseline HR value and compared with the results reported in [61], [62] and [63].

2.13.2 Inotropic Effect

In the study performed by Lewis et al. [64], the contractility of cardiac muscle is assessed utilizing the slope of the ESPVR, which represents the end-systolic elastance. This is a more accurate indicator of the inotropism than the maximum rate of left ventricle pressure rise (dP/dt_{max}). However, its acquisition is more difficult because it requires the placement of a conductance-pressure catheter inside the left ventricle. In [64], experiments are conducted on both pigs and humans under anesthesia, but these latter were affected by heart failure, therefore, we choose to base the simulation on the data from pigs.

The pig experiment is conducted in vivo with intact sympathetic innervation, dissected left vagus nerve and temporary pacing wires attached to the peripheral end for electrically stimulating the nerve. The branch of the model that carries the action potential evoked by the CNS (afferent) control was detached to reproduce the experimental set up for the model testing. In practical terms, referring to Figure 2.10, the bottom branch, which delivers $[ACh]_{pm}$ is substituted with a constant equal to 0.

As described in [64], A-VNS is applied with a set of parameters that produce a decrease in HR of 20 ± 1 bpm. The model baseline HR with the cut vagus is 100 bpm. The target HR of around 80 bpm is achieved in the model with the following stimulation parameters: current intensity = 0.78 mA, pulse width = 0.15 ms, frequency = 10 Hz.

PV loops were displayed by plotting the left ventricle volume (LVV) on the x axis and the left ventricle pressure (LVP) on the y axis. The upper left corners of the PV loops were interpolated by a straight line in the form $y = m \cdot x + p$. m represents the slope of the ESPVR, which is called end-systolic elastance (Ees).

To deliver a complete overview of the contractility changes, the end-systolic elastance was evaluated, with the same data processing procedure, simulating healthy and the HTx conditions and maintaining the same stimulation pattern.

2.13.3 Dromotropic Effect

To evaluate the dromotropic effect a comparison was performed with a study performed on dogs [56]. Here the atrioventricular conduction time (PR interval) is measured in vivo when A-VNS is applied to the cut left vagus nerve. In particular, the measure the PR interval stimulating the nerve with a fixed pulse width and current intensity while progressively increasing the stimulation frequency. The results show a linear increase in the PR interval with the increasing frequency with a certain slope.

The experiment's setup was reproduced in the model: the denervated heart condition was set and supramaximal stimulation, which involve all the fibers in the vagus nerve, was applied. This is done in the model by setting a pulse width of 0.2 ms and a current intensity of 0.9 mA.

A frequency sweep protocol was applied with 100 s ON/ 100s OFF to ensure stable PR interval achievement. The frequency was increased as follows: 0.5, 1, 1.5, 2, 2.5, 3, 4, 5 Hz. The PR interval in the 100 s ON was averaged and displayed as a function of the frequency and the slope of the PR interval-frequency relation was calculated to perform the comparison with the result reported in [64].

2.14 Hemodynamic Parameters

In a previous stage of the development of the model, extensive literature research was performed to build the basis for the implementation of the HTx condition [65]. This work's focus was placed on early HTx patients, including literature studies performed up to 1 year post-transplantation. In Table 2.3 the hemodynamic parameter obtained in resting conditions are shown.

	Healthy control	HTxR
HR [bpm]	67.24±11.04	94.71±10.60
CO [l/min]	5.33±1.00	5.34±1.27
SBP [mmHg]	119.65±14.94	114.75±27.38
DBP [mmHg]	74.87±10.34	75.90±20.74
SV [ml]	73.97±14.24	53.68±15.92

Table 2.3: Resting hemodynamic parameters obtained from a polling of data from literature. Adapted from [65].

To get an overview of the changes of the hemodynamic parameters due to the application of S/A-VNS, six simulations were performed: two are without VNS to provide the baseline values (the first simulate the healthy control and the second in the HTx condition), and other four simulations are with the application of S-VNS and A-VNS to the baseline conditions. Each condition is tested with a 100 s long simulation where VNS is

applied at $t=50$ s and maintained until the end of the simulation.

Here follows a list of the assessed hemodynamic variables and how they are obtained from the model output:

- The HR is obtained as the inverse of the heart period (HP) multiplied by 60. The HP is calculated as the time in seconds between two subsequent depolarization peaks of the SA node.
- Systolic and diastolic blood pressure (SBP and DBP) were calculated on the aortic pressure signal (P_{ao}). For each cardiac cycle, the maximum and the minimum were detected and the average of each of them gives the SBP and DBP values.
- The stroke volume (SV) is defined as the amount of blood ejected by the ventricle at each beat. It is calculated by the left ventricle volume as the difference between its maximum and minimum. The results of each beat is then averaged.
- The cardiac output (CO) is defined as the amount of blood ejected by the heart in a minute; therefore, it is simply obtained by implementing equation 2.55.

$$CO = SV \cdot HR \quad (2.55)$$

Chapter 3

Results

The model was capable of simulating different conditions to predict the cardiac response to A-VNS and S-VNS in HTxR and healthy individuals. Selecting among HTxR and healthy individuals is achieved with the user's initial definition of a boolean variable. This variable allows the load of the appropriate model parameter's values to reproduce the healthy or the HTx condition.

With the aim of building a model capable of reproducing experimental data and predicting cardiac effects, the tuning was performed using the study of Ojeda et al. [58] which provides data strictly related to the three analyzed cardiac effects by reporting their marker's values and the global sensitivity main and total indices to describe the influence of the stimulation parameters on the chronotropic, inotropic and dromotropic effect. Testing the model in the same condition reported in [58], its capability to accurately predict the three main cardiac effects when S-VNS is applied to the healthy individual was proven.

Moreover, to investigate if the condition (HTx or healthy) plays determinant role when the main and total indices are investigated or, in other words, if the effect of each stimulation parameter change in a denervated heart, the GSA was also performed in the HTx condition and its results compared to the ones of the healthy.

A GSA was also performed to the stimulation parameters of A-VNS for both the healthy and the HTx individuals. These are only preliminary results that need validation with experimental data.

To provide a validation of the model, it was then tested in condition different from the one used for the tuning. Three tests were performed, one for each cardiac effect. The prediction of the model was then compared to the experimental data reported in literature ([56, 61, 62, 63, 64]).

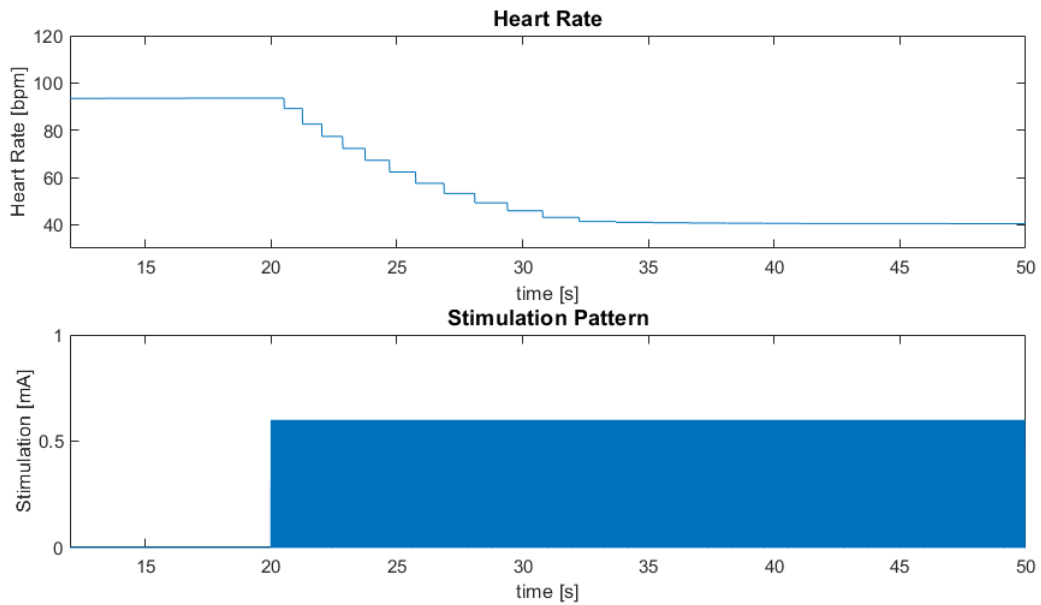


Figure 3.1: Generic simulation results for asynchronous vagus nerve stimulation (current intensity 0.6 mA, pulse width 150 μ s and frequency 25 Hz).

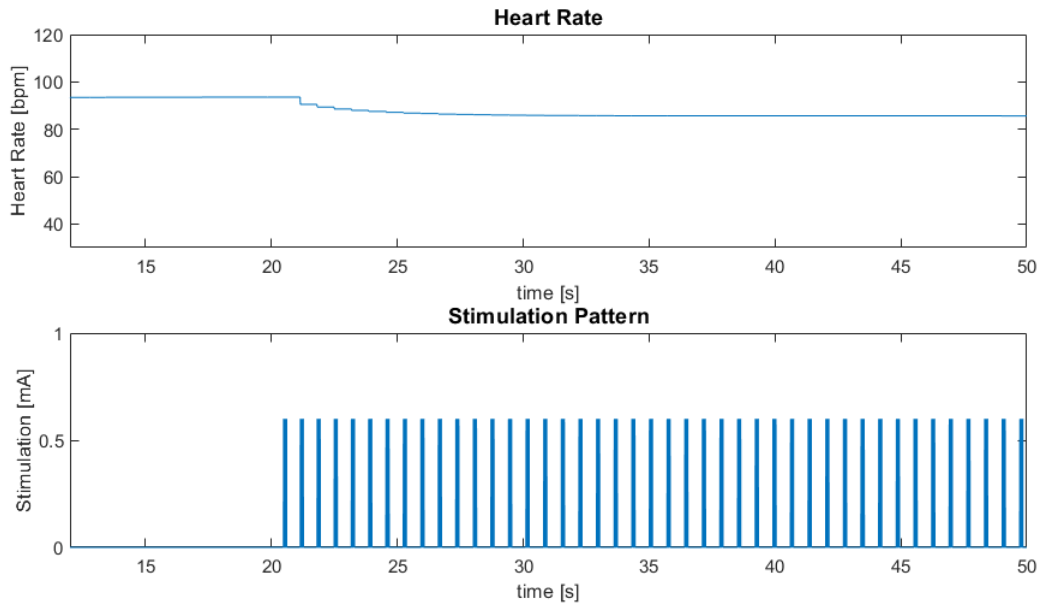


Figure 3.2: Generic simulation results for synchronized vagus nerve stimulation (current intensity 0.6 mA, pulse width 150 μ s, frequency 25 Hz, delay 156.2 ms and 4 pulses per burst).

To gain a comprehensive overview of the hemodynamics and make a quantitative comparison between the application of S/A-VNS in the healthy and in the HTx conditions, mean values of heart rate, aortic pressure, volume of the cardiac chambers, and blood flow entering or exiting from the cardiac chambers, cardiac output, and stroke volume were evaluated.

Generic simulation results showing the chronotropic cardiac effect of synchronized and asynchronous VNS applied to a HTxR are presented in Figures 3.1 and 3.2. The simulation lasts 50 s in which the first 20 s are without VNS; then, the stimulation pattern is applied in both cases and maintained until the end of the simulation. Change over time of the HR and the stimulation pattern are displayed. A higher HR of 93 bpm can be seen before the application of VNS. When VNS is applied, after a brief transitory, the HR settles to a lower value (40 bpm in the case of the A-VNS and 82 bpm in the case of the S-VNS).

3.1 S-VNS Effects on Chronotropy, Inotropy and Dromotropy

The model tuning was based on data reported by Ojeda et al [58] in which S-VNS is applied to 12 sheep with intact sympathetic and parasympathetic autonomic control (healthy condition) with 75 different parameter configurations. As described in Section 2.12.1, the three main cardiac effects induced by VNS, chronotropism, inotropism and dromotropism, are quantified using markers.

The experimental set up was reproduced in the model and in Figures 3.3, 3.4 and 3.5 the results of the markers calculated from the model output for each VNS parameter configuration is given. The graphs show six-lines plots: on the x-axis of all of them, the number of the simulation is given (from 1 to 75), while on the y-axis are given in this order from top to bottom: the marker values obtained from the model (C_M for the chronotropism, I_M for the inotropism and D_M for the dromotropism), the pulse width (P_w), the stimulation current (I_{stim}), the frequency (F), the number of pulses (N_p) and trigger delay (D). The model's predicted marker is compared to the one obtained in the reference study [58] by displaying the minimum, the maximum and the mean values obtained, elaborating the experimental data for each VNS parameter configuration applied.

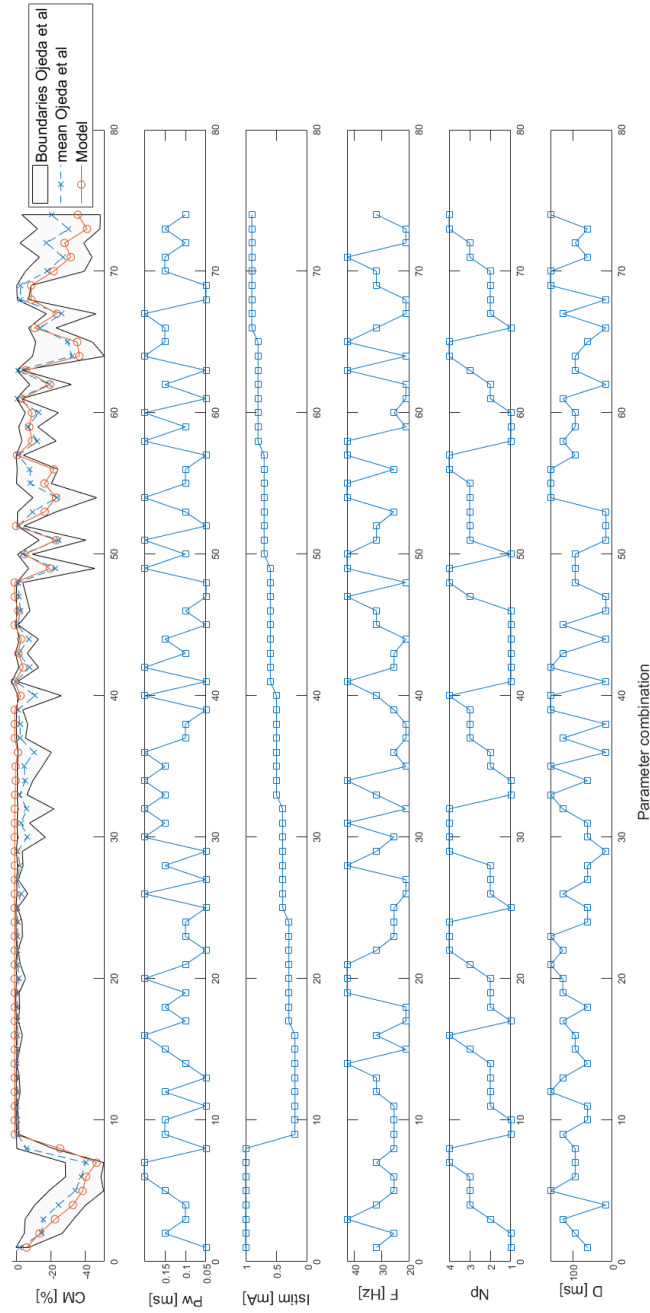


Figure 3.3: The chronotropism marker (C_M) represents the percentage change in heart rate due to stimulation. It is calculated from the model (red dot) and compared to the Ojeda et al. study results [58] (in blue the mean value and in black the maximum and minimum). For each of the 75 parameter configuration, pulse width (P_w), current intensity (I_{stim}), frequency (F), number of pulses (N_p) and trigger delay (D) are given.

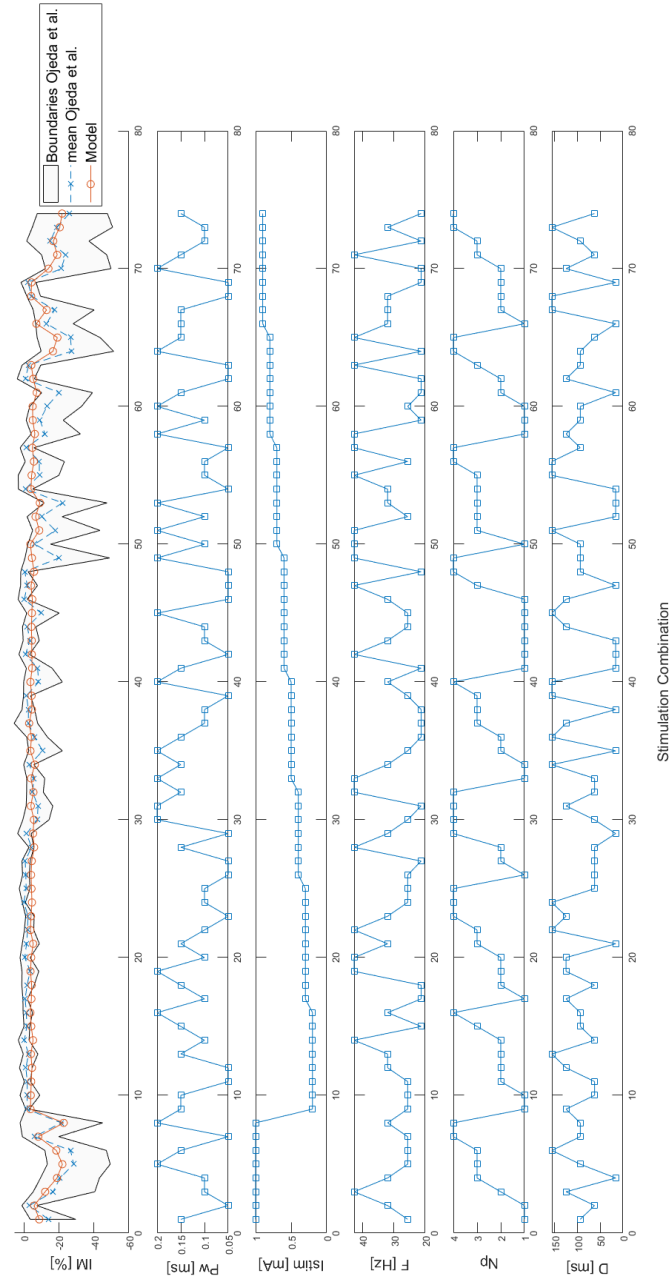


Figure 3.4: The inotropism marker (I_M) represents the percentage change of the rate of change of the left ventricle pressure due to stimulation. It is calculated from the model (red dot) and compared to the Ojeda et al. study results [58] (in blue the mean value and in black the maximum and minimum). For each of the 75 parameter configuration, pulse width (P_w), current intensity (I_{stim}), frequency (F), number of pulses (N_p) and trigger delay (D) are given.

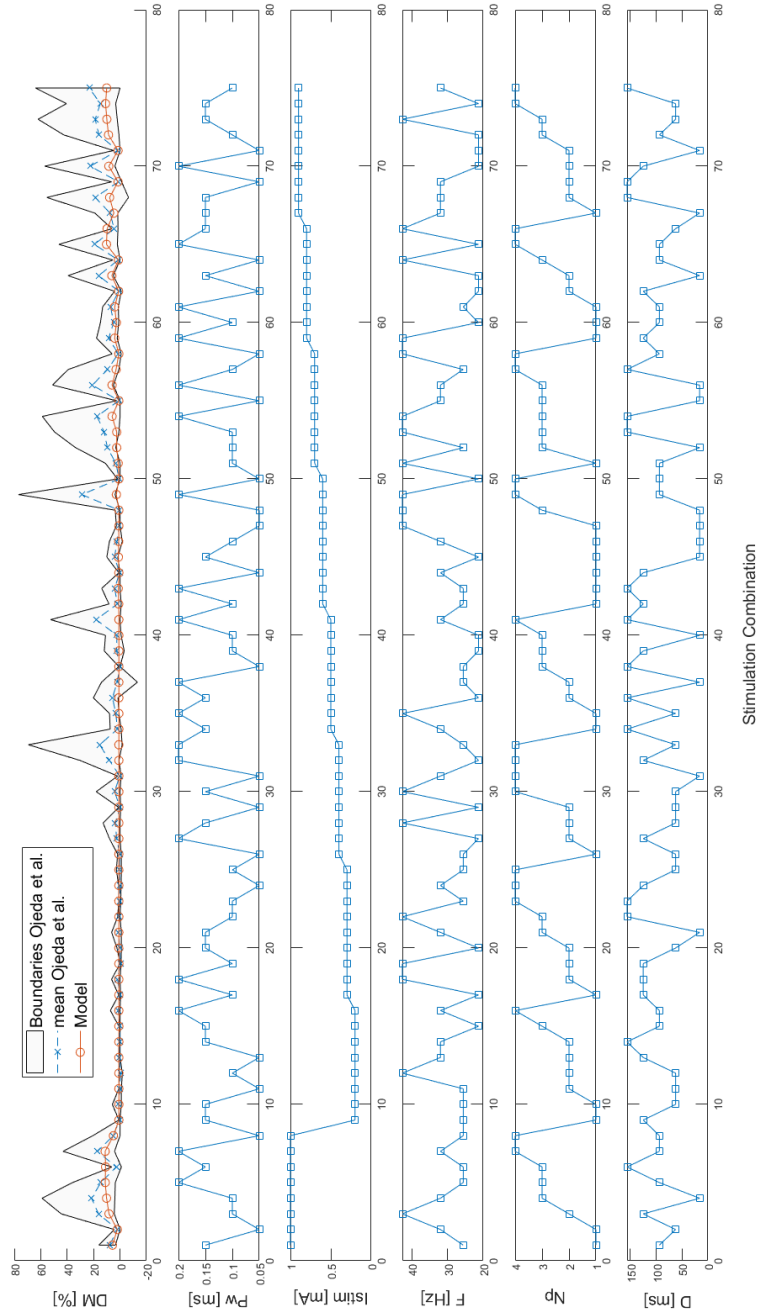


Figure 3.5: The dromotropism marker (D_M) represents the percentage change of the PR interval due to stimulation. It is calculated from the model (red dot) and compared to the Ojeda et al. study results [58] (in blue the mean value and in black the maximum and minimum). For each of the 75 parameter configuration, pulse width (P_w), current intensity (I_{stim}), frequency (F), number of pulses (N_p) and trigger delay (D) are given.

3.2 Global Sensitivity Analysis

3.2.1 S-VNS applied to Healthy condition

The second stage of the model tuning requires the implementation of the global sensitivity analysis (GSA) with Sobol's method to estimate the main and total sensitivity indices for each of the S-VNS parameters: current intensity, pulse width, number of pulses, frequency and delay using a quasi-random parameter set of 1000 combinations. The model was set in the healthy condition and the GSA results are compared with the ones provided from [58] in terms of mean and standard deviation. A graphical illustration is given in bar plots in Figure 3.6 and the exact values are reported in Table 3.1.

CHRONOTROPISM				
	Main Indices		Total Indices	
	<i>Ojeda et al.</i>	<i>Model</i>	<i>Ojeda et al.</i>	<i>Model</i>
Current	47.45±8.83	51.16±2.02	71.79±5.52	75.83±0.88
Number of pulses	6.37±2.58	5.08±0.17	14.23±4.62	13.10±3.85
Pulse width	18.60±2.97	17.78±0.62	38.01±11.21	38.05±2.58
Frequency	0.21±0.16	-0.16±0	0.64±0.41	0±4.61
Delay	0.88±1.47	-0.11±0	2.26±3.36	0.18±4.59
INOTROPISM				
	Main Indices		Total Indices	
	<i>Ojeda et al.</i>	<i>Model</i>	<i>Ojeda et al.</i>	<i>Model</i>
Current	52.82±15.32	44.41±1.84	68.70±12.45	74.37±1.04
Number of pulses	5.19±4.13	7.79±0.28	12.43±9.48	20.73±3.83
Pulse width	22.94±5.93	17.07±0.63	35.92±11.40	39.52±2.79
Frequency	0.37±0.46	0.35±0.01	1.48±1.52	0.09±5.21
Delay	0.96±1.13	-0.42±0.01	2.51±1.84	0.77±5.05
DROMOTROPISM				
	Main Indices		Total Indices	
	<i>Ojeda et al.</i>	<i>Model</i>	<i>Ojeda et al.</i>	<i>Model</i>
Current	48.26±11.71	52.62±2.09	68.31±11.67	76.41±0.88
Number of pulses	6.16±5.34	4.54±0.16	13.71±8.00	11.31±3.94
Pulse width	21.21±8.78	18.19±19	39.87±8.96	38.05±2.58
Frequency	0.13±0.09	-0.08±0	2.85±5.74	0±4.60
Delay	0.61±0.67	-0.06±0	2.86±2.83	0.06±4.59

Table 3.1: Comparison between the main and total sensitivity indices (mean±std [%]) for chronotropism, inotropism and dromotropism performed by Ojeda et al. [58] with the ones obtained from the model with a parameter set of 1000 different quasi-random combinations.

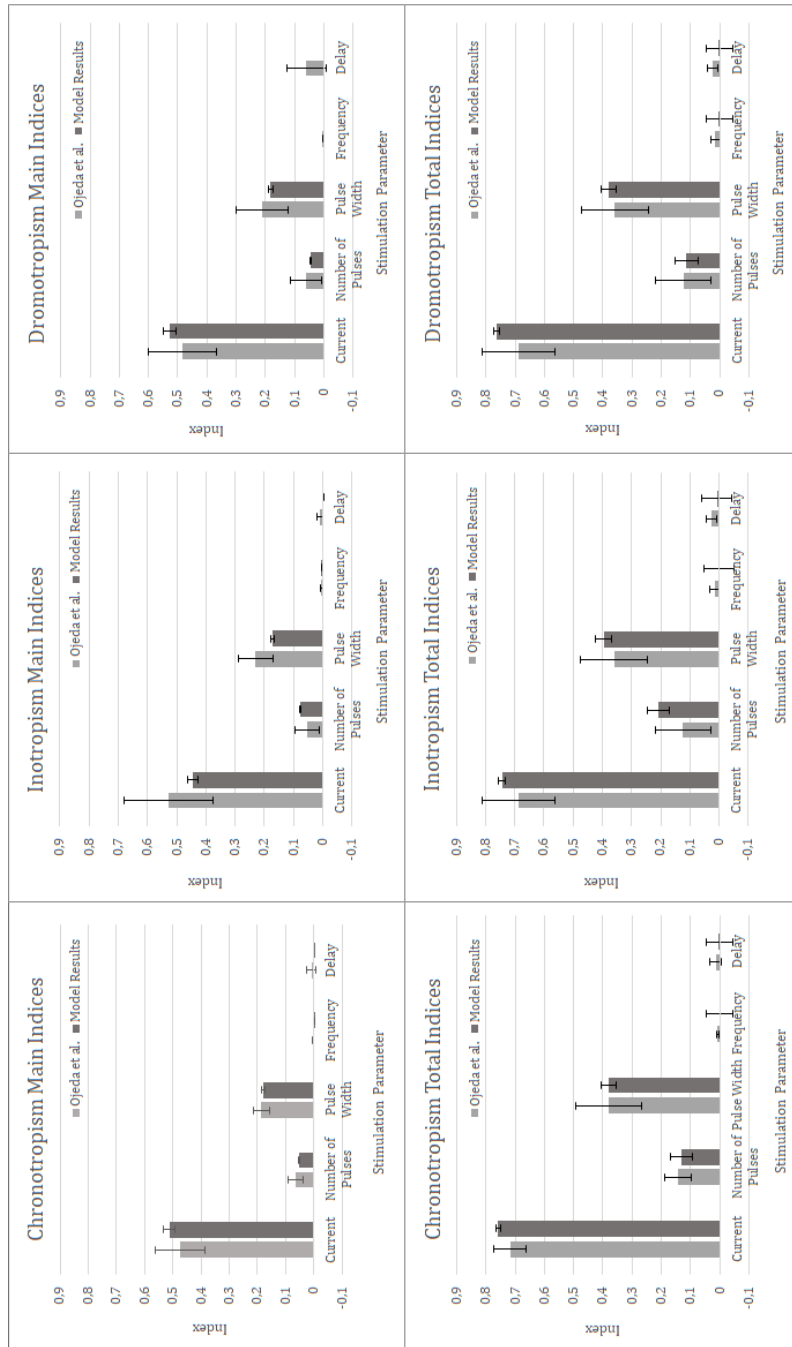


Figure 3.6: Comparison of the estimation of the main and total sensitivity indices for chronotropism, inotropism and dromotropism performed by Ojeda et al. [58] with the ones obtained from the model with a parameter set of 1000 different quasi-random combinations.

It is visible that the main and total indices obtained from the model provide a good fit of the Ojeda et al. [58] experimental data. Also, it is noticeable that the trend of both the main and the total indices for each of the analyzed cardiac effects, is similar.

Observing the main indices (top of Figure 3.6), a preponderant influence on every cardiac effect is given by the stimulation current intensity. The second most influential factor is the pulse width and the third is the number of pulses. Negligible is the effect of stimulation frequency and trigger delay.

The same trend of the indices is maintained, also looking at the total indices (bottom of Figure 3.6), but the magnitude is bigger than the main ones.

3.2.2 S-VNS applied to HTx condition

To evaluate any changes in the influence of VNS parameters on each cardiac effect in the condition of HTx with respect to the healthy condition, the GSA was performed with the same settings used in Section 3.2.1 but simulating HTx.

The comparison between the results obtained from the model in the healthy and in the HTx conditions is illustrated in Figure 3.7 and the detailed values of the HTx condition are given in Table 3.2.

It can be noted that there is good accordance between the main and total sensitivity indices of the healthy and the HTx condition when chronotropism and dromotropism are evaluated: the magnitude of the sensitivity indices are similar and the trend is maintained in the denervated heart. On the contrary, evaluating the inotropism, the magnitude of the sensitivity indices vary a lot: in the case of the main ones, magnitudes are significantly decreased and, for what concerns the total indices, they are widely increased. However, in all cases, the trend is maintained.

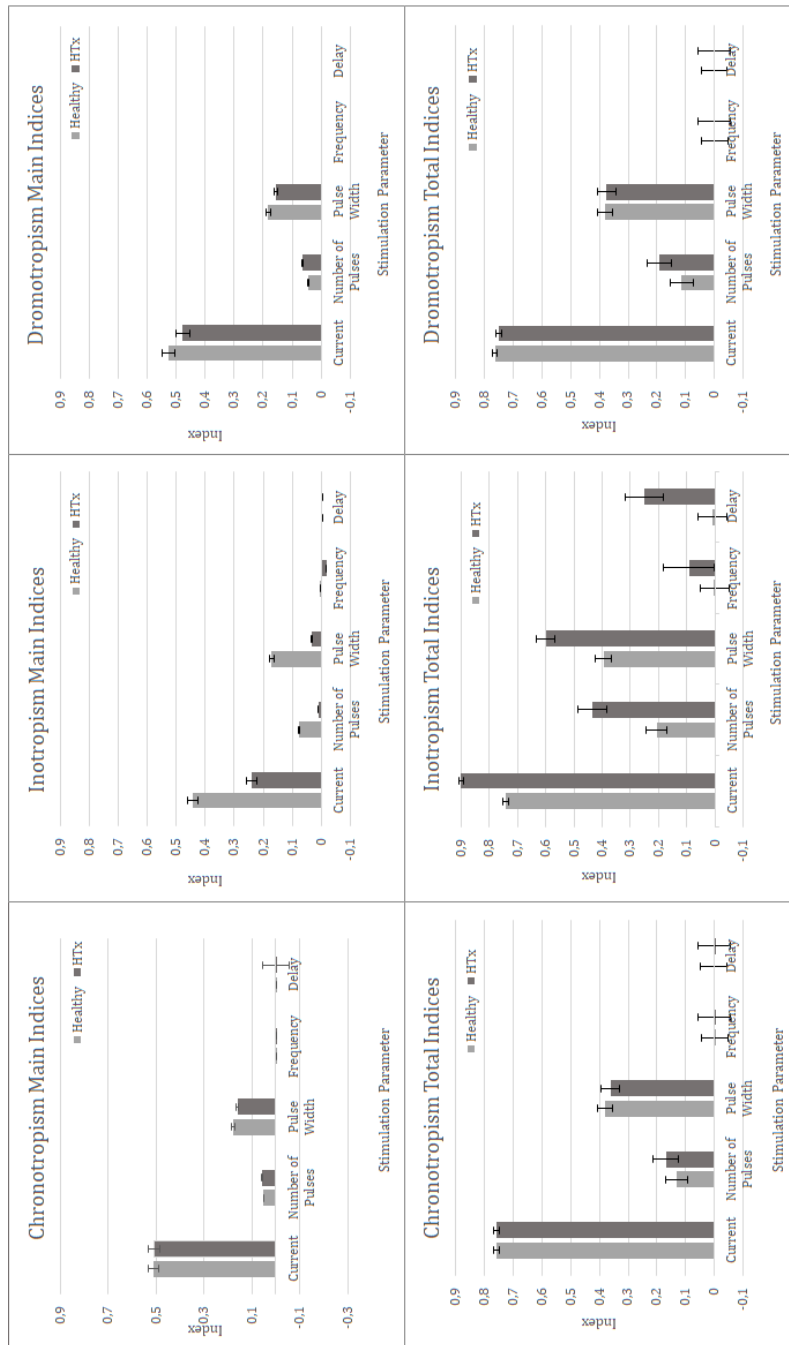


Figure 3.7: Comparison of the estimation of the main and total sensitivity indices for chronotropism, inotropism and dromotropism performed in the healthy and the HTx conditions.

CHRONOTROPISM		
	<i>Main Indices HTx</i>	<i>Total Indices HTx</i>
Current	50.72±2.43	75.79±0.97
Number of pulses	5.77±0.23	16.94±4.32
Pulse width	16.06±0.58	36.15±3.27
Frequency	-0.41±0	0±5.55
Delay	-0.41±0	0±5.55
INOTROPISM		
	<i>Main Indices HTx</i>	<i>Total Indices HTx</i>
Current	24.11±1.80	90.17±0.78
Number of pulses	0.10±0.06	43.49±5.13
Pulse width	3.38±0.23	59.99±3.23
Frequency	-1.74±0.11	9.24±9.09
Delay	-0.42±0.01	24.96±6.74
DROMOTROPISM		
	<i>Main Indices HTx</i>	<i>Total Indices HTx</i>
Current	47.66±2.30	75.01±1.01
Number of pulses	6.54±0.25	19.26±4.30
Pulse width	15.67±0.57	37.51±3.26
Frequency	-0.31±0.01	0±5.69
Delay	-0.31±0.01	0.04±5.69

Table 3.2: Estimation of main and total sensitivity indices (mean±std [%]) for chronotropism, inotropism and dromotropism obtained with the model in the HTx set up.

3.2.3 A-VNS applied to Healthy and HTx conditions

A GSA on A-VNS parameters using Sobol's method was carried out to gain a better insight and build the basis for implementing VNS parameters control strategies.

In this case, only three parameters are taken into account: current intensity, frequency and pulse width. The GSA was implemented with 1000 parameter combinations and given for both the healthy and the HTx conditions.

Results of the main and total sensitivity indices are illustrated as a comparison between the two conditions in Figure 3.8 and the detailed values are given in Table 3.3.

Between the three cardiac effects and the two condition, the trend is similar: the current have the highest magnitude in all cases and the second most influential parameter is the pulse width. The stimulation frequency has the lowest indices, but differently from the GSA performed on S-VNS parameters, it has a non-negligible role.

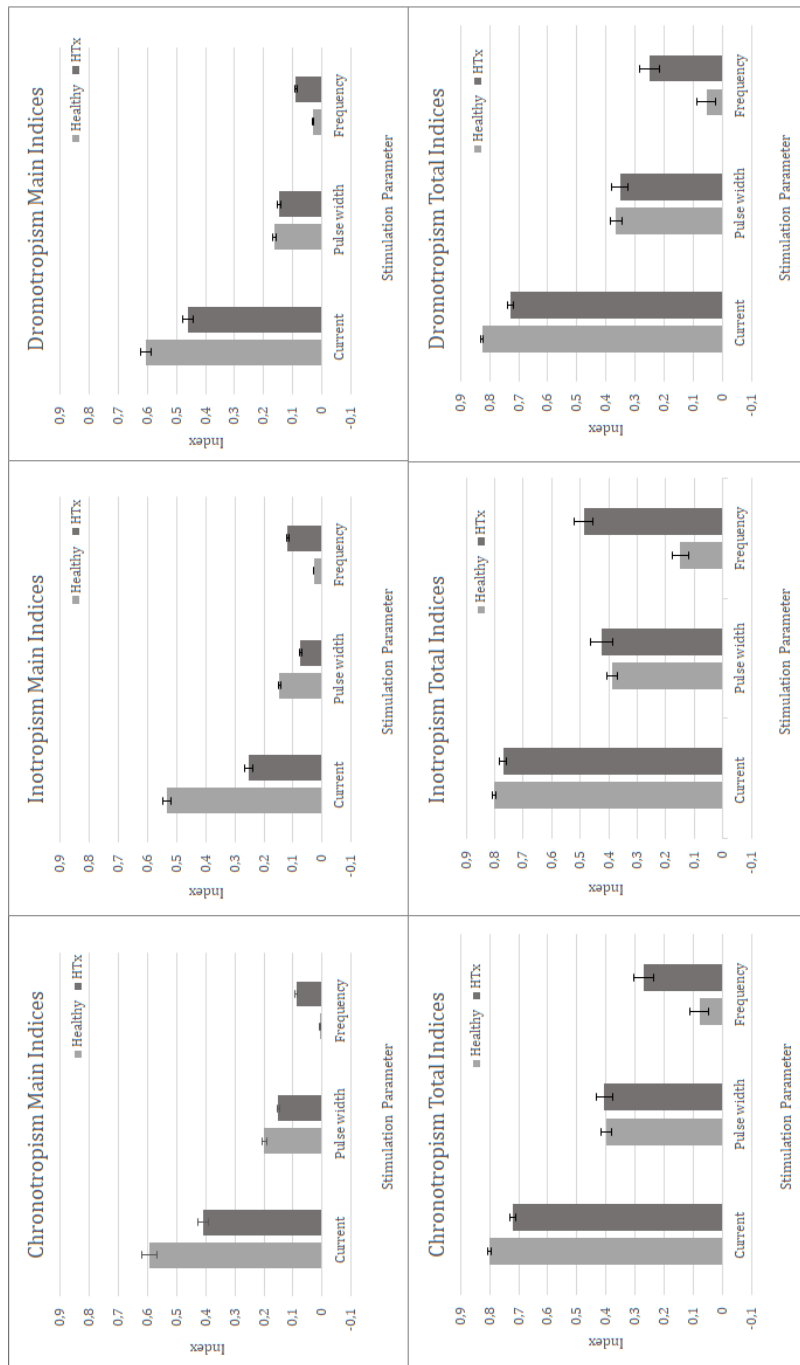


Figure 3.8: Estimation of Sobol' main and total indices for each A-VNS parameter on each cardiac effect.

CHRONOTROPISM				
	Main Indices		Total Indices	
	<i>Healthy</i>	<i>HTx</i>	<i>Healthy</i>	<i>HTx</i>
Current	59.44±2.78	41.01±1.71	80.18±0.67	72.07±1.16
Pulse width	19.98±0.83	15.05±0.55	39.78±1.90	40.58±2.77
Frequency	0.73±0.00	8.95±0.34	7.88±0.03	27.07±3.53
INOTROPISM				
	Main Indices		Total Indices	
	<i>Healthy</i>	<i>HTx</i>	<i>Healthy</i>	<i>HTx</i>
Current	53.32±1.53	25.23±1.33	80.22±0.69	77.11±1.08
Pulse width	14.66±0.48	7.38±0.28	38.93±1.87	42.38±3.88
Frequency	2.88±0.09	11.83±0.51	14.86±2.83	48.79±3.32
DROMOTROPISM				
	Main Indices		Total Indices	
	<i>Healthy</i>	<i>HTx</i>	<i>Healthy</i>	<i>HTx</i>
Current	60.47±1.74	46.15±1.90	82.63±0.53	72.76±1.10
Pulse width	16.41±0.54	14.81±0.53	36.50±1.84	35.24±2.97
Frequency	3.08±0.10	8.90±0.34	5.47±3.11	25.02±3.45

Table 3.3: Global sensitivity indices (mean±std [%]) estimated with the Sobol’s method of the asynchronized VNS parameters performed with 1000 different parameters combinations for the healthy and the HTx conditions.

3.3 Model Validation

The model was tested in conditions that are different from those imposed in the tuning stage to provide the validation of the cardiac effect’s modeling. In particular, the following tests aim to evaluate the capability of the model of reproducing data provided in ex-vivo or in-vivo studies performed by other researchers who investigate the cardiac effect of VNS [56, 61, 62, 63, 64]. Also, as previously described, the model tuning is performed on data obtained with the application of S-VNS on sheep. However, this type of vagus stimulation is still not widely used. That’s why the following tests are performed applying A-VNS having the opportunity to evaluate the capability of the model to predict the correct cardiac response in stimulation conditions different from the one used for the tuning. Moreover, the availability of human data is still restricted, but this stage allows the understanding of differences in cardiac effects given by the animal species subjected to VNS.

The setup of the studies chosen for the comparison was reproduced in the model as best as possible, without modifying any value in the model. All three implemented cardiac effects are evaluated.

3.3.1 Chronotropism

To evaluate the model capability of predict the chronotropic response, three studies were chosen ([61],[62]and [63]) whose experiments are devoted to describing the change in heart rate due to change in stimulation frequency.

As described in Section 2.13.1, to reproduce their experimental set up (isolated heart in [61], [62] and denervated heart in [63]), the model was set in the HTx condition. A frequency sweep protocol is carried out with fixed current intensity and pulse width to elicit a submaximal response.

The results are shown in Figure 3.9, where the percentage reduction in HR is displayed as a function of the frequency. The output of the model is compared with the data obtained ex-vivo in rabbits ([61],[62]) and in-vivo with a pharmacologically induced isolated setting in dogs ([63]). As expected, the HR reduction increases at increasing frequency and the model prediction is accurate with respect to the experimental data.

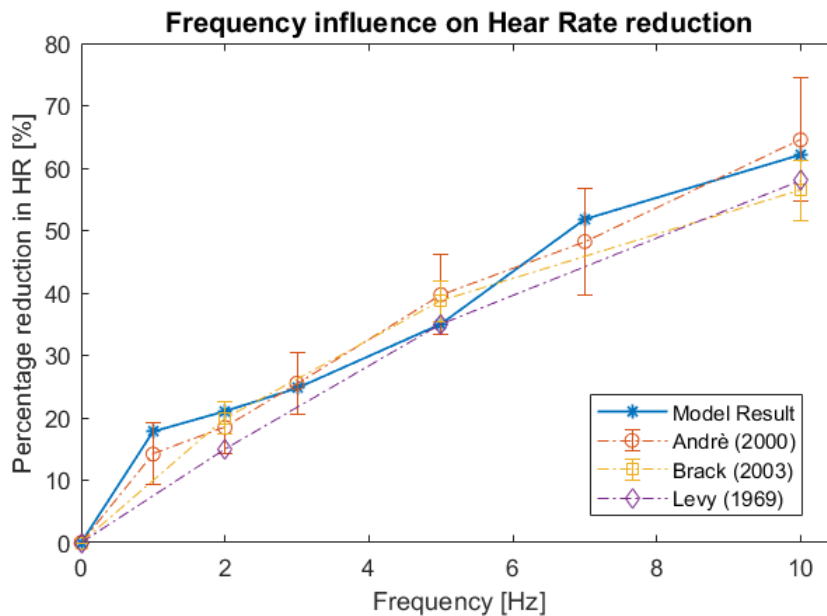


Figure 3.9: Reduction in heart rate (chronotropic effect) in an isolated heart subjected to asynchronous vagus nerve stimulation obtained by the model compared to literature data [61], [62],[63].

3.3.2 Inotropic

The simulation results were compared to the study of Lewis et al. [64] to evaluate the inotropic effects of A-VNS predicted by the model. In this study, the authors prove that in both pigs and humans, the ventricular elastance, assessed by the slope of the ESPVR, decreases with the application of VNS.

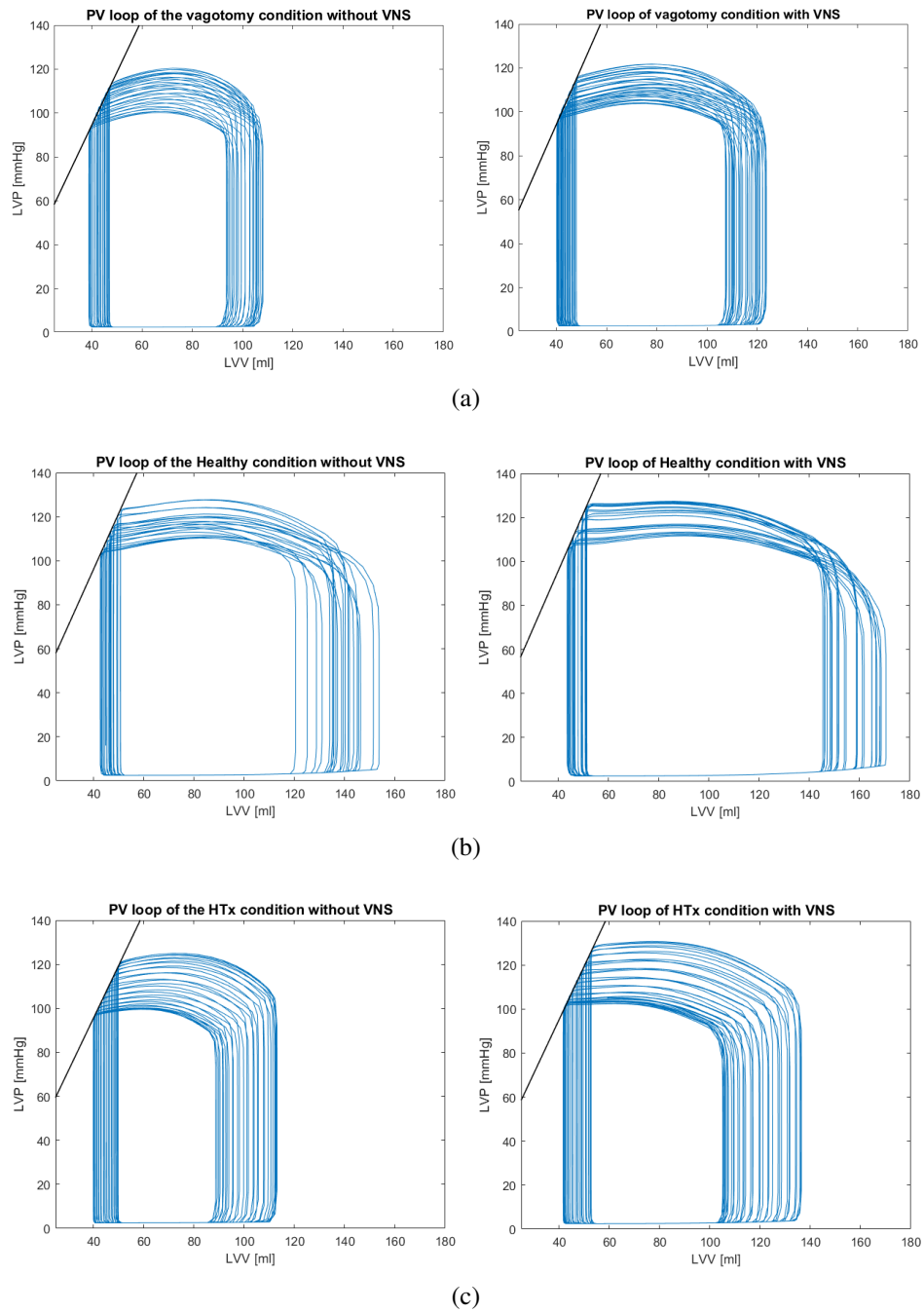


Figure 3.10: PV loops of the vagotomy (a), healthy (b) and HTx (c) conditions with (right) and without (left) the application of asynchronous VNS (current intensity = 0.78 mA, pulse width = 0.15ms and frequency = 10 Hz). The black straight line represents the ESPVR.

Asynchronous VNS was applied to the model simulating the dissected vagus as described in Section 2.13.2, leaving intact the sympathetic branch. The obtained PV loops are illustrated in Figure 3.10 (a) without (left) and during (right) VNS and the slope of the ESPVR, the end-systolic elastance, is calculated and reported in Table 3.4.

Differently from what is reported in [64], the elastance given by the model increases. To see any differences, the same procedure was also applied in healthy and HTx conditions. In Figure 3.10 (b) and (c) the PV loops are reported and the end-systolic elastance values are given in Table 3.4. In none of the cases, the expected decrease is detected.

<i>End-Systolic Elastance (Ees) [mmHg/ml]</i>		
	without VNS	with VNS
Dissected vagus	2.41	2.60
Healthy	2.54	2.61
HTx	2.39	2.43

Table 3.4: Elastance (Ees) calculated as the slope of the ESPVR for when simulating dissected vagus, healthy condition and HTxR with and without VNS (continuous stimulation: current intensity = 0.78mA, pulse width = 0.15ms and frequency = 10 Hz)

3.3.3 Dromotropism

The dromotropic effect was evaluated based on the study performed by Pirola et al. [56], who observed that the length of the PR interval increases linearly with the increase of the stimulation frequency. It is also reported the exact value of the slope increase, which was experimentally evaluated in dogs.

As described in Section 2.13.3, the experimental set up was reproduced in the model by setting the HTx condition fixing the current intensity and the pulse width to deliver supramaximal stimulation and a frequency sweep protocol was carried out.

The mean value of the PR interval is shown in Figure 3.11 as a function of the stimulation frequency and results to be linear. The slope was then calculated and it is shown in Table 3.5 compared to the one obtained in [56]. It can be observed that the model prediction is consistent with the data reported by Pirola et al. [56].

	Pirola et al.	Model
PR interval slope [ms/Hz]	6.4 \pm 4.9	6.8

Table 3.5: Comparison between of the slope of increase of the PR interval obtained in the study performed by Pirola et al. [56] and the one obtained from the model when providing a supramaximal stimulation.

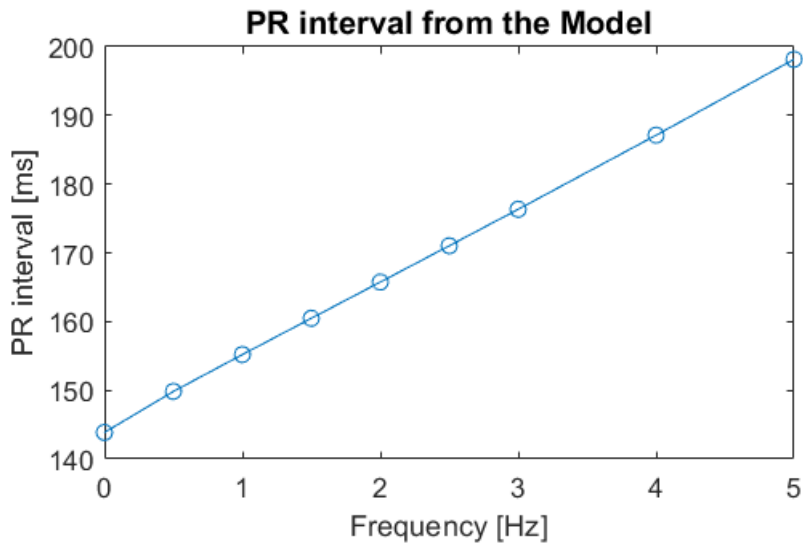


Figure 3.11: Measurement of the PR interval applying A-VNS fixing the current intensity to 0.9 mA and the pulse width to 0.2 ms and increasing the stimulation frequency from 0 to 5 Hz.

3.4 Effect of S/A-VNS on hemodynamic parameters

To get an overview of the variations due to the application of asynchronous and synchronous VNS on hemodynamic parameters in both the healthy and the HTx condition, heart rate (HR), cardiac output (CO), systolic and diastolic blood pressure (SBP and DBP), and stroke volume (SV) are calculated. As described in Section 2.14, the stimulation parameters for A-VNS and S-VNS were chosen to provoke a reduction in HR in the HTxR down to a normal resting HR (between 60 and 70 bpm). The same stimulation patterns are subsequently delivered to the healthy control.

The results are reported in Table 3.6 and for all the hemodynamic parameters, no substantial difference between the S-VNS and the A-VNS can be observed. There is a slight decrease in the CO due to the application of VNS caused by the decreased HR which is compensated by the increase in SV resulting in a normal CO. The SBP increase with the application of VNS while the DBP decreases slightly in the healthy condition and more heavily in the HTx condition.

	Healthy control	Healthy control with S-VNS	Healthy control with A-VNS	HTxR	HTxR with S-VNS	HTxR with A-VNS
HR [bpm]	66.9	49.1	47.5	93.6	66.9	63.5
CO [l/min]	5.8	5.4	5.2	5.4	5.1	5.1
SBP [mmHg]	112.7	118.1	118.1	111.6	113.4	114.7
DBP [mmHg]	72.9	71.3	71.3	81.0	70.5	69.3
SV [ml]	86.5	109.6	109.6	57.4	76.9	81.1

Table 3.6: Comparison between hemodynamic parameters (heart rate (HR), cardiac output (CO), systolic blood pressure (SBP), diastolic blood pressure (DBP) and stroke volume (SV)) of the healthy control and HTxR with and without VNS (S-VNS: current intensity = 1mA, pulse width = 0.2ms, number of pulses = 4, frequency = 25.6 Hz and delay = 156.2 us and A-VNS: current intensity = 0.7 mA, pulse width = 0.1ms and frequency = 15 Hz)

Chapter 4

Discussion

4.1 S-VNS Effects on Chronotropy, Inotropy and Dromotropy

Through the evaluation of the three cardiac effect markers in Figures 3.3, 3.4 and 3.5, it can be seen that the model output can reproduce well the data reported by Ojeda et al. [58]. In particular, for the great majority of the parameters combinations, the predicted marker resides inside the defined boundaries.

An indicator that gives an idea of the strength of the stimulation is the charge per phase [66], which is the product of pulse width and amplitude when A-VNS is applied. This concept can be adapted to S-VNS, where the stimulation strength can be seen as the product of the three most effective parameters: current, pulse width, and number of impulses. Observing the values of C_M , I_M , and D_M and evaluating the magnitude of stimulation strength as described before, it can be seen that the respective marker is close to zero for low magnitudes values. While for increasing stimulation strength, markers differ more and more with an increase in the case of the dromotropism (D_M) and a decrease in the others (C_M and I_M).

This behavior is primarily driven by a more considerable amount of involved fibers with increasing stimulation strength, which induces the vagus nerve to a major release of acetylcholine to the myocardial site. This provokes a reduction in the depolarization rate of the SA-node, a prolongation of the PR interval, and, indirectly, a depression of the ventricle contractility.

4.2 Global Sensitivity Analysis

4.2.1 S-VNS applied to the Healthy Condition

The fine-tuning involved the GSA to predict cardiac effects accurately. While performing the first stage of tuning with markers, it was seen that different model characterizations lead to a good fit of the markers provided by Ojeda et al. [58]. However, to implement the basis for a neuroprosthesis, it is essential to tune the model so that each stimulation parameter has a proper influence on the cardiac effect. If this is not the case, the risk is to have a model capable of predicting the correct response only with the combinations of stimulation parameters on which the tuning was made and making errors for all the others.

Moreover, the original approach that Ojeda et al. [58] developed allows quantifying the influence of all VNS parameters simultaneously on the main acute cardiac effects of VNS. This approach is innovative and overcomes research studies which only consider the individual stimulation parameter sensitivity on a limited (or single) number of physiological variables. This is the case of [67], which observes chronotropic sensitivity on current, or [56], which relates the stimulation frequency with the dromotropic effect.

Therefore, the GSA with Sobol's method was implemented, and from Figure 3.6 it can be seen that the model in the setting of healthy condition (intact heart) can well reproduce the sensitivity indices given in [58].

For all three cardiac effects, it can be seen that the current intensity has the highest main index, meaning that it is the most influential parameter (around 50% in all cases) on the target output. Moreover, the current intensity has a total index of 75%, indicating that controlling the current and the interactions it has with the other parameters can provide a high control of the desired output. The other two highly influential parameters are the pulse width and the number of pulses: their control provides the aforementioned interactions. The delay and the frequency of stimulation have indices close to 0% and, therefore, their role in the control of the cardiac effects is negligible.

From these considerations, it is possible to deduce that combining the primary control of the current intensity (main influential parameter) and then defining the pulse width and the number of impulses values (evaluating the interaction), it is possible to provide almost the complete control of all the three cardiac responses.

4.2.2 S-VNS applied to HTx condition

The GSA proposed by Ojeda et al. was performed on data obtained with the intact heart. However, the study's purpose is to build the basis for the implementation of cardiac control strategy on a transplanted heart. In this condition, the vagus and the sympathetic effectors are resected. Therefore, the GSA was performed by simulating the HTx condition under S-VNS.

Comparing the newly obtained sensitivity indices with the ones of the healthy condition (Figure 3.7), good accordance can be found for the chronotropic and the dromotropic effect. The trend is maintained, and only a small variation in the mean values can be observed, but they are classified as not significant because of their error bars. The similarity between the chronotropic and dromotropic indices is congruent with the direct influence that VNS has on these effects. In fact, the heart rate at rest is primarily driven by acetylcholine concentration at the cardiac site. In the case of the intact vagus nerve, the amount of acetylcholine due to VNS is summed with the baseline value driven by the central nervous system. On the contrary, when the vagus nerve is resected, the baseline concentration is absent, and the total amount of acetylcholine is only due to VNS. This behavior can be seen as a shift in acetylcholine concentration, but, reasonably, the influence of each VNS parameter stays unchanged.

The same behavior applies to the dromotropic effect. Remembering the explanation that Pirola et al. [56] gave (see Section 2.11), the PR interval length depends on the HR and on the concentration of acetylcholine and, therefore, the same consideration made for chronotropism apply to dromotropism.

This behavior does not apply to the inotropic effect. Indices obtained simulating HTx differ significantly from the ones of the healthy condition. The main indices are significantly lower while the total ones are higher than the healthy ones.

This result can be explained by considering that the elastance control is governed by the sympathetic nervous system and not by vagal outflow. Therefore, the influence of VNS on inotropism isn't a direct consequence, but the result of the indirect action of the sympathetic nervous system. In fact, the vagus nerve's direct action influences the heart rate, whose change causes a modification in the ventricle pressure value. Any changes in pressure cause the sympathetic nervous system's counteraction, which implements its control on ventricle elastance. However, the cardiac denervation interrupts the sympathetic outflow reducing its action by 95% thus, provoking an overall reduction in the influence of VNS on inotropism. According to this reasoning, inotropism's main indices are reduced in the HTx condition with respect to the healthy one.

Remembering the total index's definition, it represents the influence of the analyzed parameter in combination with all the others. In particular, the difference between the total index value and the main one indicates the interactions. Looking at the inotropism's total indices of the HTx condition in Figure 3.7, their high difference with respect to the main indices magnitude, indicates that stimulation parameters are highly inter-dependent. This highlights the main difference to the chronotropic and dromotropic effect and leads to the

observation that to control the inotropic effect, all the stimulation parameters may have to be taken into account.

4.2.3 A-VNS applied to Healthy and HTx condition

Another possibility to deliver VNS is to do it asynchronously, without observing a heart event-related trigger. In this case, only three stimulation parameters need to be set: stimulation current, pulse width, and frequency. From the GSA (Figure 3.8, one can observe that the most influential parameter for all cardiac effects remains the current, followed by the pulse width and the frequency.

Differently from the results obtained for the S-VNS, the frequency has a more relevant influence on all analyzed cardiac effects. The increased cardiac influence of the frequency when A-VNS is applied can be explained by the evidence that it is a determinant factor for the amount of acetylcholine released. The acetylcholine release model is sensitive to the arrival timing of spikes: the higher is the number of impulses delivered in the unit of time, the higher is the amount of neurotransmitter released. This is verified up to a certain frequency at which the acetylcholine in the main store cannot be reintegrated on time to be delivered at the arrival of the next action potential. In mathematical terms, the rate constants are longer than the period between one impulse and the other. Moreover, it has to be considered the range in which the frequency is defined to perform the GSA. In fact, in the S-VNS the frequency can be found in an interval between 21.3 Hz and 42.7 Hz while for the A-VNS the range is from 5 Hz to 15 Hz to make it representative of the reality. The fact that in S-VNS a certain number of pulses has to be chosen and that, in the Ojeda et al. study [58], its value is between 1 and 4 impulses, decreases the frequency effect. With simple calculations, one can verify that with the frequencies and number of impulses tested in S-VNS, the time between a beat and the other covered with stimulation is relatively short with respect to the time which elapses between the previous SA node depolarization and the next. This makes the stimulation frequency less influential when VNS is applied.

Moreover, it is interesting to see the increased relevance of the stimulation frequency in the HTx condition. For chronotropism and dromotropism, the sensitivity indices of the frequency is quite close to the one of the pulse width, meaning that their influence is quite similar. In contrast, the effect of frequency on inotropism overcomes the one of the pulse width. This behavior confirms that it is not a case that in a large number of experimental studies performed on denervated hearts, VNS effects are evaluated by switching the frequency ([56, 61, 62, 63]).

4.3 Model Validity

The model was tested evaluating the chronotropic, inotropic, and dromotropic effects in different conditions with respect to the ones used in the tuning to provide its (partial) validation. All the selected studies ([56, 61, 62, 63, 64] involved A-VNS and animal species different from sheep whose data were used for the tuning.

From Figure 3.9, it can be seen that the model can well reproduce the heart rate reduction measured in [61],[62] and [63] at different frequencies of stimulation with fixed current and pulse width. The higher the frequency, the bigger is the heart rate reduction. It is interesting to see that, even if the species on which experiments were performed (rabbits and dogs) are different between them and from the animal whose data were used for the tuning, the percentage reduction in heart rate is comparable. Also, the model reveals capable of accurately reproduce data obtained in the condition of HTx even if the tuning was performed under the healthy condition, thus confirming the successful implementation of the chronotropic response to VNS in the model.

For what concerns the assessment of the inotropic response, the model was tested by evaluating the left ventricle's contractility. This is done by calculating the slope of the end-systolic pressure-volume relation (ESPVR) called end-systolic elastance. The obtained results in Figure 3.10 and Table 3.4 show a slight increase in the value of this indicator when VNS is applied. For the sake of completeness, also the slope of the ESPVR simulating the HTx condition was calculated. Results are in contrast with the findings reported in [64] that show a decrease in the elastance provoked by VNS in both pigs and humans with intact vagus nerve.

The elastance control in the model was implemented and tuned to reproduce the data reported in [58]. However, here the elastance was evaluated as the percentage reduction of the maximum rate of change of the pressure in the left ventricle. This indicator depends on the arterial pressure (afterload-dependent) while the slope of the ESPVR is load-independent and thus more accurate when evaluating the elastance.

This unexpected behavior would deserve more research devoted to modifying the elastance control model, which can be done by either including a more accurate model or finding more literature studies that report enough data to re-tune this model subsystem.

Another aspect, which would deserve more investigation to confirm the model implementation, is that 80% of the fibers within the vagus nerve are afferent neural fibers, transducing information from visceral organs, including the heart, to the central nervous system. When VNS is applied to the intact heart, both afferent and efferent fibers are activated and may cause reflex autonomic activation. In [68], it is reported that VNS activates vagal afferent fibers that reduce cardiac efferent parasympathetic effects. It is possible that also the sympathetic efferent fibers are activated, but to date this is still not verified. However this could be an explanation to error obtained in the validation of the inotropism model.

The elongation of the PR interval due to the application of VNS is the result of the combination of the direct effect of VNS that acts to lengthen it and of the indirect effect of slowing the heart rate that acts to shorten it. The sensitivity of the atrioventricular conduction time to the stimulation frequency was experimentally studied by Pirola et al. [56] discovering the linear relation which relates them when the vagus nerve is resected and the sympathetic influence pharmacological inhibited (configuration similar to the denervated heart). In Figure 3.11, it is demonstrated that also in our model, the PR interval increase linearly with the stimulation frequency, and in Table 3.5, the comparison between the slopes states that the PR interval model perfectly reproduces those experimental data.

4.4 Hemodynamic Parameters

By observing the model output hemodynamic parameters reported in Table 3.6 without VNS applied to the healthy and HTx condition, it is possible to assess that the model prediction reflects literature data reported in Table 2.3. Congruently with the expectations, the baseline heart rate (HR) is higher in the HTxR (around 90 bpm), which is the SA node's spontaneous depolarization rate when the parasympathetic control is absent. Cardiac output (CO) is maintained constant between the two conditions, and this is due to the reduced stroke volume (SV) of the HTx condition.

No significant difference can be found in the hemodynamics when VNS is applied asynchronously or synchronously. In fact, when VNS is used, there is a reduction in HR, an increase of the systolic blood pressure (SBP), and CO, while diastolic blood pressure (DBP) and SV remain the same.

This trial aimed to see if the hemodynamics of a healthy control can be reproduced by applying VNS to an HTxR. Observing the output of the stimulation of HTxR with S/A-VNS and comparing them with the simulation of the healthy control, the values are quite similar. The biggest discrepancy can be found in the SV, which also produces a lower CO (5.8 l/min vs. 5.1 l/m).

However, knowing that the inotropism model is not accurate, as discussed in Section 4.3, these results have to be seen critically. Some experimental data are needed to verify the effect of VNS on hemodynamics. Eventually, some more model tuning will be focused on the effect of the VNS on ventricle elastance to gain more accurate hemodynamics.

Chapter 5

Conclusion and Future Work

Heart transplantation represents the last resort for individuals who suffer from end-stage heart failure. However, the direct consequence is cardiac denervation, which inhibits sympathetic and parasympathetic influence on the heart and leads to higher resting heart rate, chronotropic incompetence, and abnormal functional hemodynamic variables. From these impairments, the idea of the European NeuHeart project [41] of building a smart neuroprosthesis to restore the vagal-cardiac closed-loop connection through vagus neuromodulation.

The present work was devoted to integrating into a pre-existing computational heart model, a detailed model of the vagus nerve, and a stimulator to further investigate cardiac effects of vagus nerve stimulation (VNS) and build the basis for the implementation of cardiac control strategies.

The model was made capable of predicting the correct chronotropic, inotropic, and dromotropic responses to S-VNS. The tuning was based on data provided from Ojeda et al. [58] obtained in sheep and involved the use of markers to quantify each cardiac response and the global sensitivity analysis (GSA) with Sobol's method on stimulation parameters. The GSA was also performed in all possible model configurations, which include healthy and heart transplant (HTx) condition with synchronous (S-VNS) or asynchronous (A-VNS) VNS. From the results obtained, it stands out the preponderant role of stimulation current in the influence of each cardiac effect. The only exception is made for the inotropic effect when evaluating the HTx condition because, even if the current maintains the greatest influence, it is significantly lowered. This highlights the fact that the inotropic control is indirectly performed by the sympathetic nervous system that, due to cardiac denervation, cannot be actuated in the HTx condition. Also, it is interesting to analyze the role of stimulation frequency, which is negligible for the S-VNS but more influential when A-VNS is applied.

The model was found to accurately predict the chronotropic and dromotropic response when A-VNS is applied to the denervated heart through the validation against literature. An analysis of the hemodynamic parameters demonstrated that the synchronization or not of VNS does not change hemodynamics. Therefore, an excellent way to assess if S-VNS

can be advantageous to the commonly used A-VNS could be to evaluate power consumption. This is a crucial factor in the development of an implantable device, and it can be easily assessed with the model.

In conclusion, the model proved to be an excellent tool to investigate the effects of VNS. The GSA in the tuning stage revealed essential to implement the correct cardiac response when different stimulation parameters configurations are used. However, further investigations and tuning will be needed to simulate the correct inotropic response. A more in-depth insight into in-vivo experiments will be useful in animals with comparable human sizes (pigs and sheep) or even humans, to complete the model validation.

Appendix A

Model Parameters

A.1 Hemodynamic Model structure

A description of the hemodynamic model parameters and their assigned values are here illustrated and they refer to Equations from 2.1 to 2.7. The structure is composed by the left ventricle (Table A.1), the right ventricle (Table A.2), left and right atria (Table A.3), the four valves (Table A.4), and the arterial and venous circulation (A.5).

LEFT VENTRICLE			
Parameter	Value	Unit	Description
V^*	175	mL	Peak isovolumetric volume
P^*	270	mmHg	Peak isovolumetric pressure
V_0	27.65	mL	Ventricular unstressed volume
P_{Offset}	2.5	mmHg	
V_d	7.525	mL	Ventricular dead volume
$c3$	-0.0011	-	Coefficient of the cubic function
$c2$	0.0454	-	Coefficient of the cubic function
$c1$	0.0025	-	Coefficient of the cubic function
$c0$	-11.6244	-	Coefficient of the cubic function
α	4.127e-12	-	Constant
β	5.4122	-	Constant

Table A.1: Values used for the left ventricle model parameters

RIGHT VENTRICLE			
Parameter	Value	Unit	Description
V^*	200	mL	Peak isovolumetric volume
P^*	80	mmHg	Peak isovolumetric pressure
V_0	50	mL	Ventricular unstressed volume
P_0	0	mmHg	
P_{ec}	-4	mmHg	
K_r	14	-	Constant
a	5.3	-	Constant
b	3.3	-	Constant

Table A.2: Values used for the right ventricle model parameters

LEFT AND RIGHT ATRIA				
Parameter	Value LA	Value RA	Unit	Description
V^*	200	200	mL	Peak isovolumetric volume
P^*	30	10	mmHg	Peak isovolumetric pressure
V_0	0	0	mL	Ventricular unstressed volume
P_0	0	-5	mmHg	
E_{min}	0.125	0.100	mmHg/mL	Elastance minimum

Table A.3: Values used for the left (LA) and right (RA) atria model parameters

HEART VALVES					
Parameter	Value M	Value A	Value T	Value P	Unit
R_{dir}	0.005	0.020	0.003	0.003	$mmHg \cdot s/mL$
R_{inv}	50	50	50	50	$mmHg \cdot s/mL$
L_{li}		2.2284e-04			$mmHg \cdot s^2/mL$

Table A.4: Values used for the valve models (M=mitral, A=aortic, T=tricuspid, P=pulmonary. R_{dir} and R_{inv} are the resistance in forward and backward direction respectively and L_{li} is the inertance.

ARTERIAL LOAD			
Parameter	Systemic	Pulmonary	Unit
R_C	0.0333	0.015	$mmHg \text{ s/mL}$
C_C	1.445	3.0	$mL/mmHg$
L_C	0.0093	0.0027	$mmHg \text{ s}^2/mL$
Ca	0.155	0.7	$mL/mmHg$
Ra	1.066	0.11	$mmHg \text{ s/mL}$
VENOUS RETURN			
R_V	$0.164/P_{VS}$	0.01	$mmHg \text{ s/mL}$
C_V	50	10	$mL/mmHg$
V_{SO}	2200	200	mL

Table A.5: Values used for the arterial load and venous return parameters.

A.2 Sympathetic Cardiac Control

The sympathetic regulation mechanism is described in Equations from 2.12 to 2.18 and the relative parameter values are given in Table A.6. Here a distinction is done between the values used to model the healthy and the heart transplanted condition.

SYMPATHETIC CONTROL MODEL				
Parameter	Value Healthy	Value HTxR	Unit	Description
$P_{ao,ref}$	91	91	mmHg	Arterial baroreflex setpoint
$V_{L,ref}$	2.1	2.1	L	Pulmonary stretch reflex setpoint
Total peripheral resistance control				
G_{aRas}	0.16	0.16	$mmHg^{-1}$	Sympathetic arterial baroreflex gain
G_{pRas}	0.04	0.04	L^{-1}	Sympathetic pulmonary stretch gain
$R_{as,0}$	0.97	1.12	$mmHg \cdot s/mL$	Baseline total peripheral resistance
D_{Ras}	2	2	s	Delay of sympathetic effect
τ_{Ras}	5.1	5.1	s	Time constant of sympathetic effect
Venous unstressed volume control				
G_{aVusv}	10.6	10.6	$mmHg^{-1}$	Sympathetic arterial baroreflex gain
$V_{usv,0}$	2200	2200	mL	Baseline venous unstressed volume
D_{Vusv}	1.2	1.2	s	Delay of sympathetic effect
τ_{Ras}	2	2	s	Time constant of sympathetic effect
Ventricular elastance control (lv, left ventricle, rv, right ventricle)				
G_{aElv}	0.5	0	$mmHg^{-1}$	Sympathetic arterial baroreflex gain
G_{aErV}	0.5	0	$mmHg^{-1}$	Sympathetic arterial baroreflex gain
$E_{lv,0}$	1.15	1.15	mmHg/mL	Baseline elastance
$E_{rv,0}$	1.15	1.15	mmHg/mL	Baseline elastance
$D_{E,lv}$	2	2	s	Delay of sympathetic effect
$D_{E,rv}$	2	2	s	Delay of sympathetic effect
$\tau_{E,lv}$	0.25	0.25	s	Time constant of sympathetic effect
$\tau_{E,rv}$	0.25	0.25	s	Time constant of sympathetic effect
Circulating catecholamines				
$G_{a,am}$	0.016	0.016	$mmHg^{-1}$	Sympathetic arterial baroreflex gain
$G_{p,am}$	0	0	L^{-1}	Sympathetic pulmonary stretch reflex gain
C_{nora}	0.2	0.2	-	Proportional gain of noradrenaline release
τ_{kcirc}	1.32	1.32	s	Time constant for release of CATs
τ_{nora}	6	6	s	Time constant of noradrenaline release
Isoprenaline concentration				
$G_{a,Ts}$	0.016	0.0007	$mmHg^{-1}$	Sympathetic arterial baroreflex gain
$G_{p,Ts}$	0	0	L^{-1}	Sympathetic pulmonary stretch reflex gain
D_s	3	3	s	Proportional gain of noradrenaline release
c_s	10^{-9}	10^{-9}	-	Gain to correlate sympathetic outflow to [Iso]
iso_{base}	3.5	3.5	nM	Baseline concentration of isoprenaline

Table A.6: Values used for the sympathetic control model.

A.3 Primary Afferent Neurons

Afferent neurons drives sensory input from receptors to the central nervous system. In the model only the two most relevant ones are taken into account. Equations from 2.6 to 2.22 model them and the relative values are given in Table A.7.

AFFERENT NEURONS			
Baroreceptors			
Parameter	Value	Unit	Description
f_{min}	2.52	Hz	Minimum baroreceptor firing rate
f_{max}	47.48	Hz	Maximum baroreceptor firing rate
$P_{ao,ref}$	91	mmHg	Arterial baroreflex setpoint
G_b	23.29	$L^{-1}Hz$	Maximum baroreceptor gain
k_a	11.758	mmHg	Slope at the central point of sigmoidal function
τ_p	2.076	s	Time constants for the real pole
τ_z	6.37	s	Time constants for the real zero
Pulmonary stretch receptors			
τ_c	2	s	Time constants of the lung inflation
G_{ap}	23.29	$L^{-1}Hz$	Constant gain factor

Table A.7: Values used for the primary afferent neuron models.

A.4 Parasympathetic Premotor Neurons

The model of the efferent parasympathetic premotor neurons is describe in Equations from to and they respond integrating the signal generated by the afferent neurons. The values used are illustrated in Table A.8.

EFFERENT PREMOTOR NEURONS			
Parameter	Value	Unit	Description
$f_{ev,0,max}$	3.2	Hz	Maximal intrinsic firing rate of vagal nerves
$f_{ev,inf}$	5.95	Hz	Constant value for baroreceptor inputs
$f_{ev,0}$	5.62	Hz	Resting vagal tone
$f_{cs,0}$	25	Hz	Constant value
k_{ev}	7.06	Hz	Central point of sigmoidal function
$W_{p,v}$	0.1365	Hz	Synaptic weight applied to inputs from lung stretch receptors
θ_v	-0,23	Hz	Offset term

Table A.8: Values used for the efferent premotor neuron models.

A.5 CRRSS Model

The CRRSS model model the single nerve fiber which resides in the vagus nerve. To implement the CRRSS model, Equations from 2.25 to 2.42 are used and the variable values are given in Table A.9. It can be seen that most of the values are not fixed, but diameter (D) dependent: each fiber has a proper D which influences some the other CRRSS parameter values giving to the fiber its own properties.

CRRSS MODEL			
Parameter	Value	Unit	Description
D	variable	mm	Nerve fiber diameter
d	0.46 D	mm	Axon diameter
l_n	$1.5 \cdot 10^{-4}$	cm	Node length
l_{in}	100 D	cm	Internode length
c_m	1 F/cm	cm^2	Specific membrane capacitance
ρ	0.07	$k\Omega \text{ cm}$	Axoplasmic resistivity
ρ_e	0.35	$k\Omega \text{ cm}$	Extracellular medium resistance
g_m	1	mS/cm^2	Passive membrane conductivity
N	$75 D \cdot 10^4$	-	Number of myelin sheath layers
g_{Na}	1445	mS/cm^2	Sodium channel conductivity
g_{lk}	128	mS/cm^2	Leakage channel conductivity
V_{Na}	115	mV	Sodium channel reversal potential
V_{lk}	-0.01	mV	Leakage channel reversal potential
T	37		Temperature

Table A.9: Values used for the CRRSS model.

A.6 Acetylcholine Release Model

To model the release of acetylcholine to the myocardial site a three-compartment model is used as described in Equations from 2.43 to 2.48. The relative values are reported in Table A.10.

ACETYLCHOLINE RELEASE MODEL			
Parameter	Value	Unit	Description
k_H	0.15	s^{-1}	Hydrolysis rate constant
k_D	0.5	s^{-1}	Diffusion rate constant
k_E	0.5	s^{-1}	Washout rate constant
k_1	0.01	s^{-1}	Rate constant for release into neuroeffector junction
k_2	0.0005	s^{-1}	Rate constant of release into adjacent extrajunctional space
$[ACh]_T$	0.04	mM	Initial [ACh] in main store
F_{ms}	1	-	Relative volume of the main store
F_{ex}	1	-	Relative volume of the extrajunctional space

Table A.10: Values used for the ACh release model.

A.7 Vagus Nerve

The vagus nerve was built by assembling 400 nerve fibers modeled with the CRRSS model. However, the computational cost to include in the model 400 different CRRSS model was too high and a dimensionality reduction was applied. The entire system, with its integration with the ACh release model, is illustrated in Figure 2.10 and the values are given in Table A.11.

VAGUS NERVE REDUCED MODEL			
Parameter	Value	Unit	Description
l_N	4	mm	Nerve length
N_A	120	-	Amount of A fibers
N_B	280	-	Amount of B fibers
d_A	9.3 ± 0.75	μm	A fibers diameters (mean \pm std)
d_B	2.5 ± 0.5	μm	B fibers diameters (mean \pm std)
d_{el}	1.56 ± 0.94	cm	Electrode distances (mean \pm std)
$G_{ACh,stim}$	16	-	Gain factor $[ACh]_{stim}$
$G_{ACh,pm}$	4.5	-	Gain factor $[ACh]_{pm}$

Table A.11: Values of the vagus nerve reduced model.

A.8 PR Interval Model

When VNS is applied, a decrease in the atro-ventricular conduction speed follows causing a prolonged PR interval. This behavior is the consequence of two simultaneous effects: indirect and direct effects. Equations 2.49, 2.50 and 2.51 allow its calculation and the parameters values are given in Table A.12.

PR INTERVAL MODEL			
Parameter	Value	Unit	Description
$PR_{baseline}$	0.1766	s	baseline PR interval
$c_{PR,ind}$	0.351e-3	s/bpm	HR gain, indirect effect
$c_{PR,dir}$	2150	s/M	[ACh] gain, direct effect
$\tau_{PR,dir}$	1.5	s	time constant, direct effect

Table A.12: Values used for the PR interval model.

Bibliography

- [1] Cindy L Stanfield et al. *Principles of human physiology*. Benjamin Cummings, 2011.
- [2] D Burkoff. “Mechanical properties of the heart and its interaction with the vascular system”. In: *Cardiac Physiology* 46 (2002), pp. 1–23.
- [3] Richard Klabunde. *Cardiovascular physiology concepts*. Lippincott Williams & Wilkins, 2011.
- [4] JE Darnell et al. “Overview of neuron structure and function”. In: *Molecular cell biology*. WH Freeman and Company, 2000.
- [5] Iftikhar Abbasov. *Psychology of Visual Perception*. Jan. 2019.
- [6] CNX OpenStax. “Anatomy & physiology”. In: *Human Anatomy & Physiology* (2014).
- [7] Marcos Gridi-Papp. “Human Anatomy”. In: (2015).
- [8] Laurie Kelly McCorry. “Physiology of the autonomic nervous system”. In: *American journal of pharmaceutical education* 71.4 (2007).
- [9] Michel Kana. “Mathematical models of cardiovascular control by the autonomic nervous system”. In: *arXiv preprint arXiv:1901.05071* (2018).
- [10] *Neurotransmission*. Online; accessed 24-June-2020. 2020. URL: <https://basicmedicalkey.com/neurotransmission-2/#ch05>.
- [11] MN Levy and H Zieske. “Autonomic control of cardiac pacemaker activity and atrioventricular transmission.” In: *Journal of Applied Physiology* 27.4 (1969), pp. 465–470.
- [12] MARGARET R Warner and JEROD M Loeb. “Beat-by-beat modulation of AV conduction. I. Heart rate and respiratory influences”. In: *American Journal of Physiology-Heart and Circulatory Physiology* 251.6 (1986), H1126–H1133.
- [13] Anna Végh et al. “Part and Parcel of the Cardiac Autonomic Nerve System: Unraveling Its Cellular Building Blocks during Development”. In: *Journal of Cardiovascular Development and Disease* 3 (Sept. 2016), p. 28. doi: 10.3390/jcdd3030028.
- [14] Robert H Howland. “Vagus nerve stimulation”. In: *Current behavioral neuroscience reports* 1.2 (2014), pp. 64–73.

- [15] Sirkku Peltonen, Maria Alanne, and Juha Peltonen. “Barriers of the peripheral nerve”. In: *Tissue Barriers* 1.3 (2013), e24956.
- [16] Niels Hammer et al. “Cervical vagus nerve morphometry and vascularity in the context of nerve stimulation-A cadaveric study”. In: *Scientific reports* 8.1 (2018), pp. 1–9.
- [17] Frank Rattay. *Electrical nerve stimulation*. Springer, 1990.
- [18] Polona Pečlin and Janez Rozman. “Alternative paradigm of selective vagus nerve stimulation tested on an isolated porcine vagus nerve”. In: *The Scientific World Journal* 2014 (2014).
- [19] Junichiro Hayano. “Introduction to heart rate variability”. In: *Clinical assessment of the autonomic nervous system*. Springer, 2017, pp. 109–127.
- [20] Fred Shaffer and JP Ginsberg. “An overview of heart rate variability metrics and norms”. In: *Frontiers in public health* 5 (2017), p. 258.
- [21] Noor Aimie-Salleh, M Balakrishnan Malarvili, and Anna C Whittaker. “Fusion of heart rate variability and salivary cortisol for stress response identification based on adverse childhood experience”. In: *Medical & Biological Engineering & Computing* 57.6 (2019), pp. 1229–1245.
- [22] Piotr Ponikowski et al. “2016 ESC Guidelines for the diagnosis and treatment of acute and chronic heart failure: The Task Force for the diagnosis and treatment of acute and chronic heart failure of the European Society of Cardiology (ESC). Developed with the special contribution of the Heart Failure Association (HFA) of the ESC”. In: *European journal of heart failure* 18.8 (2016), pp. 891–975.
- [23] M Federmann and OM Hess. “Differentiation between systolic and diastolic dysfunction”. In: *European heart journal* 15.suppl_D (1994), pp. 2–6.
- [24] Kiran K Khush et al. “The International Thoracic Organ Transplant Registry of the International Society for Heart and Lung Transplantation: Thirty-sixth adult heart transplantation report—2019; focus theme: Donor and recipient size match”. In: *The Journal of Heart and Lung Transplantation* 38.10 (2019), pp. 1056–1066.
- [25] AIDO, Associazione Italiana per la Donazione di Organi, Tessuti e Cellule. Online; accessed 1-August-2020. 2020. URL: https://www.aido.it/dati_statistici/risultati.htm#.
- [26] Morcos Awad et al. “Early denervation and later reinnervation of the heart following cardiac transplantation: a review”. In: *Journal of the American Heart Association* 5.11 (2016), e004070.
- [27] Alan L Hodgkin and Andrew F Huxley. “A quantitative description of membrane current and its application to conduction and excitation in nerve”. In: *The Journal of physiology* 117.4 (1952), pp. 500–544.

- [28] George L Morris III et al. “Evidence-Based Guideline Update: Vagus Nerve Stimulation for the Treatment of Epilepsy: Vagus Nerve Stimulation for the Treatment of Epilepsy”. In: *Epilepsy Currents* 13.6 (2013), pp. 297–303.
- [29] JJ Ardesch et al. “Cardiac responses of vagus nerve stimulation: intraoperative bradycardia and subsequent chronic stimulation”. In: *Clinical neurology and neurosurgery* 109.10 (2007), pp. 849–852.
- [30] John P O’Reardon, Pilar Cristancho, and Andrew D Peshek. “Vagus nerve stimulation (VNS) and treatment of depression: to the brainstem and beyond”. In: *Psychiatry (Edgmont)* 3.5 (2006), p. 54.
- [31] Gaetano M De Ferrari et al. “Chronic vagus nerve stimulation: a new and promising therapeutic approach for chronic heart failure”. In: *European heart journal* 32.7 (2011), pp. 847–855.
- [32] Gaetano M De Ferrari and Peter J Schwartz. “Vagus nerve stimulation: from pre-clinical to clinical application: challenges and future directions”. In: *Heart failure reviews* 16.2 (2011), pp. 195–203.
- [33] Daniel Lawson and Glenn Marion. “An introduction to mathematical modeling”. In: *Bioinformatics and statistics Scotland* (2008), pp. 3–13.
- [34] Mona Abdolrazaghi, Mahdi Navidbakhsh, and Kamran Hassani. “Mathematical modelling and electrical analog equivalent of the human cardiovascular system”. In: *Cardiovascular Engineering* 10.2 (2010), pp. 45–51.
- [35] Yubing Shi, Patricia Lawford, and Rodney Hose. “Review of zero-D and 1-D models of blood flow in the cardiovascular system”. In: *Biomedical engineering online* 10.1 (2011), p. 33.
- [36] Nico Westerhof, Jan-Willem Lankhaar, and Berend E Westerhof. “The arterial windkessel”. In: *Medical & biological engineering & computing* 47.2 (2009), pp. 131–141.
- [37] Kamran Hassani, Mahdi Navidbakhsh, Mostafa Rostami, et al. “Simulation of the cardiovascular system using equivalent electronic system”. In: *Biomedical Papers-Palacky University in Olomouc* 150.1 (2006), p. 105.
- [38] Simon M Danner, Cornelia Wenger, and Frank Rattay. “Electrical stimulation of myelinated axons: An interactive tutorial supported by computer simulation”. In: *Saarbrücken (VDM 2011)* (2011).
- [39] George Qian and Adam Mahdi. “Sensitivity analysis methods in the biomedical sciences”. In: *Mathematical Biosciences* 323 (2020), p. 108306.
- [40] Andrea Saltelli et al. “Variance based sensitivity analysis of model output. Design and estimator for the total sensitivity index”. In: *Computer physics communications* 181.2 (2010), pp. 259–270.

- [41] *NeuHert Project*. <https://cordis.europa.eu/project/id/824071>. [Online; accessed 26-May-2020]. 2020.
- [42] Francesco Moscato et al. “Use of continuous flow ventricular assist devices in patients with heart failure and a normal ejection fraction: a computer-simulation study”. In: *The Journal of thoracic and cardiovascular surgery* 145.5 (2013), pp. 1352–1358.
- [43] A C Guyton, T G Coleman, and H J Granger. “Circulation: Overall Regulation”. In: *Annual Review of Physiology* 34.1 (1972). PMID: 4334846, pp. 13–44. doi: 10.1146/annurev.ph.34.030172.000305. eprint: <https://doi.org/10.1146/annurev.ph.34.030172.000305>. URL: <https://doi.org/10.1146/annurev.ph.34.030172.000305>.
- [44] Francesco Moscato. “Investigating the interaction between the cardiovascular systems and an axial flow ventricular assist device: mathematical model and acute animal study”. PhD thesis. University of Calabria, Italy, 2007.
- [45] Mauro Ursino and Elisa Magosso. “Role of short-term cardiovascular regulation in heart period variability: a modeling study”. In: *American Journal of Physiology-Heart and Circulatory Physiology* 284.4 (2003), H1479–H1493.
- [46] Mauro Ursino. “Interaction between carotid baroregulation and the pulsating heart: a mathematical model”. In: *American Journal of Physiology-Heart and Circulatory Physiology* 275.5 (1998), H1733–H1747.
- [47] SY Chiu et al. “A quantitative description of membrane currents in rabbit myelinated nerve.” In: *The Journal of physiology* 292.1 (1979), pp. 149–166.
- [48] JD Sweeney, JT Mortimer, and D Durand. “Modeling of mammalian myelinated nerve for functional neuromuscular stimulation”. In: *IEEE 9th Annual Conference of the Engineering in Medicine and Biology Society*. Vol. 3. 1987, pp. 1577–1578.
- [49] Frank Rattay and Matthias Aberham. “Modeling axon membranes for functional electrical stimulation”. In: *IEEE Transactions on Biomedical Engineering* 40.12 (1993), pp. 1201–1209.
- [50] Socrates Dokos, Branko Celler, and Nigel Lovell. “Vagal control of sinoatrial rhythm: a mathematical model”. In: *Journal of theoretical biology* 182.1 (1996), pp. 21–44.
- [51] Danilo Šćepanović. “A model of sinoatrial node cell regulation by the autonomic nervous system”. PhD thesis. Massachusetts Institute of Technology, 2011.
- [52] Erika E Fanselow. “Central mechanisms of cranial nerve stimulation for epilepsy”. In: *Surgical neurology international* 3.Suppl 4 (2012), S247.
- [53] EJ Peterson, O Izad, and Dustin J Tyler. “Predicting myelinated axon activation using spatial characteristics of the extracellular field”. In: *Journal of neural engineering* 8.4 (2011), p. 046030.

- [54] Alan Fabbri et al. “Computational analysis of the human sinus node action potential: model development and effects of mutations”. In: *The Journal of physiology* 595.7 (2017), pp. 2365–2396.
- [55] Stefano Severi et al. “An updated computational model of rabbit sinoatrial action potential to investigate the mechanisms of heart rate modulation”. In: *The Journal of physiology* 590.18 (2012), pp. 4483–4499.
- [56] Francine T Pirola and Erica K Potter. “Vagal action on atrioventricular conduction and its inhibition by sympathetic stimulation and neuropeptide Y in anaesthetised dogs”. In: *Journal of the autonomic nervous system* 31.1 (1990), pp. 1–12.
- [57] SG Carruthers et al. “Relationships between heart rate and PR interval during physiological and pharmacological interventions.” In: *British journal of clinical pharmacology* 23.3 (1987), pp. 259–265.
- [58] David Ojeda et al. “Sensitivity analysis of vagus nerve stimulation parameters on acute cardiac autonomic responses: chronotropic, inotropic and dromotropic effects”. In: *PloS one* 11.9 (2016).
- [59] Laure Rousselet et al. “Influence of vagus nerve stimulation parameters on chronotropism and inotropism in heart failure”. In: *2014 36th Annual International Conference of the IEEE Engineering in Medicine and Biology Society*. IEEE. 2014, pp. 526–529.
- [60] MATLAB Central File Exchange. *Global Sensitivity Analysis Toolbox*. <https://www.mathworks.com/matlabcentral/fileexchange/40759-global-sensitivity-analysis-toolbox>. [Online; accessed -July-2020]. 2020.
- [61] Kieran E Brack, John H Coote, and G André Ng. “Interaction between direct sympathetic and vagus nerve stimulation on heart rate in the isolated rabbit heart”. In: *Experimental physiology* 89.1 (2004), pp. 128–139.
- [62] G André Ng, Kieran E Brack, and John H Coote. “Effects of direct sympathetic and vagus nerve stimulation on the physiology of the whole heart—a novel model of isolated Langendorff perfused rabbit heart with intact dual autonomic innervation”. In: *Experimental physiology* 86.3 (2001), pp. 319–329.
- [63] MATTHEW N Levy and HARRISON Zieske. “Comparison of the cardiac effects of vagus nerve stimulation and of acetylcholine infusions”. In: *American Journal of Physiology-Legacy Content* 216.4 (1969), pp. 890–897.
- [64] ME Lewis et al. “Vagus nerve stimulation decreases left ventricular contractility in vivo in the human and pig heart”. In: *The Journal of physiology* 534.Pt 2 (2001), p. 547.
- [65] Max Haberbusch, Daniela De Luca, and Francesco Moscato. “Changes in Resting and Exercise Hemodynamics Early After Heart Transplantation: A Simulation Perspective”. In: *Frontiers in Physiology: Coputational Physiology and Medicine* (2020).

BIBLIOGRAPHY

- [66] Kurt Y Qing et al. “B fibers are the best predictors of cardiac activity during Vagus nerve stimulation”. In: *Bioelectronic Medicine* 4.1 (2018), p. 5.
- [67] Hendrik P Buschman et al. “Heart rate control via vagus nerve stimulation”. In: *Neuromodulation: Technology at the Neural Interface* 9.3 (2006), pp. 214–220.
- [68] Kentaro Yamakawa et al. “Vagal nerve stimulation activates vagal afferent fibers that reduce cardiac efferent parasympathetic effects”. In: *American Journal of Physiology-Heart and Circulatory Physiology* 309.9 (2015), H1579–H1590.